Applications of resistive droop control to grid connected low-voltage, single phase distributed generators in microgrids

by

Peter Bontorno

B.S., State University of New York Maritime College, 2009

A THESIS

submitted in partial fulfillment of the requirements for the degree

MASTER OF SCIENCE

Department of Electrical and Computer Engineering
Carl R. Ice College of Engineering

KANSAS STATE UNIVERSITY
Manhattan, Kansas

2020

Approved by:

Major Professor
Dr. Behrooz Mirafzal

Copyright

Abstract

A common understanding of the future grid structure consists of microgrids connected together (also called grid of microgrids). The microgrid concept includes a collection of loads and distributed generators (e.g. photovoltaic, microturbine, wind, etc.). The intelligent control of microgrids is a widely studied area. Traditionally the grid is controlled by central generators (e.g. nuclear, hydro and coal power stations) which establish the voltage and current setpoints and profiles throughout the grid. As distributed generators are introduced and microgrids are formed the opportunity for decentralized control of grid parameters is realized. While decentralized control can be accomplished by means of communication cables between generators, techniques such as droop control allow distributed generators to locally monitor parameters while collective manage voltage, current and power flow through the microgrid. This paper focuses on decentralized control without the use of communication cables by means of droop control methodologies.

Today many low voltage distributed generators, such as rooftop mounted photovoltaic arrays, are implemented using a control method that maximizes power output. This paper investigates the methods of applying droop control in place of maximum power point tracking to small scale, low voltage photovoltaic (PV) distributed generators. The study is performed in the context of rooftop mounted PV, where the distributed generators contribute primarily to residential loads. The study begins by investigating the design of a single phase 240 VRMS inverter. The design of the inverter uses traditional methods such that either maximum power point tracking or droop control could be applied as the control method for the inverter. The investigation continues by reviewing the principles of droop control and developing the droop control method that is most representative of the low voltage system, referred to in this paper as resistive droop control. The control method is then applied to the inverter design and a microgrid of distributed generator inverters and loads is simulated. The performance of the decentralized control method is analyzed. Potential benefits and applications of this method in the control of microgrids are presented.

Table of Contents

List of Figures

List of Tables

Acknowledgements

It has been said that nothing of significance was ever accomplished alone. This is true of the work that culminated in this thesis. This effort has been very challenging to me and I am grateful to have been supported by many along the way.

I would like to express my gratitude to my advisor, Dr. Behrooz Mirafzal for remembering me as one of his students, even though I was not present on campus. I am also extremely grateful for the help and guidance and instant support of my colleagues in the power electronics research lab, who also very willingly supported me from afar. Of particular note among these colleagues are Mr. Mohsen Pilehvar, who introduced me to PSCAD and willingly answered even the most basic of questions, Mr. Aswad Adib, who coached me through the final and most challenging stages of inverter design, and Mr. Fahmid Sadeque, who wisely identified what to trim and where to focus in order for my work and study to transform into a thesis.

I am very grateful to the faculty and staff at Kansas State University who supported and enabled my learning experience as a Masters student. I'd like to thank Dr. Fariba Fateh and Dr. Anil Pahwa for willingly fulfilling the role of committee members and supporting a summer final examination. I am also thankful to Dr. Andrew Rys for permitting me to carry my studies to completion, despite my slower than average pace. And when I consider those who I regularly counted on to help me, I have to mention Ray Clotfelter, director of the College of Engineering IT. As a distance student I depended daily on the ability to remotely log in to K-state labs and resources, and there were many days when Ray came to my rescue, preventing significant lost time.

Above all, my gratitude overflows for my wife and children who gave up Daddy time and many family experiences to see this effort through with me. Their commitment to me and to my research has been tremendous and stands as a monument to the caliber of people that they are.

Thank you!

Dedication

For Myna, Michaelangelo, Peter Elias and Ashley – my microgrid of distributed generators.

Chapter 1 - Introduction

This chapter introduces the present work of study. This work consists of modeling and demonstrating the application of resistive droop control to single phase, grid connected distributed generators, operating in parallel. Distributed Generation (DG) refers to the use of small ($\leq$50KW) scale power generators located at homes and businesses which have the ability to power a local load and transfer excess energy to the electric grid. This differs from centralized generators which exist for the express purpose of providing continuous reliable power to the electric grid for the use by multiple loads. The advent of growth in distributed generation has been made possible over the last several years as the cost of small scale power generation sources has decreased significantly. Photovoltaic arrays, consisting of solar panels wired in parallel strings, and often installed on residential or commercial rooftops, are the source of a significant amount of the growth in distributed generation. As the benefits of distributed generation become ever more apparent, so does the need to understand the various control methods that can be used to manage the microgrids to which these distributed generators are connect.

This paper is a collection of research performed to understand the design and control of paralleled inverters in a low voltage microgrid. This paper does not attempt to cover all of the methods that have been explored. Rather it selects one of the prevailing power management control strategies, resistive droop control, and presents information relative to this strategy. That information is presented in the form of equations, figures, tests and simulations throughout the chapters that follow.

1.1 Research Motivation

As these DG systems become more prevalent, it is possible that grid designers will need to undergo a mental shift, no longer looking at the grid as being powered by centralized generators and supported by additional distributed generators, but instead considering decentralized control that is possible when distributed generation serves as a primary power

source. When this is the case, distributed generators will take on a new role and responsibility for ensuring grid stability.

As this future state is considered, power electronic engineers will need to have the tools and information to design inverter controllers that seek to support grid voltage and frequency through power management. One of the most popular methods for contributing to the control of voltage and frequency is via droop control, due to the simplicity of implementation, and the fact that control can be shared by multiple generators without the need for interconnecting communication systems or supervisory control.

This paper seeks to understand the latest in droop control strategies, with particular consideration for its application to low voltage, single phase distributed generators. It is the authors hope that the information gathered by this paper will be useful to the many inverter designers who in the near future will wish to implement these strategies on a large scale.

1.2 Background and Previous Research Performed

The application of droop control to inverter design has been a study of many researchers. The majority of the focus has been on the application of traditional droop control for use in higher voltage systems. These studies have proposed solutions to many of the challenges of traditional droop control such as power sharing during islanded microgrid operation [1], balancing reactive power sharing despite variations in feeder impedances [2], and the need for hierarchical supervisory control when managing multiple microgrids of distributed generators [3]. However, over the last decade there has been an increase in recognition by researches that a major application of distributed generation will occur at the low voltage and single phase level, where the feeders are not expected to be highly inductive. Some researchers have addressed this reality by applying virtual impedance to the controller, simulating a more inductive feeder, to support the continued use of traditional droop control [3], [4]. Meanwhile other researchers have abandoned traditional droop control for resistive droop control, citing benefits such as a more damped system overall, improved harmonic current sharing, and protection of active power sharing against phase errors [5]. In [6], resistive droop control is

used to demonstrate improved power sharing during islanded operation. The previously mentioned concept of a virtual impedance was modified to an even simpler concept of virtual resistance to ensure performance, even in an inductive grid [5]. Finally, research is also covering the potential benefit of a combined controller in which active and reactive power are both managed during changes in either voltage or frequency. This concept is presented in [7] as a method to apply better power management in the presence of non-linear loads.

1.3 Methods

To accomplish this research, a model of the electrical distribution system of interest first was developed. To accomplish this, the simulation software Power Systems CAD (PSCAD) was selected. This software package allows for an electrical power system with multiple sources to be built and tested at a high speed. The software also contains many of the mathematical and logic functions needed to build power electronic controllers, such as those required to implement an inverter and control system. The use of software allows for easy and rapid modification, enabling an array of tests to be performed following the development of a single model. The limitation, however, is that assumptions are required to be made in the development of a model that may not always be correct in an equivalent real-world hardware application. However, as long as the assumptions are generally conservative the results will be largely consistent with real world results.

After selecting the software, a model was constructed consisting of a microgrid with multiple distributed generators feeding multiple loads. The model also includes the power electronic controllers for the distributed generator inverters. The model was tested to demonstrate important features of droop control relative to low voltage grid connected inverters.

This effort is documented in this paper as follows. The microgrid design is presented in Chapter 2. The design of the power electronic control system for the inverter, up to the power reference signal, is presented in Chapter 3. The design of the droop controller that provides the power reference signals to the inverter controller is presented in Chapter 4. The tests performed and associated results are presented in Chapter 5. A wrap up of conclusions and a

brief discussion of future research based on this study is presented in Chapter 6. From these tests a useful decentralized integrated microgrid control function is demonstrated.

1.4 Thesis Contributions

This research seeks to support the growing research on droop control methods. While this paper is specifically intended to demonstrate the implementation of resistive droop control in a single phase microgrid, it is the hope of the author that this information will be used alongside existing information on traditional droop controllers to allow the future designers of inverter controllers to develop the best possible control systems for establishing autonomous microgrids.

1.5 Conclusion

As future inverter controllers are developed to support the growing demand for microgrid operation, designers will need a vast array of information across the many inverter control systems that have been proposed. The information in this paper is intended to support those designers by providing information specific to low voltage, single phase, droop controlled power inverters.

Chapter 2 - System Description

2.1 Introduction

The purpose of this chapter is to present the parameters and design of the system under study. This paper investigates operation of a grid connected microgrid with significant distributed generator capacity. The theorized microgrid is a small portion of a larger grid network, that is separated from the larger grid by some amount of impedance. More specifically, in this paper a small scale microgrid is theorized consisting of only a few low voltage loads and sources. The loads are selected to be representative of a small or efficient home. The sources are

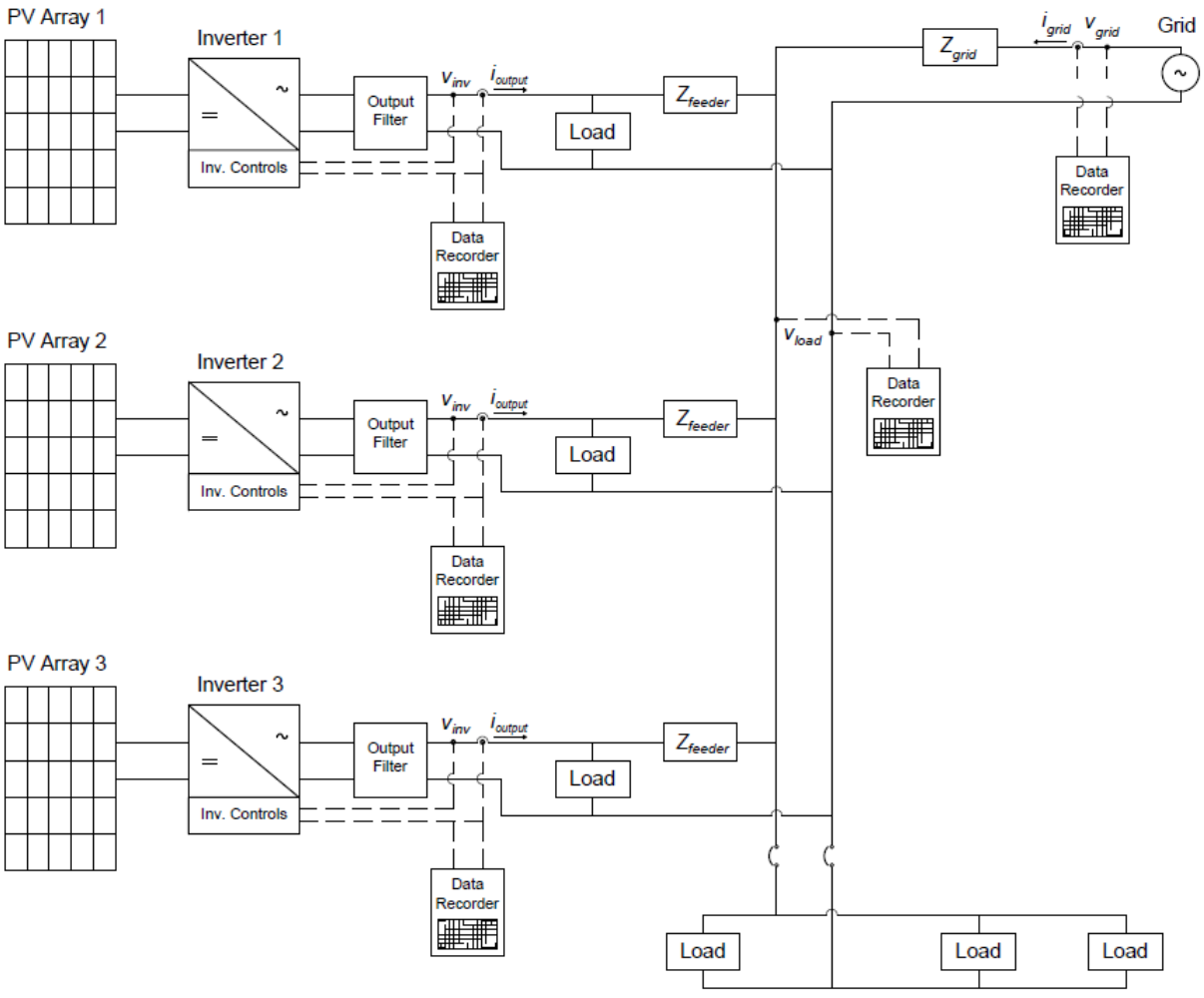

Figure 2.1 Block Diagram of the Theorized Microgrid

representative of a rooftop mounted photovoltaic array under full light. The system is a single phase 240 VRMS, 60 Hz system, equivalent to what might be seen in North America. The building blocks of this theorized grid network are presented in this chapter, while during testing specific parameters may vary with each simulation run. Any differences are presented in the discussion of the specific simulations in Chapter 5 -System Analysis and Tests.

2.2 Grid Network Description

The block diagram of the microgrid that is studied is presented in Figure 2.1. The data recorders are inserted to make clear the location and direction of power flow at the points of measurement that are used in tests performed in this paper. Important values and content of many of the blocks in the block diagram are presented in the following discussion.

2.2.1 Voltage Sources

Two power source types are used to supply power to this grid network. One ideal centralized alternating current (AC) power source of infinite capacity is used to represent the grid. More specifically, this source represents the output of a single phase transformer, regulating the local grid voltage (V_{grid}) to 240 VRMS line to line, and a frequency (f) of 60 Hz. Additionally, there are multiple photovoltaic arrays, considered as rooftop mounted systems, tied to the grid via

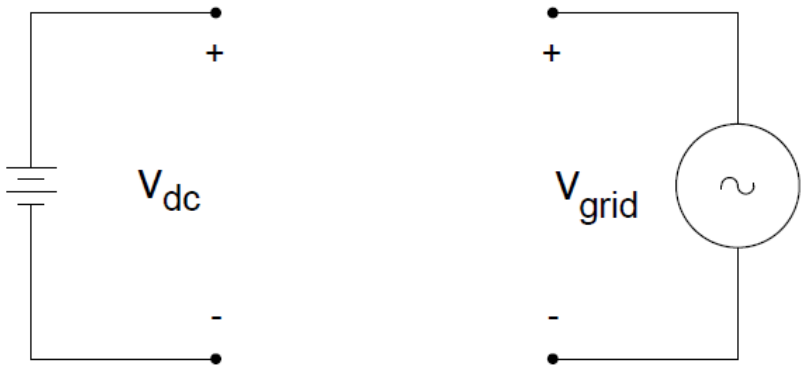

Figure 2.2 Power Source Schematics

single-phase DC/AC photovoltaic inverters. To simplify simulation and improve simulation time, the PV arrays are simulated as a constant, ideal direct current (DC) power source providing a stable voltage source (V_{dc}) to the DC link of the inverter.

The inverter also serves as a power source to the microgrid, assisting in establishing the grid operating parameters. A description of the inverter is provided in Chapter 3. The output of the inverter (V_{inv}) is 240 VRMS line-to-line, operating at 60 Hz with a phase angle (δ) to the grid voltage. The phase angle is a result of line impedance on the microgrid between the grid source and the inverters, and the phase angle of operation of each of the loads.

$$V_{rms} = 240\ VRMS \tag{2.1}$$

$$f = 60\ Hz \tag{2.2}$$

$$V_{grid} = 339.4 \sin(2\pi 60t) \tag{2.3}$$

$$V_{inv} = 339.4 \sin(2\pi 60t - \delta) \tag{2.4}$$

$$V_{dc} = 600\ VDC \tag{2.5}$$

2.2.2 Grid Side Transformer

The grid network is a single-phase 240 VRMS network. Though the larger grid is likely distributed as three phases at a higher voltage, the portion of the grid of interest has only one phase. Residential single phase is typically acquired from a single phase low voltage transformer, which is assumed to exist but not modeled in any of the simulations used for this paper. A typical transformer is presented here in order to provide an explanation for the voltages and configuration of the microgrid presented in this study. A three phase system will often feed multiple single phase transformers of equal sizes to achieve balanced loading. Residential single phase transformers make use of a center tap to ground to achieve the characteristic 240 VRMS line to line and 120 VRMS line to ground.

$$V_{Load\ (Line\ to\ Line)} = 240\ VRMS \tag{2.6}$$

$$V_{Load\ (Line\ to\ Ground)} = 120\ VRMS \tag{2.7}$$

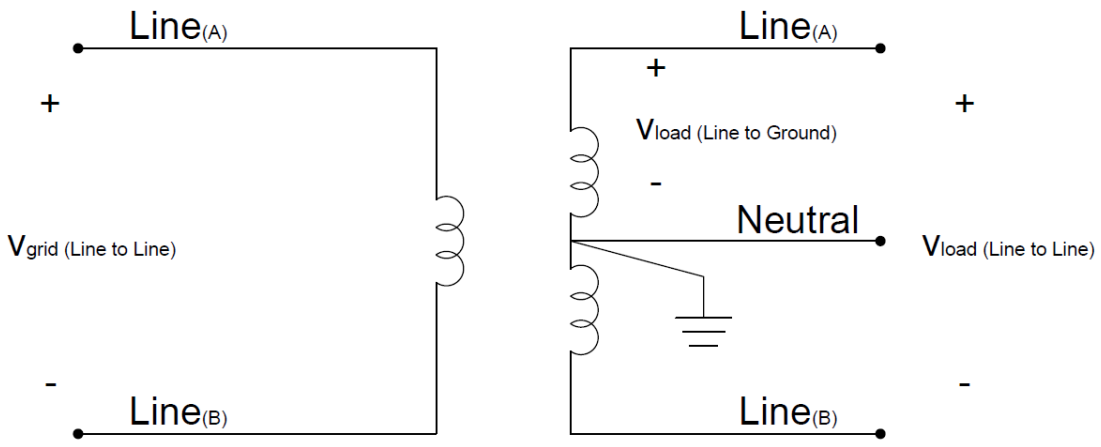

Figure 2.3 Single phase center tapped residential 240 VRMS transformer supplying microgrid, tapped from two legs of a three phase distribution system, schematic diagram

In Chapter 5 -System Analysis and Tests, the concept of a smart transformer is presented. Though the transformer is not developed in this paper, it can be assumed to perform the same functions as the transformer presented above. However, the voltage change would be achieved by a power electronic full bridge gate array, similar to the one used in an inverter, rather than by means of induction. This difference would allow for the output voltage to vary, according to the voltage setpoint desired for the system.

2.2.3 Inverter Output Filter

The inverter output filter reduces high frequency harmonics that would otherwise be propagated to the loads because of the high frequency switching of the full bridge inverter. An LCL filter is used with the larger inductor being placed closest to the full bridge switches to maximize control of current out of the inverter, thereby minimizing the potential *dv/dt* spikes across the capacitor.

$$L_1 = 2\text{mH} \tag{2.8}$$

$$L_2 = 1\text{mH} \tag{2.9}$$

$$C = 50\ \text{uF} \tag{2.10}$$

Two resistors are used to further reduce current flow through the capacitive branch, thereby minimizing voltage spikes on the system. The resistor in parallel with the capacitor has a very high resistance and functions only to shunt current during a voltage spike. Under normal conditions no appreciable value of current will pass through this resistor.

$$R_H = 1 \times 10^{16}\ \text{Ohm} \tag{2.11}$$

$$R_L = 1\ \text{Ohm} \tag{2.12}$$

A resonant frequency (f_R)can be estimated by combining the inductors in series and applying the resonant frequency formula.

$$f_R = \frac{1}{2\pi\sqrt{LC}} \tag{2.13}$$

By convention the output filter will minimize harmonic distortion if the filter resonance frequency falls between $^1/_6$ and $^1/_2$ of the pulsewidth modulation frequency (f_{PWM}). The inverter pulsewidth modulators are set to 2.500 KHz and the resonant frequency of the output filter has a resonant frequency of $^1/_6$ this frequency.

$$f_R = 0.41\ \text{KHz} \tag{2.14}$$

$$f_{PWM} = 2.5\ \text{KHz} \tag{2.15}$$

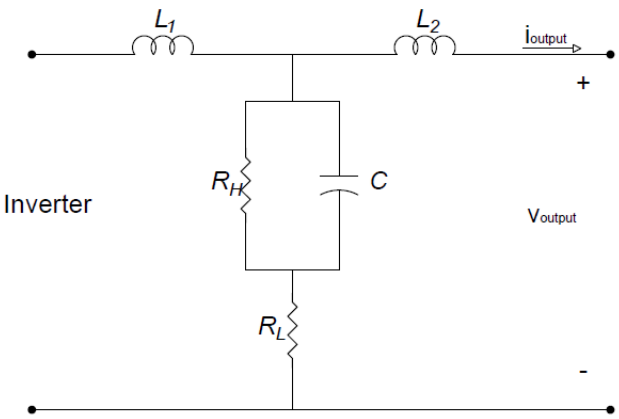

Figure 2.4 Inverter Output Filter Schematic

2.2.4 Busses

The busses of the microgrid are represented schematically in the block diagram Figure 2.1. They consist of a grid bus, a load bus and the individual distributed generator busses. The microgrid refers to the combination of the distributed generator busses and the load bus. The load bus is isolable from the microgrid by means of breakers which can be set to operate during simulations to illustrate the effect of adding and removing load to and from the microgrid. The reader should not be confused into believing that isolating the load bus will remove all load from the system. It should be noted that each distributed generator bus also contains a local load which is not separated by impedance from the inverter. This setup allows for simulations to be run with only local loads, or with a combination of local and remote loads, depending on the position of the load bus breakers.

2.2.5 Line Impedance

Line impedance is inserted into the grid network to simulate the natural impedance of distribution lines and to ensure each inverter operates independently, separated from each of the other sources by an impedance angle (δ). This is accomplished by adding an inductor (L) and resistor (R) in series with one line of each inverter, representing the feeder impedance (Z_{feeder}). Knowing the feeder impedance is useful to anticipate the voltage and frequency response during droop control. Since voltage and current are measured on the feeder side of

the output filter, the output filter impedance can be neglected when considering the feeder impedance. The impedance of the output filter is compensated for by the inverter controller. An inductor and resistor are also placed on the grid side of the network representing the grid source impedance (Z_{grid}).

$$L_{feeder} = 0.1\ mH \tag{2.16}$$

$$L_{grid} = 0.5\ mH \tag{2.17}$$

$$Z\angle(\theta_i)_{feeder} = 0.1884 + j0.0377\ Ohms \tag{2.18}$$

$$Z\angle(\theta_g)_{grid} = 0.1884 + j0.1885\ Ohms \tag{2.19}$$

$$\frac{R_{feeder}}{X_{feeder}} = 5 \tag{2.20}$$

$$\frac{R_{grid}}{X_{grid}} = 1 \tag{2.21}$$

Reference [8] describes line inductance in terms of inductive reactance and provides characteristic examples of impedance values for various situations. For a low voltage distribution system, higher inductive reactance values will be observed in overhead aerial lines then would be observed in underground conduit. In the case where power is supplied to a neighborhood via a pole mounted transformer and aerial lines, the inductance in the network would be higher than if power was distributed underground. If cables from a pole mounted transformer descended underground at the entrance of a neighborhood and were distributed to the homes underground, the transformer side inductive reactance would be larger than the inductive reactance between homes. If all power is routed underground and the transformer is ground mounted on a slab, the inductive reactances throughout the network might be low and near to zero.

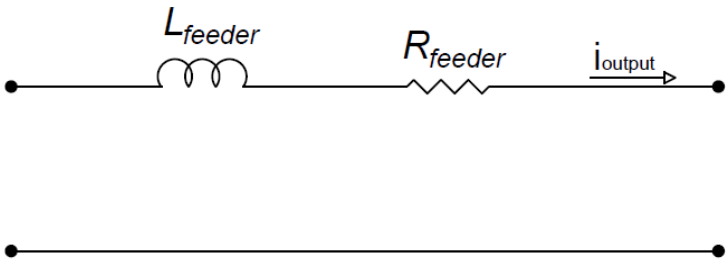

Figure 2.6 Feeder Line Impedance Schematic

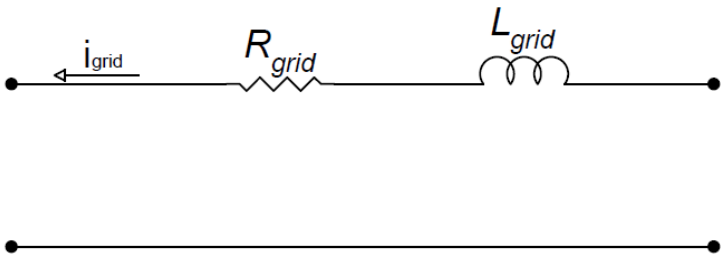

Figure 2.6 Grid Line Impedance Schematic

Using the tabulated values for inductive reactance available in reference [8] and reference [9], inductance values were selected for use in this research. An inductance value of .5mH was selected to represent overhead distribution up to 1 mile in distance. An inductance value of 0.1mH was selected to represent underground distribution up to 700 ft in distance.

2.2.6 Loads

The loads for this grid network consist of a parallel resistor and inductor set. One typical load is designed for use wherever a load is applied in the microgrid. The load can be simply referred to as a 10 KW load, however a power factor (pf) of 0.98 is applied to account for the possibility of inductive elements in the load.

$$V = 240\ VAC \tag{2.22}$$

$$P = 10\ KW \tag{2.23}$$

$$\sigma = 11.4° \tag{2.24}$$

$$S = \frac{P}{\cos\sigma} \tag{2.25}$$

$$Z = \frac{V^2}{S} \tag{2.26}$$

$$R = Z\cos\sigma = 5.56\ Ohms \tag{2.27}$$

$$X = Z\sin\sigma \tag{2.28}$$

$$L = \frac{X}{2\pi f} = 3.0\ mH \tag{2.29}$$

The use of a 10KW load and a power factor that is close to 1 is assumed to be representative of a standard residential load profile. Additionally, it is assumed that the residential 120 VRMS

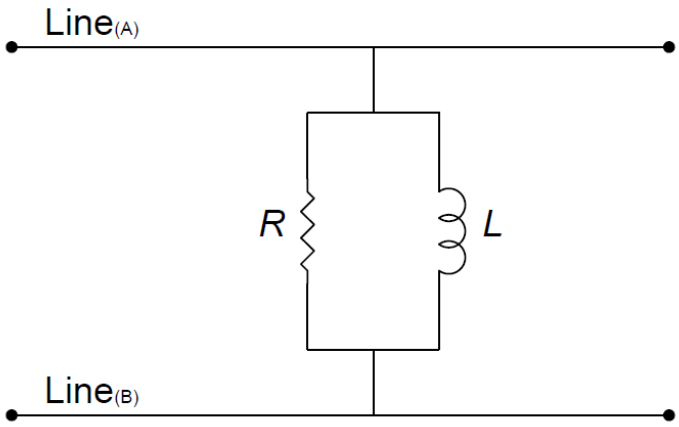

Figure 2.7 Standard Load Schematic

loads are balanced such that they can be simulated by applying the 240 VRMS load directly from phase to phase. All loads applied to the grid are assumed to be the same. These assumptions simplify the simulation without compromising the fidelity of simulation results.

2.3 Conclusion

This chapter presented the design of the system under study, and a number of the key system parameters. These parameters are consistent with the parameters that would be expected to be observed in a physical mockup of this electrical system. These parameters are summarized in Table 2.1.

Table 2.1 Key System Parameters

Voltage Sources			
$v_{rms\ grid}$	240 VRMS	f_{grid}	60 Hz
$V_{DC\ photovoltaic}$	600 VDC		
Grid and Inverter Output Voltage Waveforms			
v_{grid}	$339.4\sin(2\pi 60t)$	v_{inv}	$339.4\sin(2\pi 60t-\delta)$
Inverter Output Filter			
$L_{1\ Output\ Filter}$	2 mH	$L_{2\ Output\ Filter}$	1 mH
$R_{H\ Output\ Filter}$	1 x 10^{16} Ohm	$R_{L\ Output\ Filter}$	1 Ohm
$C_{\ Output\ Filter}$	50 uF	f_R	0.41 KHz
f_{PWM}	2.5 KHz	$\frac{f_R}{f_{PWM}}$	0.164
Line Impedance			
L_{feeder}	0.1 mH	L_{grid}	0.5 mH
$Z\angle(\theta_i)_{feeder}$	$0.1884 + j0.0377\ Ohms$	$Z\angle(\theta_g)_{grid}$	$0.1184 + j0.1885\ Ohms$
$\frac{R_{feeder}}{X_{feeder}}$	5	$\frac{R_{grid}}{X_{grid}}$	1
θ_i	11.3°	θ_g	57.9°
Loads			
L_{Load}	3 mH	R_{Load}	5.56 Ohms
P_{Load}	10 KW	Q_{Load}	2 KVAR
S_{Load}	10.2 KVA	σ	11.4°

Chapter 3 - Single-Phase Inverter Operation

3.1 Introduction

The purpose of this chapter is to present the design details of a power electronic inverter with the purpose of injecting power from a photovoltaic array into a low voltage grid distribution system.

A unique characteristic of many distributed generation systems is the fact that these power sources tie-in to low voltage grid distribution lines. Traditional large centralized power generators are normally tied-in to high and medium voltage transmission lines. Additionally, central generators typically provide three phase power, while smaller distributed generators, such as roof top photovoltaic arrays, may only provide single phase power. Residential photovoltaic systems must be able to inject power into the grid via the single-phase distribution lines that power homes.

Many inverter designs exist or have been proposed to accomplish this purpose. This chapter presents a single-phase inverter design that supports single phase power conversion and can operate in both the maximum power point tracking (MPPT) mode, as well as the droop control mode.

This chapter will present the basic building blocks of the power inverter and provided a basic level of explanation for their function (Figure 3.1). These building blocks are largely based on the research of others. References to the work of others is provided throughout the chapter in order for the reader to gain a deeper understanding of these components.

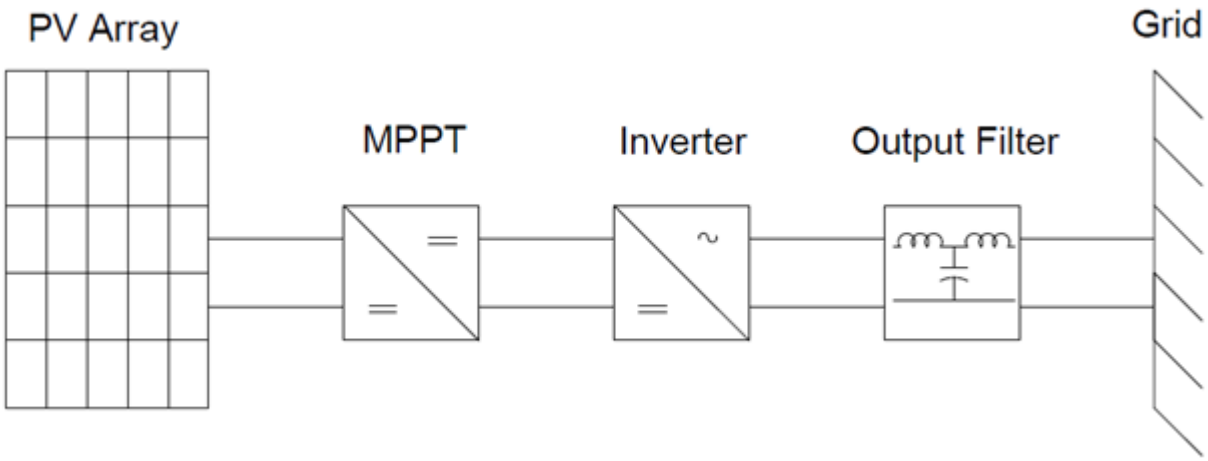

Figure 3.1 Typical Roof Top Mounted Photovoltaic Array and Grid Integration Functions Block Diagram

3.2 Single-Phase inverter operation

A single-phase inverter is a power electronic component designed to convert DC electrical power from a local generator (such as a photovoltaic array) to grid synchronized AC electrical power, and to maximize power transfer from the DC source to the grid. Traditional inverters for photovoltaic application employ two power electronic stages to complete these tasks [10] [11] [12] [13]. The first stage maximizes photovoltaic power output by establishing the output voltage consistent with the maximum power point. The second stage converts this DC output voltage to AC current and establishes voltage and phase characteristics necessary to transfer power to the grid. A DC link provides stability and isolation between each of these stages. An output filter reduces harmonic injection to the grid by smoothing the high frequency switching perturbations carried by the low frequency output waveform. Each of these stages and features are discussed below (Figure 3.2).

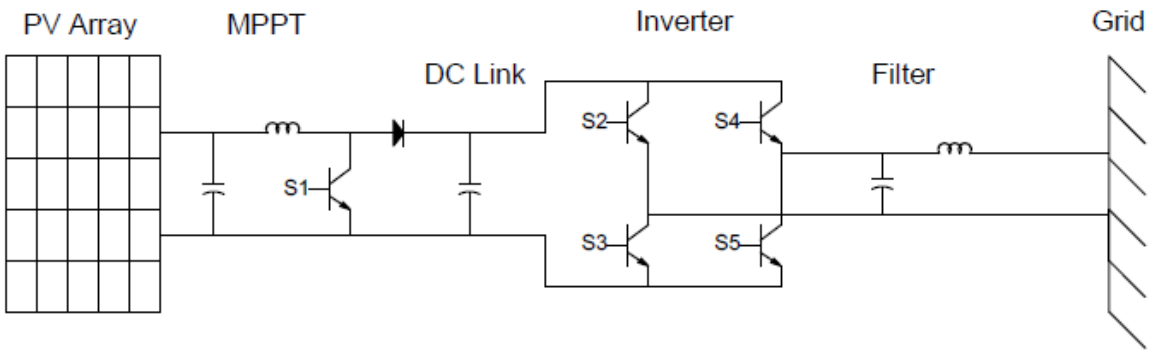

Figure 3.2 Single Phase Schematic Diagram

3.3 Maximizing Photovoltaic Power Output (Maximum Power Point Tracking)

In order to understand how to maximize photovoltaic output, a basic understanding of the function of a photovoltaic cell is required. A thorough discussion of photovoltaic cell operation is provided in [14] and summarized here. A solar cell can be seen as a current source driven by the sun. The amount of "insolation" or sun intensity at the surface of the solar cell establishes the amount of current that can be generated. Under short circuit conditions the amount of current that can be generated is finite, and dependent on the characteristic of the solar cell. As an increasing load is applied, the associated voltage drop affects the current profile as shown in Figure 3.3 (a). This figure shows that there is a limiting voltage drop that can be applied, at which point the PV effect is overcome and current falls to 0. Taking the integral of Figure 3.3 (a) produces the power to voltage relationship shown in Figure 3.3 (b). This relationship makes it apparent that each photocell has a single maximum power point of operation.

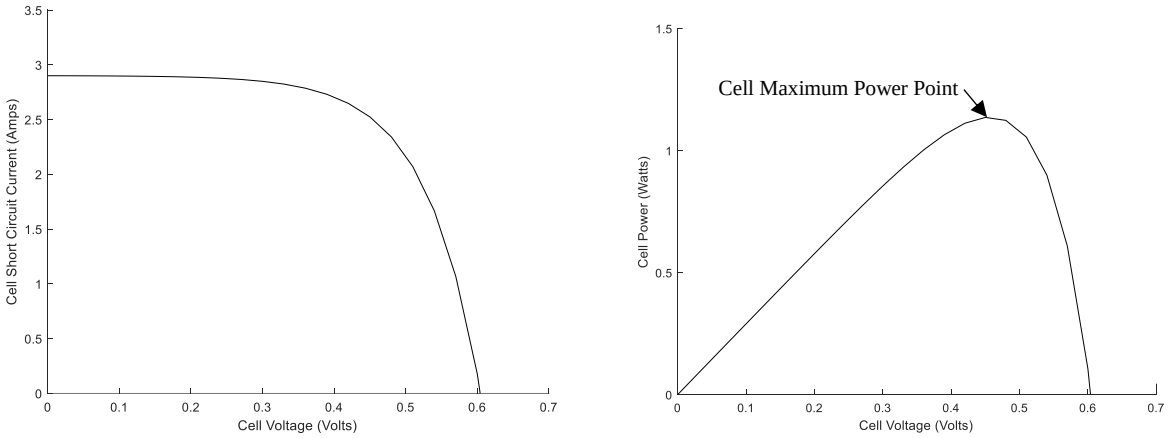

(a) (b)

Figure 3.3 Properties of a photovoltaic cell under various conditions of Irradiation. (a) Relationship of voltage and current of a single solar cell. (b) Relationship of power and voltage of a single solar cell.

Because of this relationship between voltage across a load and photovoltaic current, only a single load profile will maximize the power output of the solar cell. In a practical photovoltaic system, many solar cells are connected in series to create solar panels. The solar panels are then connected in parallel to form the system. Using an algorithm to determine the maximum power point of the photovoltaic system under the given conditions of temperature and illumination, a simulated load can be applied by adjusting the voltage across the solar panels using a boost converter [15]. The boost converter must seek the "Maximum Power Point" of the solar panel and adjust voltage as necessary to maximize system current output. Using a boost converter in this way is called "maximum power point tracking". Thus, the first stage of the photovoltaic inverter is a DC to DC stage in which voltage is adjusted to obtain the maximum power point of the photovoltaic system (see Figure 3.2).

Power from the maximum power point tracking DC DC converter is stored in a capacitor, called a DC link, for use by the inversion stage of the photovoltaic inverter (Figure 3.4).

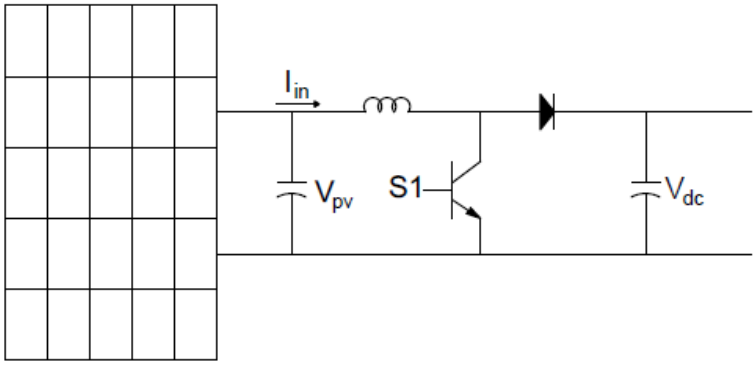

Figure 3.4 Maximum Power Point Tracking Circuit with DC Link at Output [16]

3.4 Transferring Power to the Grid (Inversion and Filtering)

Power stored in the DC link on the output of the maximum power point DC DC boost converter is transferred to the grid via a full bridge converter. The full bridge converter requires a stable DC voltage source for an input. This function is performed by the DC link. The DC link is a capacitor that stores the energy from the maximum power point tracker and establishes a reference voltage. This reference voltage may vary with variations in the maximum power point caused by changes in temperature and irradiation. Therefore, the inversion stage must be able to accommodate variations in input voltage. Since variations in temperature and irradiation are not expected to occur rapidly, the high switching frequency required to enable DC inversion should be sufficient in all cases to adequately respond to the resulting input voltage variations.

DC power inversion is achieved by a standard full bridge (also referred to in literature as a H-bridge) inverter (Figure 3.5). Though a variety of topographies have been proposed for performing inversion, the full bridge inverter is commonly used for its simplicity of design, range of operation, and relatively high efficiency.

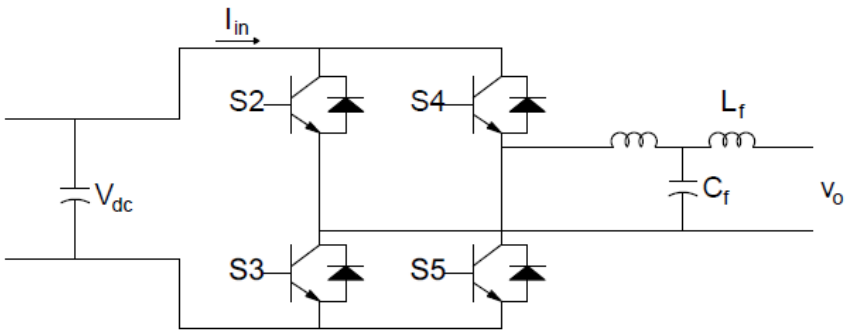

Figure 3.5 Standard Full Bridge Inverter and Output Filter

3.4.1 Full Bridge Inverter

The full bridge inverter functions by rapid operation of semiconductor switches. These switches are usually implemented as metal oxide semiconductor field effect transistors (MOSFETs) but may also be integrated gate bipolar junction transistors (IGBTs) or bipolar transistors, depending on the intended voltages. The switches operate in pairs, with switch S3 and S4 going shut to establish positive voltage at the output, and switches S2 and S5 going shut to establish negative voltage at the output. It is important that both pairs of switches do not ever operate at the same time since that would result in a short circuit. The diodes operate in parallel with the switch to allow effective bi-directional current flow through the switch. Though current is not ever expected to flow in the opposite direction of the transistor due to the voltage imposed by the circuit across the switch, in practice large instantaneous voltages are known to develop across the switch at turn off, due to the semiconductor properties of the switch. The diodes provide a current shunt path to dissipate these shutoff voltages prior to the switch ratings being exceeded. Because the voltage applied by the full bridge is instantaneously equal to either Vdc or -Vdc (the DC link voltage), it is necessary to store electrical energy to provide the average voltage and current profile to the grid. This is achieved by the output filter.

3.4.2 Output Filter

The output filter consists of an inductor, a capacitor and an inductor. In steady state, the current across the first inductor (i_{output}) rises when the instantaneous output voltage (v_{output}) is positive. The current across the inductor falls when the instantaneous output voltage is

negative. The average charge is stored in the capacitor which establishes a stable AC voltage profile for the grid. The second inductor ensures that rapid fluctuations in current are not propagated to the loads. A properly sized output filter is essential to reduce the total harmonic distortion and establish a stable AC voltage source before the point of common connection with the grid.

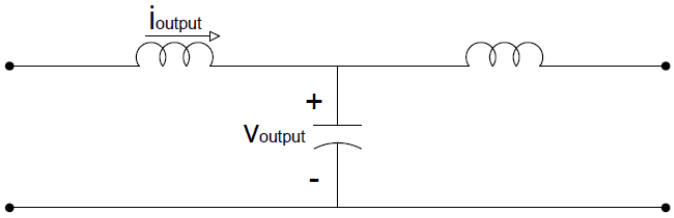

Figure 3.6 Typical LCL Inverter Output Filter

3.4.3 Pulsewidth Modulation

The driver for the switches is a high frequency pulse width modulation (PWM) control circuit [16]. This circuit implements step changes in voltage to achieve average voltage and current properties of the grid at the point of common connection. The duration over which the instantaneous output voltage completes a single positive and negative cycle is referred to as the period (Ts). The period is constant and is a feature of the pulsewidth modulator design. The ratio of the duration (D) of the positive voltage to the period is referred to as the duty cycle (Ds) (Figure 3.7).

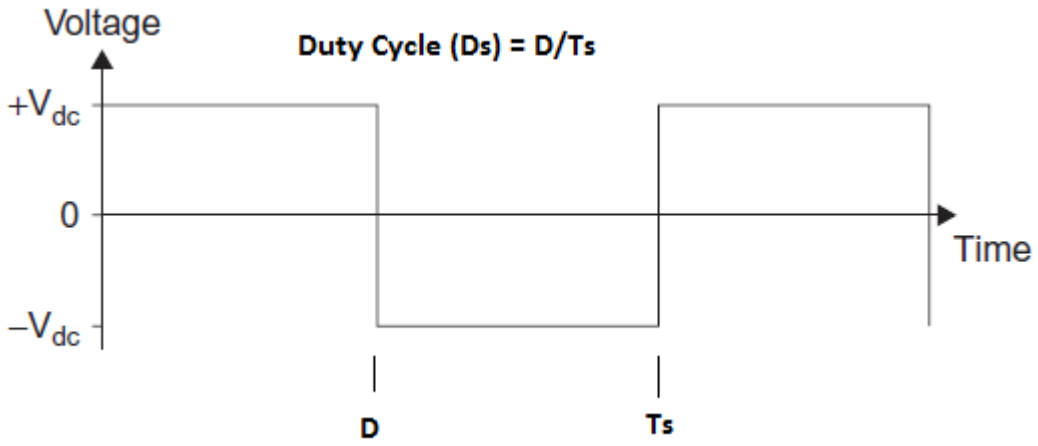

Figure 3.7 Instantaneous High Frequency Output of Full Bridge Circuit

During the positive portion of a 60 Hz AC sinewave the duty cycle is greater than 0.5. During the negative portion of a 60 Hz AC sinewave the duty cycle is less than 0.5. This can be understood when looking at the voltage across the filter inductor v_L. During the positive partial period (D) the voltage across the inductor is given in (3.1).

$$v_L = V_{dc} - v_C \tag{3.1}$$

Where v_C is the instantaneous voltage of the filter capacitor. During the negative partial period ($Ts - D$), the voltage across the inductor is given in (3.2)

$$v_L = -(V_{dc} + v_C) \tag{3.2}$$

The average voltage across the inductor during any given period can be given by (3.3)

$$v_L = D(V_{dc} - v_C) - (Ts - D)(V_{dc} + v_C) \tag{3.3}$$

Though the current through the inductor rises and falls with every operation of the full bridge switches, if the duty cycle is greater than 0.5 the inductor current increases. If the duty cycle is less than 0.5 the voltage across the inductor current decreases (3.4).

$$v_L = L\frac{di_L}{dt} \tag{3.4}$$

Thus, the average output voltage and rate of change of inductor current will increase or decrease based on the duty cycle. To achieve an AC output waveform, the duty cycle must vary proportional to the desired output waveform. Therefore, the reference signal supplied to the pulsewidth modulator must be proportional to the desired output waveform (Figure 3.8).

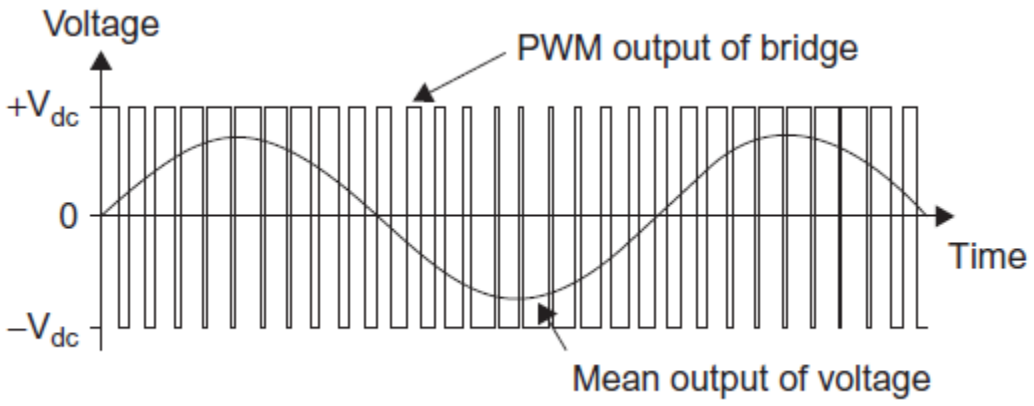

Figure 3.8 Voltage Profile on Filter Input, and Approximated Voltage Profile on Filter Output

3.4.4 Grid Isolation (Isolation Transformer)

Equally important to providing clean power to the grid is the importance of preventing ground loop leakage between the grid and the distributed generator. This loop leakage is possible due to parasitic capacitance in the photovoltaic inverter and at the point of common connection. Ground leakage current not only reduces the efficiency of the distributed generator but also poses threats to both equipment and personnel safety. A transformer is required to provide electrical isolation between the grid and distributed generation ground loops. Two common methods of transformer implementation include a high frequency transformer within the photovoltaic inverter, or a low frequency transformer after the output filter (Figure 3.9). A benefit of the high frequency transformer is the smaller size. A benefit of the low frequency transformer is less complexity to implement.

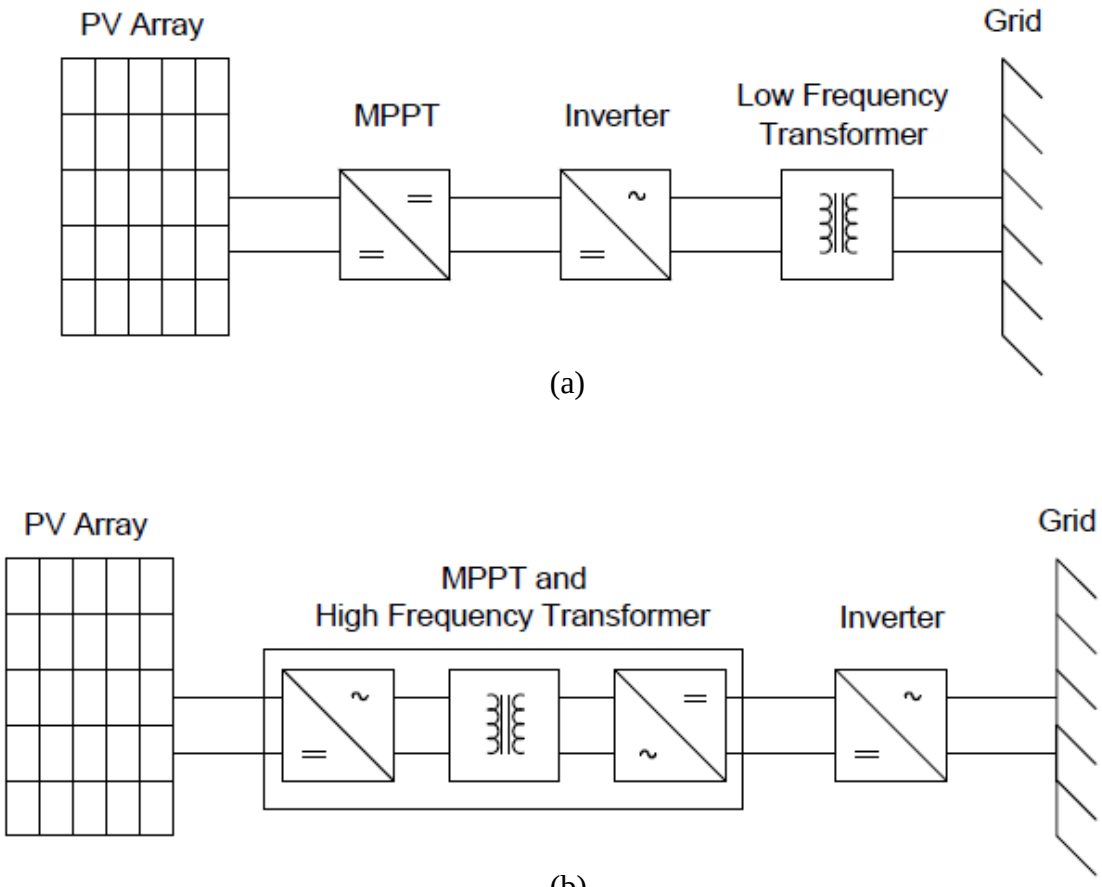

Figure 3.9 Grid Isolation Implemented via Low Frequency Transformer (a), and Implemented via High Frequency Transformer (b), [16]

3.5 Control Functions

Over the past decades several methods of controlling power electronic converters have been explored. One of the first considerations to be made is with regard to the type of power source that supplies the converter. A voltage source converter is supplied by a stable voltage, regardless of fluctuations in current. A current source converter is supplied by a stable current, regardless of fluctuations in voltage.

1. The maximum power point tracker can be implemented as either a voltage source or current source converter, by placing either a capacitor or an inductor before the

transistors. If the photovoltaic array is placed directly in line with the maximum power point tracker, the tracker will function as a current source converter since photocells function as current sources.

2. The full bridge inverter is implemented as a voltage source inverter when a DC link capacitor is used to supply input power.

A second consideration when selecting a control methodology is to determine whether the converter will be controlling voltage or current. A current controller is a control system that regulates output current, regardless of output voltage. A voltage controller is a control system that regulates output voltage, regardless of output current.

1. The maximum power point tracker must be implemented as a voltage controller since the function of the maximum power point tracker is to establish the optimal voltage across the photovoltaic array.

2. The full bridge inverter operating in grid feeding mode must be implemented as a current controller since its function is to inject current into the grid to ensure full utilization of the distributed generator. A full bridge inverter operating in grid forming mode (such as a universal power supply (UPS)) must be implemented as a voltage controller. Grid supporting inverters may operate as either a current or voltage controller, depending on the control method selected, in order to help regulate the grid voltage and phase angle [4].

A third consideration is whether the input and output parameters are AC or DC. A converter that receives AC power on the input and produces DC output power (AC DC converter) is called a rectifier. A converter that receives DC power on the input and produces DC output power (DC DC converter) is called a DC DC converter. A converter that receives DC power on the input and produces AC output power (DC AC converter) is called an inverter. A converter that receives AC power on the input and produces AC output power (AC AC converter) is called a transformer.

Unless special waveforms are required, transformers will not usually be implemented by means of power electronics.

1. The maximum power point tracker is a DC DC converter.

2. The full bridge inverter is a DC AC converter.

The method of control is hierarchal as discussed in [17]. At the lowest level a control signal is tracked by the pulse width modulator to drive the output current waveform. This is called the modulation level. The control signal is provided by the next higher level called the current or voltage control level. The maximum power point tracker only requires two levels of control to achieve DC boost conversion. The full bridge inverter, however, has more levels of control, depending on the application, as will be discussed.

3.6 Maximum Power Point Tracker Control Functions

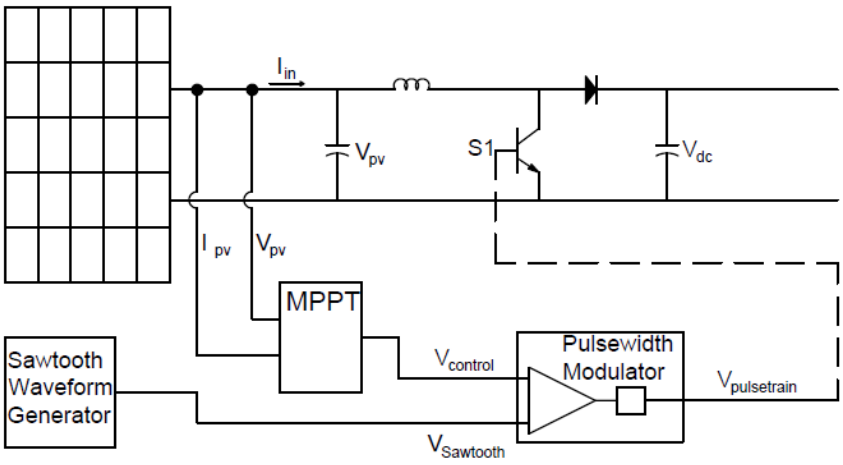

Figure 3.10 MPPT Boost Converter with Control System Block Diagram

The maximum power point tracker is implemented as a current source voltage regulating DC DC converter. The parameters of the solar array and the parameters of the DC link output are

measured at voltage control level to establish the modulation control signal. The modulation control signal is applied to the pulsewidth modulator to generate a pulse train. The pulse train is used to control the switch of the MPPT boost converter.

3.6.1 Voltage Control Level

At the voltage control level, PV output voltage and current are measured to determine output power. This output power is compared to a maximum power point reference signal to generate an error signal. The error signal is passed through a proportional integral (PI) controller and provided as the modulating control signal for the pulse width modulator.

The PI controller generates the control signal ($E_{control}$) by multiplying the error signal (E_{error})by a gain factor (K_P) and integrating the error over time using the integrating constant (K_I), then summing the results (Figure 3.11).

The proportional part of the PI controller provides two major functions:

1. The proportional element provides the gain necessary to maximize use of the full band of the sawtooth waveform.

2. The proportional element ensures adequate controller response to minimize high frequency errors.

The integral part of the PI controller provides two similar functions:

1. The integral element provides a non-zero signal to the comparator needed to maintain steady state switching while the instantaneous error is at zero.

2. The integral element ensures adequate controller response to minimize low frequency errors.

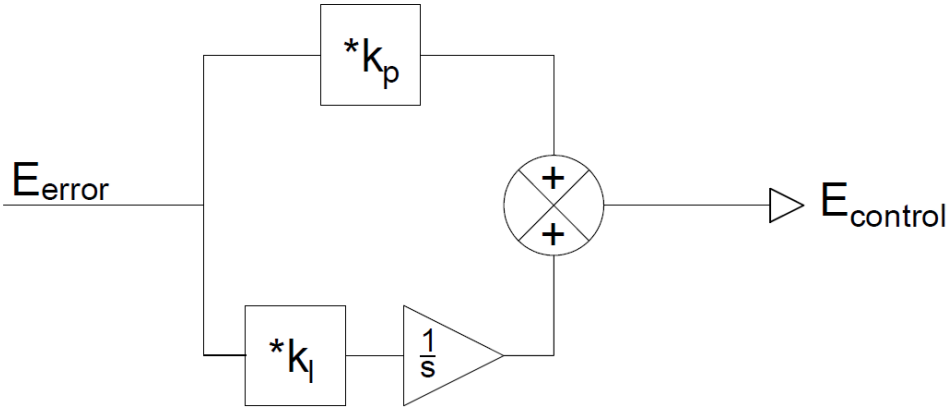

Figure 3.11 Block diagram of a PI controller

The PI controller must be tuned for the application in which it is used. Tuning is accomplished by adjusting the gain (k_P) and the time constant (k_I). A high gain equates to a higher response magnitude. If the gain is too high the controller will become unstable and unable to achieve steady state. Adjusting the gain will directly affect the amount of system overshoot of the reference signal. A high time constant equates to a longer response time. If the time constant is too large the control signal will be unable to track rapid system changes. If the time constant is too small, the control signal will overshoot the reference signal and may be unable to stabilize. Adjusting the time constant will directly affect the slope of the system response signal.

The maximum power point reference signal may be generated using a variety of methods which will not be covered in this work (see reference [18] chapter 24). One of the most commonly recognized methods is the 'Perturb and Observe' method. This simple method causes periodic perturbations in the duty cycle of the pulsewidth modulator. The controller recognizes the response from these perturbations as negative or positive error when compared to the previous output power, and responds by raising or lowering the reference signal, respectively. This tracking method is popular for its simplicity and generally continuous efficiency and

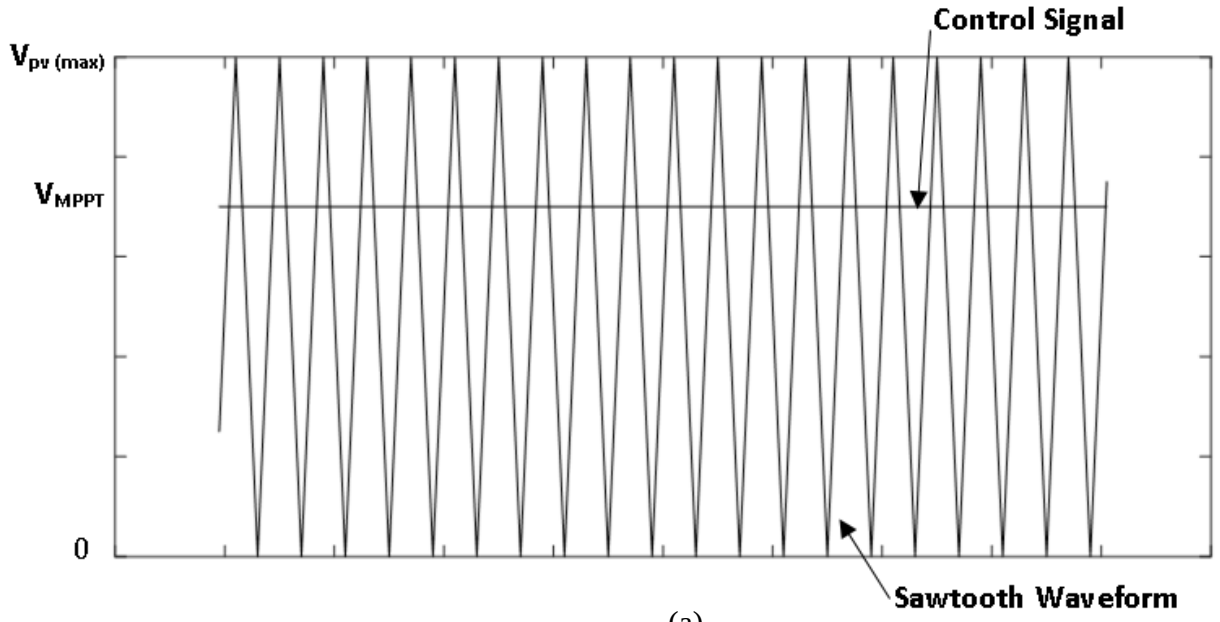

(a)

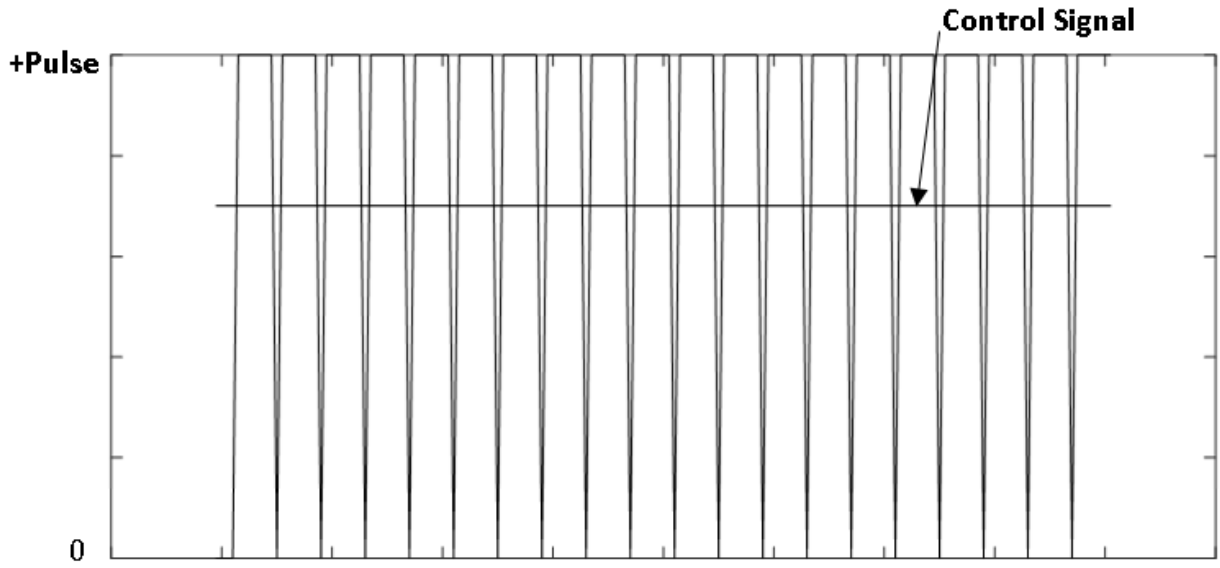

(b)

Figure 3.12 Reference Signal Provided to the Pulsewidth Modulator (Control Signal), Transposed on the Sawtooth Waveform (a); Control Signal Transposed on the Resulting Pulse Train at the Output of the Pulsewidth Modulator (b)

accuracy. This tracking method is known to fall short during rapidly changing atmospheric conditions due to its low tracking speed.

3.6.2 Modulation Level

In the modulation level, the control signal is fed into a high frequency comparator circuit (pulsewidth modulator) to generate the pulses that drive the switches. The control signal establishes the duty cycle which establishes an average voltage output value. Unlike AC pulsewidth modulation, the control signal is a DC value. This DC value operates between 0 and the Maximum voltage for the PV array. The high frequency sawtooth waveform operates between 0 and a value greater than or equal to V_{pv}. A single pulse train results, producing an average voltage that is proportional to the reference signal.

3.7 Full Bridge Inverter Control Functions

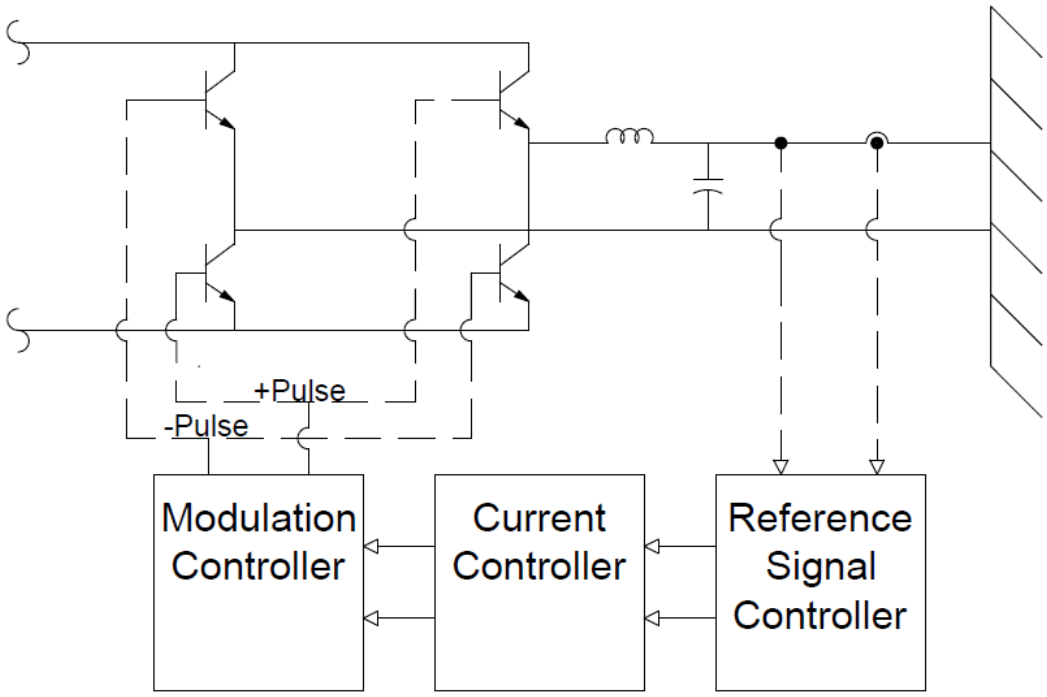

Figure 3.13 Block Diagram of the Full Bridge Voltage Source Current Regulating Inverter Control System

The full bridge inverter is implemented as a voltage source current regulating inverter. The basic block diagram for this type of inverter is shown in Figure 3.13. A sophisticated controller is required to drive the full bridge. Though many methods of implementing control loops are possible, some common methods are discussed here. The full bridge inverter, like the maximum power point tracker, uses a hierarchal control structure. This structure consists of three levels with the highest level being the reference signal control level. The reference signals are fed into the current and voltage control level along with the inverter output voltage and current waveforms. These are compared in order to establish the desired modulation control signal. In the modulation level the current control signal is compared to a sawtooth waveform to establish the gate firing pulsetrain to operate the full bridge converter.

3.7.1 Modulation Level

Modulation is accomplished by a comparator which compares a reference signal to a sawtooth pulse train. These components are common to both the maximum power point control loop and the full bridge inverter control loop. However, additional considerations exist when performing pulsewidth modulation on an AC signal. For example, the period of the sawtooth waveform must be chosen to meet the following objectives.

1. The frequency of the sawtooth waveform is sufficiently high that a large gap exists between the fundamental harmonic and the pulse switching harmonics to allow ease of harmonic discrimination.

2. The period of the sawtooth waveform is sufficiently short that the modulating signal appears as a constant signal, even though lower frequency variations exist in the modulating signal waveform. This will prevent the comparator from experiencing the case in which fluctuations in the modulating signal waveform result in multiple crossings of the sawtooth waveform within the same period.

3. The period of the sawtooth waveform must be long enough to minimize switch operation and the associated losses.

4. When using simulation software, the period must be long enough that the processing speed of the software can properly identify each modulating signal crossing with sufficient accuracy to produce time variant waveform

In order to generate an AC waveform, the shape of the control signal should be proportional to the intended output voltage waveform.

A practical method to implement AC modulation is to use two comparators and two pulse generators. One set to handle the positive half cycle of the modulating signal, and one to handle the negative half cycle of the modulating signal. During modulation of the positive half cycle of the control signal, the comparator outputs pulses at the frequency of the sawtooth waveform. When the modulating signal is close to zero the duration of the high pulse (D) is short within the period. As the modulating signal approaches the peak value the duration of the high pulse (D) is longer within the period. The pulses are supplied as the firing pulses for the pair of full bridge thyristors associated with the positive direction of current flow. Thus a conventional buck converter circuit is established that generates an oscillating output waveform from zero to maximum (I_{max}) and back to zero with the average instantaneous value (I_{avg}) of the waveform equal to (3.5).

$$I_{avg} = I_{max}\, D \tag{3.5}$$

During modulation of the negative half cycle of the modulating signal, the other comparator outputs pulses at the frequency of the sawtooth waveform. When the modulating signal is close to zero the duration of the high pulse (D) is short within the period. As the modulating signal approaches the peak negative value the duration of the high pulse (D) is longer within the period. The pulses are supplied as the firing pulses for the pair of full bridge thyristors associated with the negative direction of current flow. The same buck converter circuit is established and operated in the opposite direction.

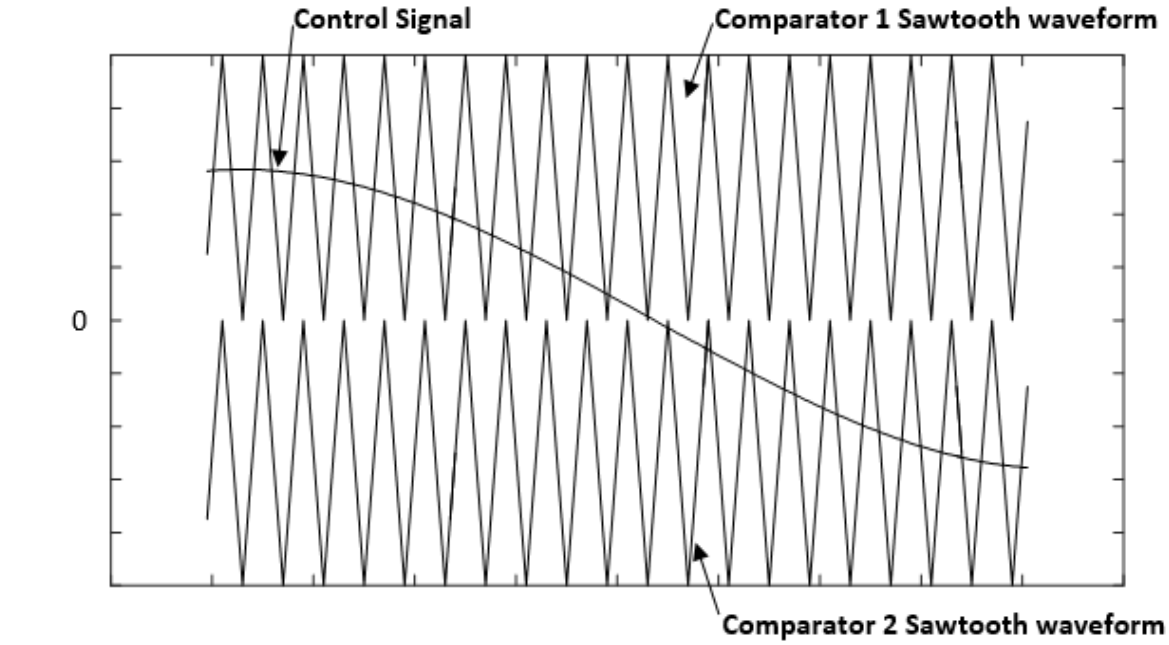

(a)

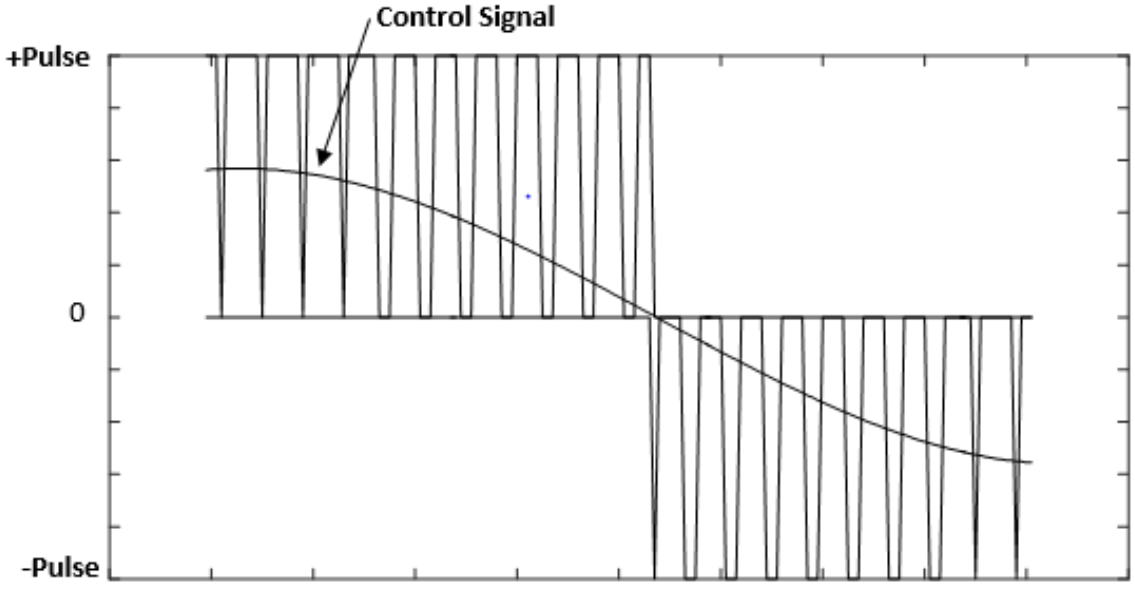

(b)

Figure 3.14 Two Comparator Method: Control Signal Provided to the Pulsewidth Modulator, Transposed on the Sawtooth Waveform (a); Control Signal Transposed on the Resulting Pulse Train at the Output of the Pulsewidth Modulator (b)

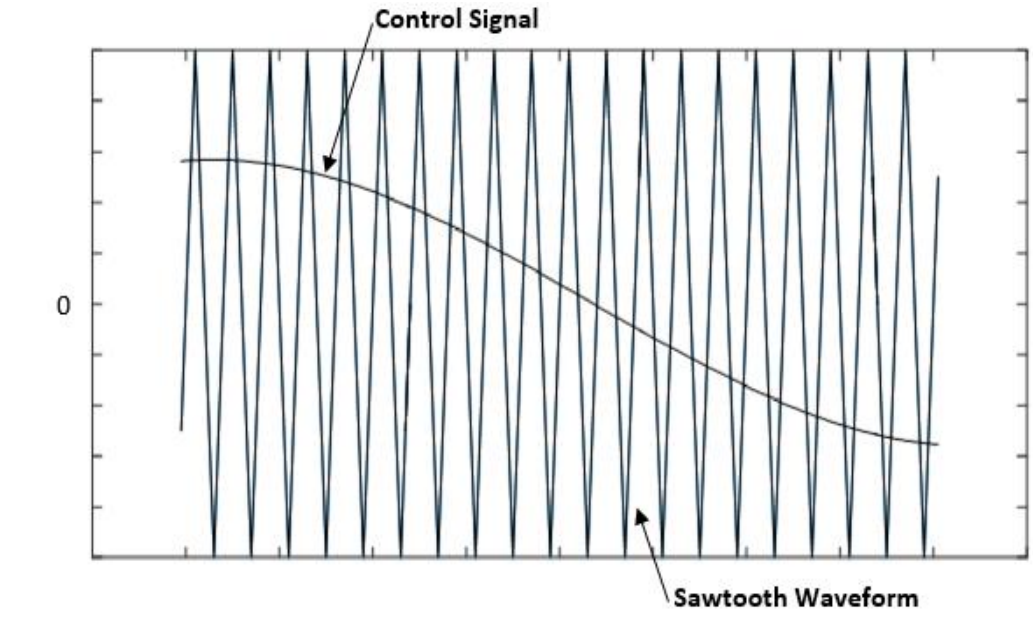

(a)

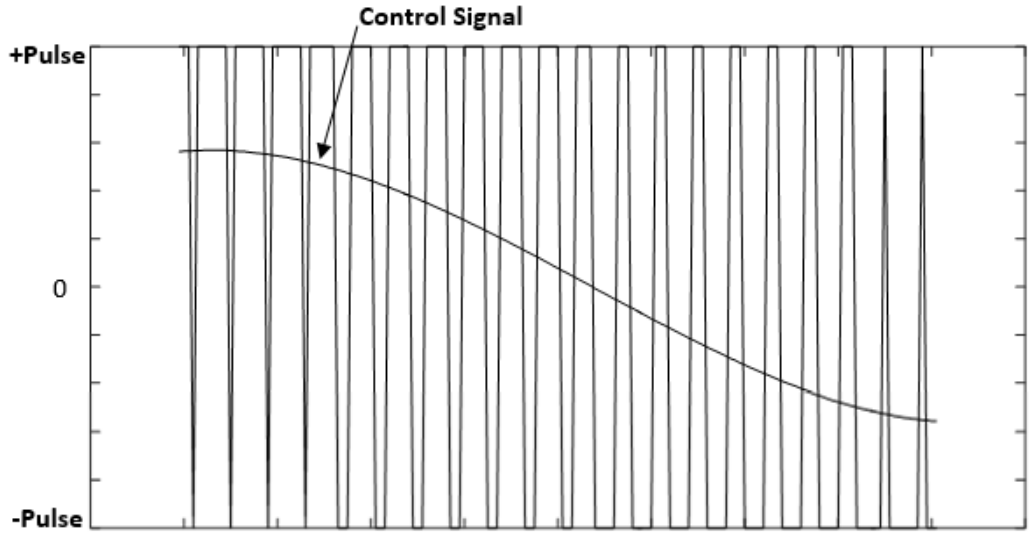

(b)

Figure 3.15 Single Comparator Method: Control Signal Provided to the Pulsewidth Modulator, Transposed on the Sawtooth Waveform (a); Control Signal Transposed on the Resulting Pulse Train at the Output of the Pulsewidth Modulator (b)

An alternative to this method is to use a single comparator to evaluate the entire control signal waveform during both positive and negative half cycles. In this case the sawtooth waveform must operate from the maximum to the minimum possible output value. The principle of operation is the same as previously described, however both the positive switch pulse and the negative switch pulse are provided during each period, and during both the positive and negative half cycle. This method maximizes the accuracy of the output signal, but also requires more switch operations and larger passive components to handle the larger power variations that are experienced. In this case the average voltage v_{avg} imposed on the output filter by the inverter during any given period can be represented by the following equation.

$$v_{avg} = 2(V_{dc})\, D - V_{dc} \tag{3.6}$$

3.7.2 Current and Voltage Control Level

Since the sensed parameters in the current regulating inverter are AC signals, using PI controllers, like the one used in the maximum power point tracker (Figure 3.11), is not the best option for generating an error signal. The PI controller uses a fixed gain and time interval when performing the proportional and integral conversions. Though a fixed gain and time interval work well when the sensed parameter is DC and provide a steady control point to the pulse width modulator, they do not work well with continuously varying AC error signals. Specifically, the effect of the gain is greatest during zero crossings of the fundamental frequency. In consequence of this fact, this control method is subject to error in the phase and amplitude. These errors constitute error in the fundamental output waveform and are called steady state errors. A common method to achieve zero steady state error in AC controllers is to convert the AC signals to equivalent DC reference signals by transposing the sensed AC parameters to the synchronous rotating frame [19] [20].

The synchronous rotating frame controller performs a d-q transformation of the sensed current signal, where d and q represent the direct and quadrature attributes of the AC signal. The d-q attributes of the sensed AC current are DC values. Since a pure sine wave can be defined by two constants, a real AC signal can be defined also by two DC values. The transformation is performed mathematically, usually by a microprocessor. In a three phase system the required

input parameters are each of the phase currents (i_a, i_b *and* i_c) and phase (ωt). Though phase cannot be directly measured, it can be generated using a phased locked loop. From this information, the current waveforms of a three phase system can be defined mathematically using the standard notation shown in (3.7).

$$i_a = A\sin(\omega t) \tag{3.7}$$

$$i_b = A\sin(\omega t + \frac{2\pi}{3}) \tag{3.8}$$

$$i_c = A\sin(\omega t - \frac{2\pi}{3}) \tag{3.9}$$

With these parameters defined, the current signals can be converted into the synchronous rotating frame where they become the DC values i_d, i_q and i_0. These values represent the direct (i_d) and quadrature (i_q) elements of the signal, and the plane of reference (i_0)This conversion is discussed in [21] and shown in (3.10).

$$\begin{bmatrix} i_d \\ i_q \\ i_0 \end{bmatrix} = \frac{2}{3}\begin{bmatrix} cos(\omega t) & cos(\omega t - \frac{2\pi}{3}) & cos(\omega t + \frac{2\pi}{3}) \\ sin(\omega t) & sin(\omega t - \frac{2\pi}{3}) & sin(\omega t + \frac{2\pi}{3}) \\ \frac{1}{2} & \frac{1}{2} & \frac{1}{2} \end{bmatrix}\begin{bmatrix} i_a \\ i_b \\ i_c \end{bmatrix} \tag{3.10}$$

Since the current signals will ultimately need to be transformed back to the stationary reference frame, the inverse conversion is presented in (3.11).

$$\begin{bmatrix} i_a \\ i_b \\ i_c \end{bmatrix} = \begin{bmatrix} cos(\omega t) & sin(\omega t) & 1 \\ cos(\omega t - \frac{2\pi}{3}) & sin(\omega t - \frac{2\pi}{3}) & 1 \\ cos(\omega t + \frac{2\pi}{3}) & cos(\omega t + \frac{2\pi}{3}) & 1 \end{bmatrix}\begin{bmatrix} i_d \\ i_q \\ i_0 \end{bmatrix} \tag{3.11}$$

Once the sensed current signals are transformed to the d-q reference frame they become DC signals. They can then be compared to reference DC signals, generated at the current control level, to generate a DC error signal. A PI converter can then be used in the same way as the maximum power point tracker to generate a modulating control signal. This DC modulating control signal must then be transformed back to AC via an inverse d-q transformation 3.11. The

AC signal undergoes pulse width modulation to generate the firing signals for the full bridge thyristors.

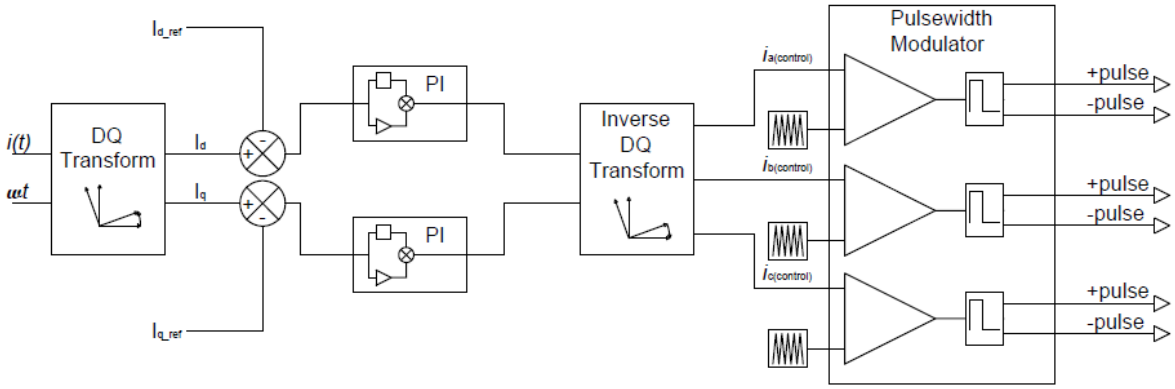

Figure 3.16 Three Phase d-q Synchronous Rotating Frame PI Controller

Obviously the calculations presented in 3.10 and 3.11 will not support a single phase inverter in which only a single current phase is sensed. To overcome this, an equivalent control methodology is developed in [22] and modified in [23], [24], and [25]. Use of a rotating frame transformation requires that a least two orthogonal waveforms are present. Since a single phase system has only one current waveform, a second imaginary waveform is defined. The imaginary waveform (i_i) is generated by delaying the sensed current waveform (i_r) by one quarter period. A sample and delay register can be used to perform this function. The two waveforms can then be defined mathematically equivalent to (3.12) and (3.13), as follows.

$$i_r = A\sin(\omega t) \tag{3.12}$$

$$i_i = A\sin\left(\omega t - \frac{\pi}{2}\right) = -A\cos(\omega t) \tag{3.13}$$

A simplification of the transformations presented in (3.10) and (3.11) can now be applied. The stationary to d-q rotating reference frame transformation is presented in (3.14). The d-q rotating reference frame back to stationary reference frame transformation is presented in (3.15).

$$\begin{bmatrix} i_d \\ i_q \end{bmatrix} = \begin{bmatrix} \sin(\omega t) & -\cos(\omega t) \\ \cos(\omega t) & \sin(\omega t) \end{bmatrix} \begin{bmatrix} i_r \\ i_i \end{bmatrix} \quad (3.14)$$

$$\begin{bmatrix} i_r \\ i_i \end{bmatrix} = \begin{bmatrix} \sin(\omega t) & \cos(\omega t) \\ -\cos(\omega t) & \sin(\omega t) \end{bmatrix} \begin{bmatrix} i_d \\ i_q \end{bmatrix} \quad (3.15)$$

Once the *d* and *q* components of the single phase current and voltage are realized, reference signals can be generated using setpoint comparators and PI controllers.

The function of the current and voltage control level of the full bridge controller is to compare a reference signal at the input with the sensed signal in order to determine system error, and generate a corrected reference signal at the output. The reference signal at the input is developed dependent on the intended function of the inverter. In the case of a photovoltaic grid feeding inverter, the function is to export as much current as possible, without causing disturbances or distortion to the power grid. Since the sensed signals are converted to i_d, i_q, v_d and v_q, a reference setpoint must be identified for each of these parameters.

3.8 Reference Signals

In order to control grid parameters, reference signals must be developed for this purpose. Multiple methods exist for managing power flow from a grid feeding inverter. This paper will present a method that can be built upon for performing grid supporting functions as well.

3.8.1 Power Reference Signals

To achieve power control, the system must be able to detect output power. This can be accomplished by measuring inverter output current (*i*) and voltage (*v*). From these parameters, both a real (*P*) and a reactive (*Q*) power value can be determined.

$$P = (vi)\cos(\theta) \quad (3.16)$$

$$Q = (vi)\sin(\theta) \quad (3.17)$$

$$\theta = \cos^{-1}(pf) \quad (3.18)$$

$$pf = \frac{X}{R} \quad (3.19)$$

In these equations the power angle (θ) is measured directly by measuring the angle between the current (i) and voltage (v) waveforms. If the system reactance (X) and resistance (R) were known they could be used to calculate the power factor (pf), from which the phase angle could also be determined.

Since power is a DC value, it can be fed directly into comparators with real and reactive power reference signals. The real power reference signal (P_{ref}) can be inferred from the MPPT. The reactive power reference signal (Q_{ref}) can be assumed to be 0 for a grid feeding inverter. This is because the inverter is not intended to perform grid supporting functions, and therefore should not be providing compensating waveforms. Thus, reactive power will be provided to the loads only by the grid in this case.

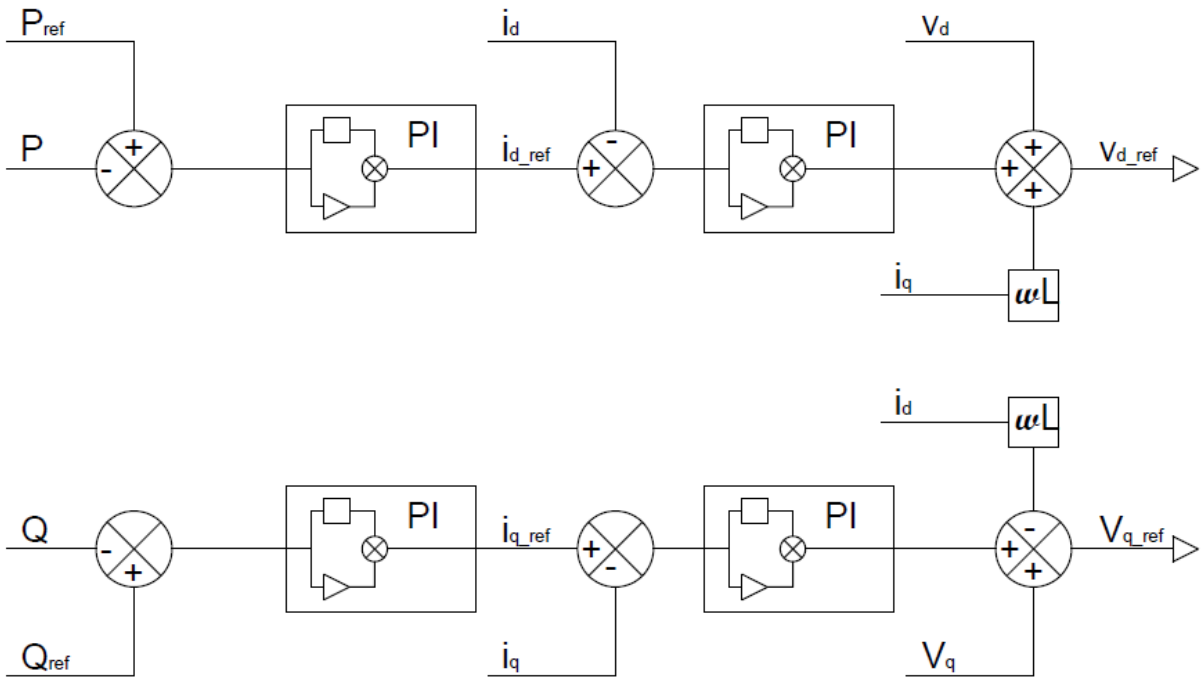

Figure 3.17 Power Signal Comparators and Control Signal Generation

The two error signals, generated by these comparators are then each passed through PI controllers, turning them into reference signals for the direct (d) and quadrature (q)

components of the current signal. This enables the changes in power from the reference point to result in changes in current to compensate.

3.8.2 Current and Voltage Reference Signals

The d-q current reference signals must then be compared to the actual d-q values derived from the current waveform. The error is then passed through a PI controller, creating the reference signals for the desired current waveform. However, since the DC link establishes the full bridge inverter as a voltage source inverter, the output waveform must be converted to the voltage waveform. Thus, the reference signals from the current controller, instead of being used directly as the reference signal for the modulation level, are instead added as compensating errors to the direct and quadrature components of the voltage waveform. This results in a voltage signal that matches the desired output signal with the desired power transfer.

This signal would be provided as the final control signal to the pulsewidth modulator, however the source of the voltage and current signal (point of system measurement) is after the output filter of the inverter. Therefore, a voltage drop is expected from the full bridge inverter to the measurement point. Therefore, the signal needs to be corrected to add the voltage drop expected from the output filter. Assuming the voltage drop to be entirely caused by the output inductance this voltage drop can be accurately estimated by the following relationships.

$$v_{filter} = iX = (i_d + ji_q)(0 - j\omega L) \tag{3.20}$$

$$v_{d\_filter} + jv_{q\_filter} = i_q\omega L - ji_d\omega L \tag{3.21}$$

$$v_{d\_filter} = i_q\omega L \tag{3.22}$$

$$v_{q\_filter} = -i_d\omega L \tag{3.23}$$

From these relationships it can be seen that a simple multiplication factor can be applied to the already known i_d and i_q values and added to the voltage d-q values to correct for the expected voltage drop across the output filter. Thus, the final reference signal is a sum of the current

error signals with the voltage d-q values and the d-q values of the expected voltage drop across the output filter.

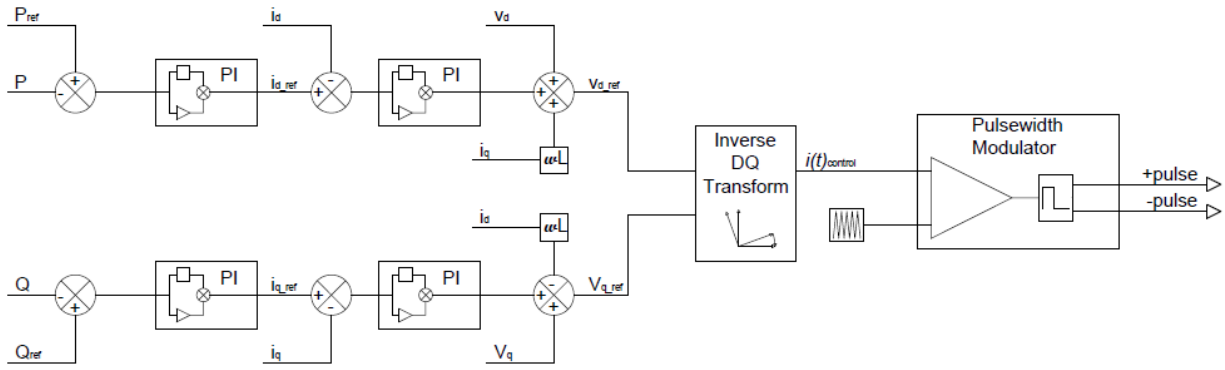

Figure 3.18 Current and Voltage Reference Signals Applied to the Current and Voltage Controller in Order to Generate the Output Reference Control Signal to the PWM to Establish the Grid Feeding Inverter Full Bridge Pulse Generation Scheme

3.8.3 Grid Feeding Inverter Control System

The final control signal must be fed into the pulsewidth modulator as previously discussed. With these control elements combined together, a grid feeding power inverter control system is realized. To recap, this control system starts by detecting the maximum power point of the PV array, and measuring the AC output of the inverter. Power signals are compared in PI controllers to generate current reference signals. Current signal errors and output filter voltage drops are applied to the detected voltage waveform, and a control signal is generated. The control signal is converted to a pulse train in the pulsewidth modulator, which drives the full bridge transistor gates, generating an output AC waveform from the inverter.

3.9 Other Inverter Designs

The inverter presented in this chapter is one of many possible designs that attempts to use well known and proven methodologies. No attempt is made to introduce novel or new techniques. The design is intended to be robust, simple and able to function as a grid supporting inverter in

droop control mode. However, it should be acknowledged that many other inverter designs exist and have been proposed.

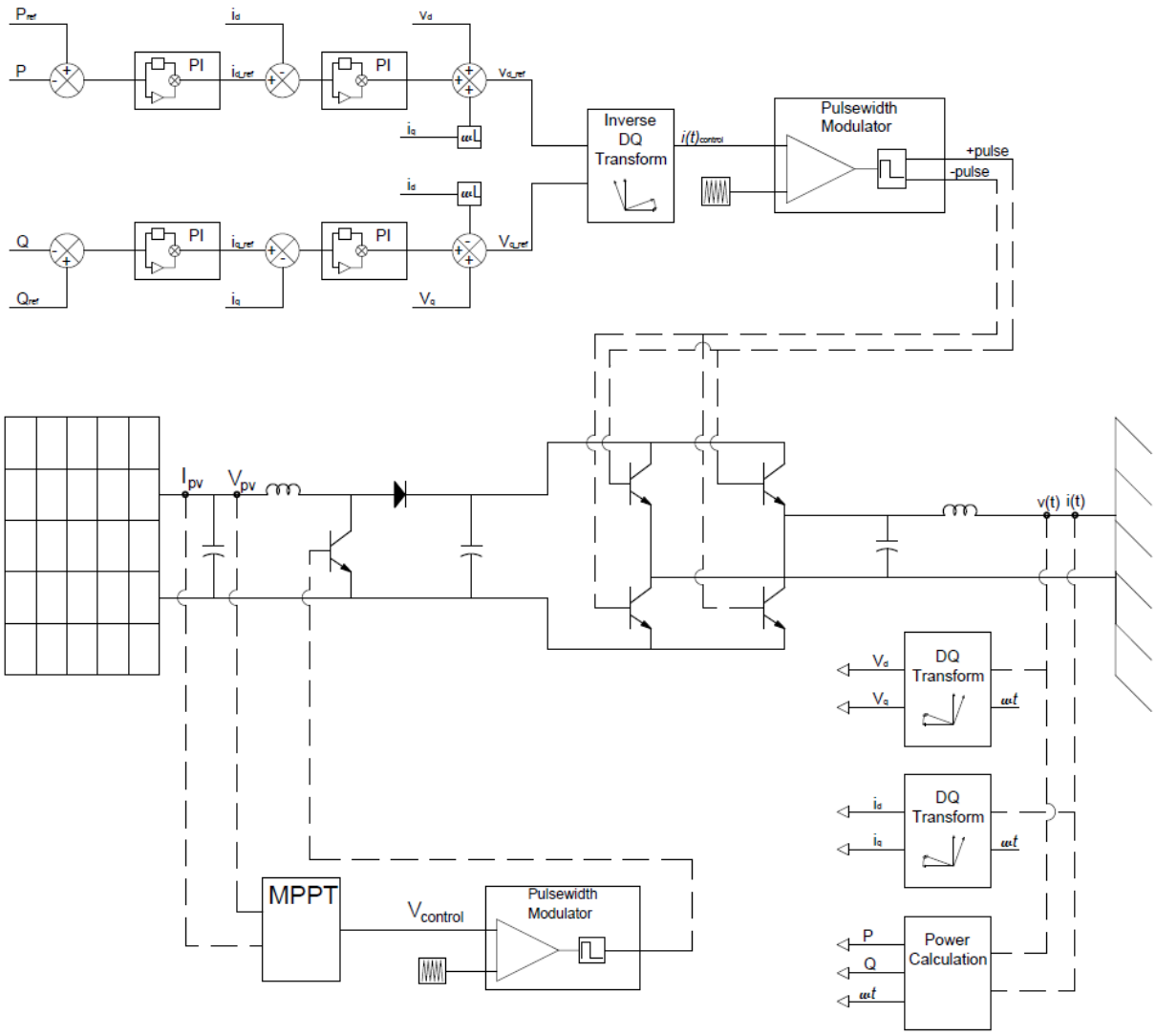

Figure 3.19 Complete Grid Feeding Inverter Control System

The inverter presented has two clearly defined power electronic stages. The first stage performs DC DC conversion for maximum power point tracking. The second stage performs DC AC conversion for power transfer to the AC grid. In order to reduce the number of inverter components and thereby achieve higher power conversion efficiency by reducing inverter

losses, many single stage inverter designs have been proposed. These inverters perform the functions of maximizing photovoltaic power output and grid power transfer via a single power electronic stage. One of the major challenges these inverters face is in the ability to provide clean power to the grid over the large range of input voltages to which these inverters are subjected. However, a significant amount of research is ongoing to develop these single stage systems further [26], [27], [28], [29], [30]. Success in this area could lead to lower cost and higher efficiency inverters.

It should be noted that the design of the inverter will impact the inverter response during droop control operation. Therefore, although this research will draw conclusions regarding droop control operation with the inverter described in this chapter, it cannot be asserted that these conclusions will directly apply for all inverter designs. A variety of inverter designs within a single system may allow for significant variations in system response during droop control operation. The conclusions of this effort are only intended to present a limited dataset for reference and comparison with future studies.

3.10 Conclusion

This chapter presented the basic building blocks of a power inverter and provided a basic level of explanation for their function. These building blocks are largely based on the research of others, which should be reviewed to gain a deeper understanding. Though many possible inverter designs may be used, this chapter presents an excellent single phase design that will be easily adapted for droop control operation in the following chapter.

Chapter 4 - Droop Control

4.1 Introduction

The purpose of this chapter is to present the theory and background of the droop control method and the application of this theory to the inverter control system described in the previous chapter. This chapter first presents the conventional droop method, derived from the operation of parallel generators with large prime movers. Next a droop method that is more appropriate for low voltage resistive systems is derived. Finally, the implementation of this resistive form of droop control to the previously described inverter control system is presented.

4.2 Role of a Droop Controller

The previous chapter presented a full inverter control system, that is able to maximize power output from the distributed generator to the grid. This form of control is used to make what is called a grid feeding inverter. A grid feeding inverter is beneficial to the distributed generator in that no power is wasted. However, it may not always be beneficial to the grid network, since it operates independently of the needs of the grid.

Droop control, on the other hand, is a control method that exports power specifically to meet the needs of the grid. This form of control is used to make what is called a grid supporting inverter. Only a slight variation is required to convert the previously described grid feeding inverter control system into a grid supporting inverter control system, by the addition of a droop controller. By implementing droop control into the inverters control system, the inverter gains the ability to share load equally with other inverters within a microgrid environment, even when PV capacity or grid load changes. This is accomplished by managing the local voltage and frequency.

4.3 Traditional Droop Control

The droop control method is originally derived from the application of large prime movers, such as a diesel generator, being placed in parallel with the grid or other generators to supply local

loads. The significant inertia and inductive nature of traditional large prime movers resulted in a high level of control of power flow by adjusting the operating frequency or voltage peak of the generator, in accordance with the following well known, inductive droop control equations.

$$f = f_0 - k_f(P) \tag{4.1}$$

$$V_{rms} = V_{0(rms)} - k_v(Q) \tag{4.2}$$

In these equations, f is the system frequency and f_0 is the nominal frequency of the system, V_{rms} is the system RMS voltage and $V_{0(rms)}$ is the nominal voltage of the system. P is the active power provided to the grid by the distributed generator necessary to cause the specified change in frequency, and Q is the reactive power provided by the distributed generator necessary to cause the specified change in voltage. K_p and K_q are the droop coefficients (slope) that define the rate at which these parameters change relative to one another.

4.4 Resistive Droop Control (Low Voltage Systems)

In Chapter 2 -System Description it is shown that the output line impedance from each inverter has a R/X ratio of greater than one. The high R/X ratio is consistent with low voltage distribution systems [4], which typically carry higher current over shorter distances, than high voltage systems. The conventional droop relationships presented in (4.1) and (4.2) should not be applied in this condition as they are based on the assumption that the inverter output line impedance between generators is nearly perfectly inductive. Thus, revised relationships must be developed with the revised assumption that the inverter output line impedance is nearly perfectly resistive.

4.4.1 Revised Power Relationships

To revise this conclusion the following steady state equations for calculating active (P) and reactive (Q) power drop across the output line impedance are used [31].

$$P = \left(\frac{EV}{Z}\cos\delta - \frac{V^2}{Z}\right)\cos\theta_Z + \frac{EV}{Z}\sin\delta\sin\theta_Z \tag{4.3}$$

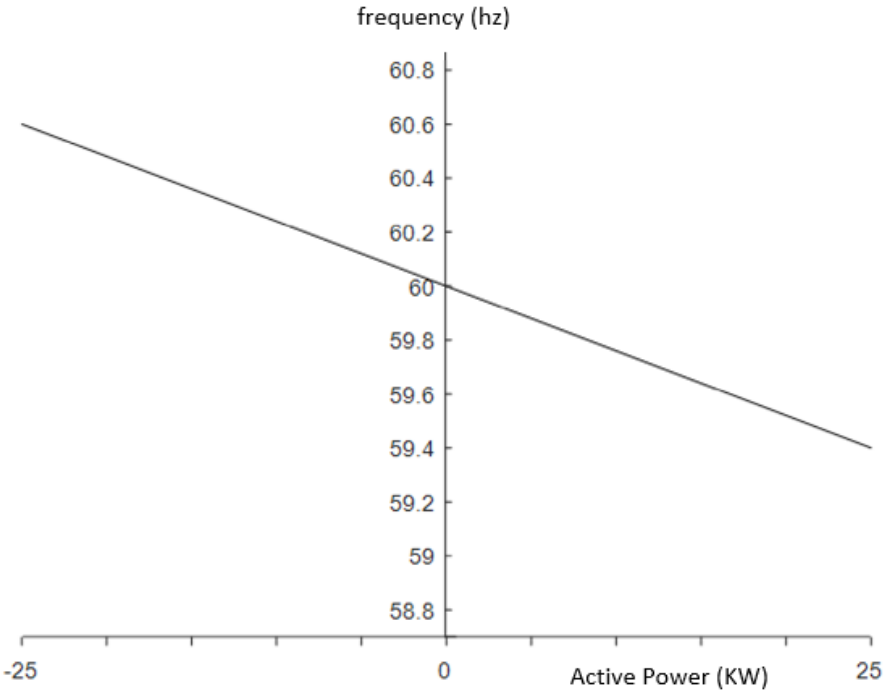

(a)

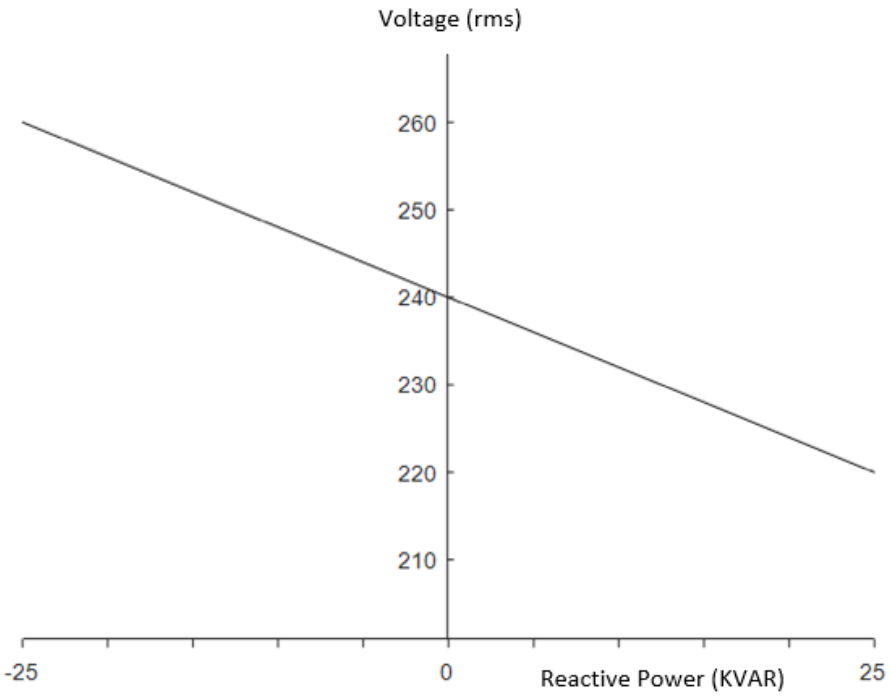

(b)

Figure 4.1 Conventional Droop Relationships for a Highly Inductive System (a) P-f droop, (b) Q-V droop

$$Q = \left(\frac{EV}{Z}\cos\delta - \frac{V^2}{Z}\right)\sin\theta_Z - \frac{EV}{Z}\sin\delta\cos\theta_Z \tag{4.4}$$

In these equations, *E* is the amplitude of the inverter voltage. *V* is the amplitude of the voltage at the common bus. The power angle is δ. *Z* and θ_Z are the magnitude and phase of the feeder impedance from the inverter to the common bus.

In a low voltage system, the impedance of the feeder can be assumed to be dominantly resistive. With this assumption *Z* can be replaced with *R*, and θ_Z can be assumed to be close to *0*, therefore cos $\theta_Z \approx 1$ and sin $\theta_Z \approx 0$. The following simplifications are realized when these assumptions are applied to (4.3) and (4.4).

$$P \approx \left(\frac{EV}{R}\cos\delta - \frac{V^2}{R}\right) \tag{4.5}$$

$$Q \approx -\frac{EV}{R}\sin\delta \tag{4.6}$$

It can also be assumed that the voltage phase angle (δ) is small for an operational low voltage residential grid, and therefore cos $\delta \approx 1$ and sin $\delta \approx \delta$. This assumption allows us to simplify the equations enough to show the droop relationship for a resistive grid.

$$P \approx \left(\frac{V}{R}(E - V)\right) \tag{4.7}$$

$$Q \approx -\frac{EV}{R}\delta \tag{4.8}$$

From this it can be seen that *P* is linearly dependent on the voltage drop across the feeder. It can also be seen that *Q* is linearly dependent on voltage angle δ which varies with system frequency as in seen in (4.9).

$$\frac{d\delta}{dt} = \omega = 2\pi f \tag{4.9}$$

It should be noted that (4.7) expresses the active power consumed across the feeder. Therefore, it can be interpreted to represent the power output needed to be supplied by the inverter to restore nominal parameters at the inverter output. This equation is useful if voltage amplitude is able to be measured at both the filter capacitor (*E*) and the load bus, or end of the

feeder (*V*). However, it is impractical to implement voltage measurement and feedback at each end of each inverter feeder in an actual power system, due to the need for additional measuring devices and communication lines. Because of this, a nominal voltage setpoint (V_0) is selected and programmed into each inverter independently, representing the voltage at the feeder end (*V*). Variations in this nominal setpoint between inverters will result in variations in inverter output, similar to the variations seen based on differences in the programmed droop coefficients. These variations will not impact the inverter general response to changes in load conditions and power sharing.

Similarly, (4.8) expresses the reactive power consumed across the feeder. As more reactive power is consumed across the feeder, a larger change in phase angle is experienced across the feeder, and therefore a larger change in frequency is observed. The magnitude of this change in frequency can be determined in a similar fashion to the change in voltage across the feeder, by assuming the frequency at the load bus to be a nominal frequency setpoint (f_0) and evaluating the difference between the nominal frequency and the measured frequency at the inverter (*f*).

4.4.2 Resistive Droop Equations

Applying these nominal values to (4.7) and (4.8) and reducing constants into a single variable results in the following relationships between voltage, frequency and power consumed across the feeder.

$$(k_v)P_{inv} \approx (V_{rms} - V_{0(rms)}) \tag{4.10}$$

$$(k_f)Q_{inv} \approx (f_0 - f) \tag{4.11}$$

These equations correctly represent power consumed across the feeder from the perspective of the inverter. When power is greater than zero it is being provided by the inverter. When power is less than zero it is being provided by the grid. The inverter can now establish a setpoint equal to the amount of power being consumed by the load by inverting the calculated power produced by the grid. By inverting the power and rearranging the previous equations,

(4.1) and (4.2) can be derived again as the droop control equations representative of a resistive feeder.

$$V_{rms} = V_{(0)rms} - k_v(P_{setpoint}) \tag{4.12}$$

$$f = f_0 + k_f(Q_{setpoint}) \tag{4.13}$$

These equations are represented graphically slightly differently than the traditional inductive version of these equations, as shown.

4.4.3 Combined Droop Equations

Both the traditional and the resistive droop control equations are dependent on the assumption that the feeder impedance is almost entirely resistive or inductive. A combination of these assumptions is possible by working backwards from (4.1), (4.2), (4.12) and (4.13). In the event that the feeder impedance angle is known or can be estimated, this combined set of equations provides more accurate power point estimating [7].

$$V_{rms} = V_{0(rms)} - k_V(P\cos\theta + Q\sin\theta) \tag{4.14}$$

$$f = f_0 - k_f(P\sin\theta - Q\cos\theta) \tag{4.15}$$

When droop control is applied to the inverter control system, the inverter becomes a grid supporting inverter. It is no longer tasked with maximizing output from its associated distributed generator but is instead tasked with maintaining voltage and frequency values on the grid. When multiple inverters are operated this way in parallel, the inverters will each pick up a fair share of the load, in accordance with their programmed droop equation, until all inverters are working together to maintain voltage and frequency of the grid near to the nominal values. Thus, intelligent power sharing is possible between multiple independent inverters without the use of interconnecting communication modules and cables and a centralized network control system.

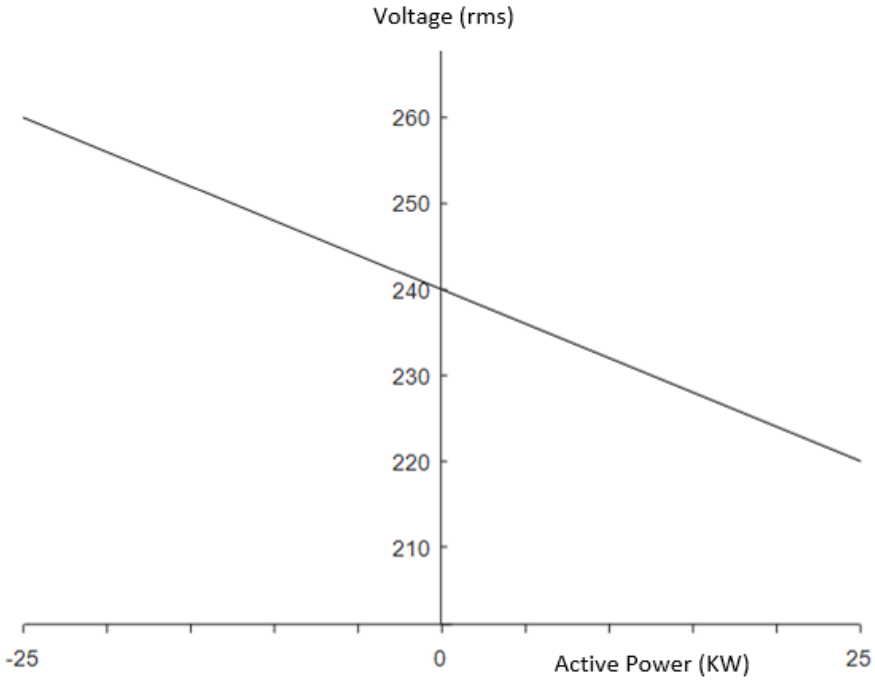

(a)

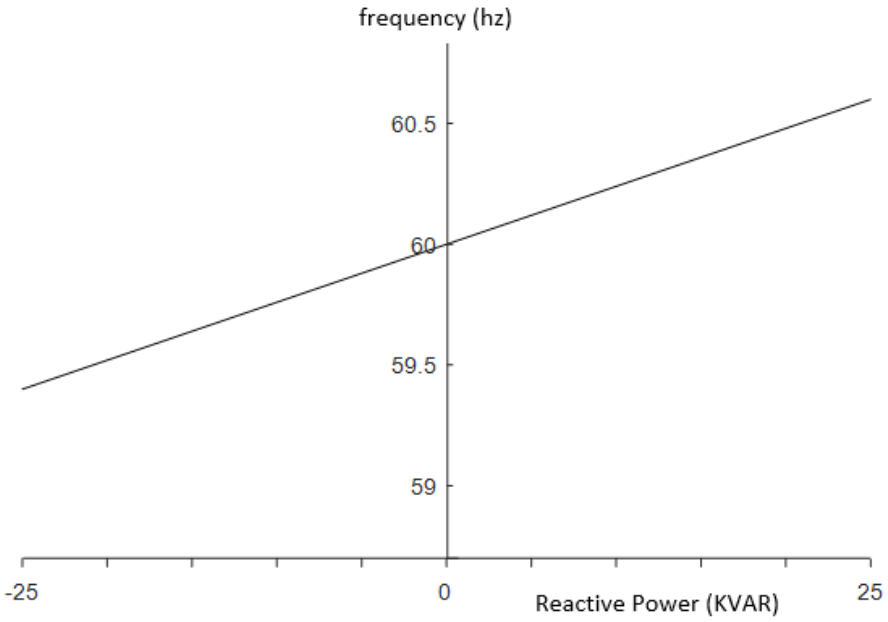

(b)

Figure 4.2 Droop Equations for a Resistive System (a) P-V droop, (b) Q-f droop

4.5 Implementation of Resistive Droop Control in the Inverter Controller

To apply droop control to the inverter control system developed in the previous chapter, the droop controller must generate power reference signals. To do this, the droop equations must be rearranged to solve for the desired setpoint. In this case, the equations must evaluate the known and expected values of frequency and voltage and generate active (P_{droop}) and reactive (Q_{droop}) power setpoints that the inverter should try to achieve to restore the grid to its nominal parameters. The following rearrangement of (4.12) and (4.13) perform this function.

$$P_{droop} = -\frac{1}{K_V}(V_{rms} - V_{0(rms)}) \tag{4.16}$$

$$Q_{droop} = \frac{1}{K_f}(f - f_0) \tag{4.17}$$

These equations could be implemented in the grid feeding inverter control system as the setpoint generators for the control system, replacing the 0 setpoint for Q and the MPPT setpoint for P. However, this change will only be effective instantaneously, since as soon as the inverter begins to respond to the new power setpoints, the system voltage and frequency parameters will respond as well. Thus, the new setpoints will adjust and the control system will be unable to achieve steady state.

4.5.1 Power Reference Signal Generation

To overcome this problem and to achieve a steady state setpoint the measured active (P) and reactive (Q) power must be added to the calculated droop power setpoints to achieve a real (P_{ref}) and reactive (Q_{ref}) reference signal. Thus, the droop controller generates the error signal, which when added to the measured power generates a reference signal.

$$P_{ref} = P + P_{droop} \tag{4.18}$$

$$Q_{ref} = Q + Q_{droop} \tag{4.19}$$

The final controller can be represented mathematically as a combination of (4.16), (4.17), (4.18) and (4.19).

$$P_{ref} = P + \frac{V_{rms} - V_{0(rms)}}{(-k_V)} \tag{4.20}$$

$$Q_{ref} = Q + \frac{f - f_0}{k_f} \tag{4.21}$$

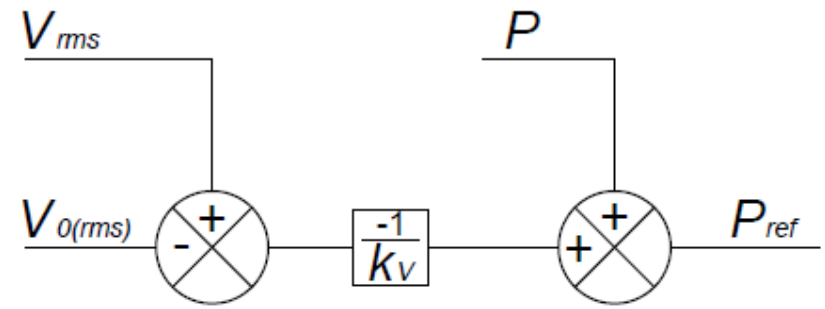

(a)

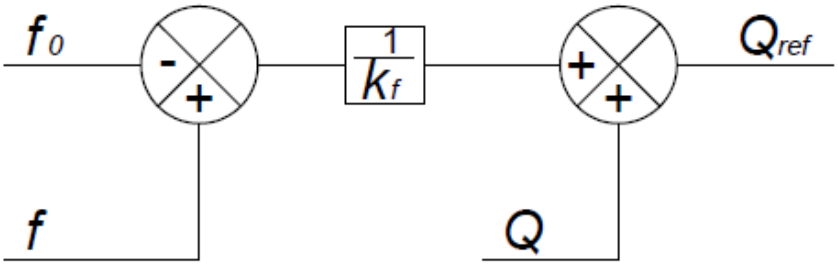

(b)

Figure 4.3 Control System Block Diagram for Generating Active (a) and Reactive (b) Power Reference Points Using Droop Control

4.5.2 Correction for an Inertialess Grid

While the equations and figures above provide a representation of the practical implementation of droop control in an actual grid system, the system presented in this paper requires one further variation. The simulated system differs from a true system in that it does not simulate inertia at the generator. Therefore, no changes in frequency are expected to be

caused by changes in power flow. Because of this, (4.17) can be used directly to establish a reference reactive power setpoint for the given frequency conditions as follows.

$$Q_{ref} = \frac{f - f_0}{k_f} \tag{4.22}$$

This is easily incorporated into the model by removing the summation block shown in Figure 4.3 (b).

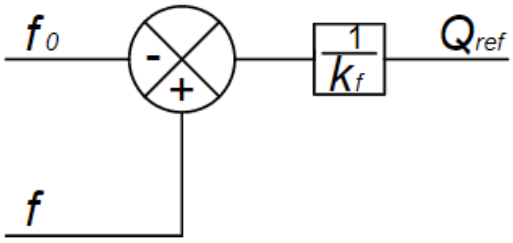

Figure 4.4 Control System Block Diagram for Generating Reactive Power Reference Setpoint in a grid without inertia.

4.5.3 Droop Coefficients Calculation

The droop coefficients k_v and k_f function similar to gain in a linear controller. The value chosen effects local and remote loads differently. The voltage at the local load will be entirely managed by the local inverter. Therefore, the power transferred by the local inverter will be directly proportionate to the voltage drop caused by the local load, in accordance with the droop coefficient. In other words, raising or lowering the droop coefficient will directly raise and lower the contribution of active power by the local inverter.

On the other hand, remote loads are separated by some impedance from each inverter. In this case the inverters operate only as necessary to maintain voltage levels at the local grid and not at the load bus. The inverter feeder impedance becomes the dominant factor in managing power transfer to the remote loads. Therefore, regardless of the droop coefficient, the inverter that is closest (has the lowest impedance to) the remote load will transfer the most power.

Since the local load will have a dominant effect on power drawn from the local inverter, the droop coefficients should be chosen to prevent the inverter from exceeding its capacity. This can be accomplished with the following derivations of (4.16) and (4.17).

$$k_v = \frac{v_{min} - v_0}{P_{capacity}} \tag{4.23}$$

$$k_f = \frac{f_{max} - f_0}{Q_{Capacity}} \tag{4.24}$$

In these equations v_{min} *and* f_{max} are the minimum voltage and maximum frequency parameters under which the load is expected to operate safely, while $P_{capacity}$ and $Q_{capacity}$ are the rated capacity of the photovoltaic arrays. This method ensures that the load will not be driven to operate outside of the design operating limits, by correlating those limits with the limits of the power source.

4.6 Complete Grid Supporting Inverter Control System

By modifying the grid feeding inverter control system with the addition of droop control, the inverter becomes a grid supporting inverter control system. This is done by combining Figure 3.19 with Figure 4.3 and Figure 4.4, connecting them at the points labeled P_{ref} and Q_{ref}. Notice when these figures are combined that both *P* is added into the droop controller, and then subtracted out of the current controller. Thus, the controller can be further simplified by feeding the voltage error signal directly into the current controller without having to take any active power measurement.

The additional elements needed to add the grid supporting functionality are strictly logic elements applied to the signal voltages and currents. Thus, there are no additional high power or high frequency components required which are normally associated with increased cost. The result is an inverter control system with significantly increased functionality and diversity of application, but without a significantly increased number of components or cost.

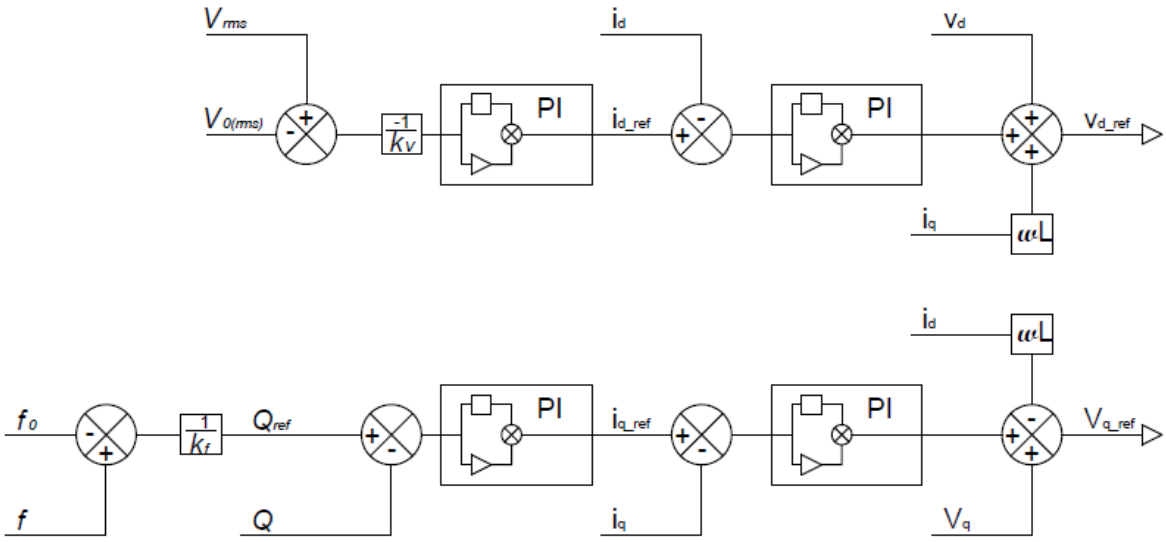

Figure 4.5 Droop Controlled Grid Supporting Inverter Control System

4.7 Conclusion

This chapter presented the droop control method used in this study. The selected method is a derivation of the traditional droop method used by generators that operate at higher voltages and have large prime movers and inertia. This derivation is more applicable to low voltage systems which are characterized by less inductance and more resistance in the distribution system. This derivation also takes into account operation in a microgrid with no inertia. The implementation of this form of droop control to the previously presented inverter control system is simple and does not require the use of expensive components.

Chapter 5 - System Analysis and Tests

5.1 Introduction

The purpose of this chapter is to test the performance of the inverter and droop controller design that was developed in the previous chapters, within a microgrid environment. The tests are selected with the purpose of gaining a greater understanding of some of the unique characteristics of the droop controller when applied to low voltage distributed generators, and to demonstrate some of their potential benefits in future grids. Three test cases are presented in this chapter.

The first test case has the purpose of demonstrating the ability of the inverter to contribute to grid voltage and frequency regulation, as required by the droop controller.

The second test case is selected to highlight one of the unique features of applying droop control to low voltage distributed generators. Unlike centralized generators, low voltage distributed generators are often intended to operate in the vicinity of a local load. This test is intended to demonstrate the unique differences in droop controlled inverter response when regulating a local load versus when regulating a remote grid load. This test case shows that the inverter governs each type of load differently and provides an explanation for these differences.

The third test case is selected to demonstrate the autonomous control of a microgrid when the droop controlled inverters are operated in parallel with a smart voltage controlling transformer. One of the key advantages of a microgrid is the ability to operate in island mode. This test demonstrates that by a simple voltage control technique, a smart transformer can leverage the benefits of droop control to establish a power sharing condition in which the microgrid is fully powered by the distributed generators, thus establishing the conditions needed for seamless islanding. The other test of this test case demonstrates that when the inverters are unable to meet the demand of the microgrid, the external grid will automatically fill the need. These

concepts are presented to illustrate some of the decentralized control capabilities of resistive droop control in the smart grid environment.

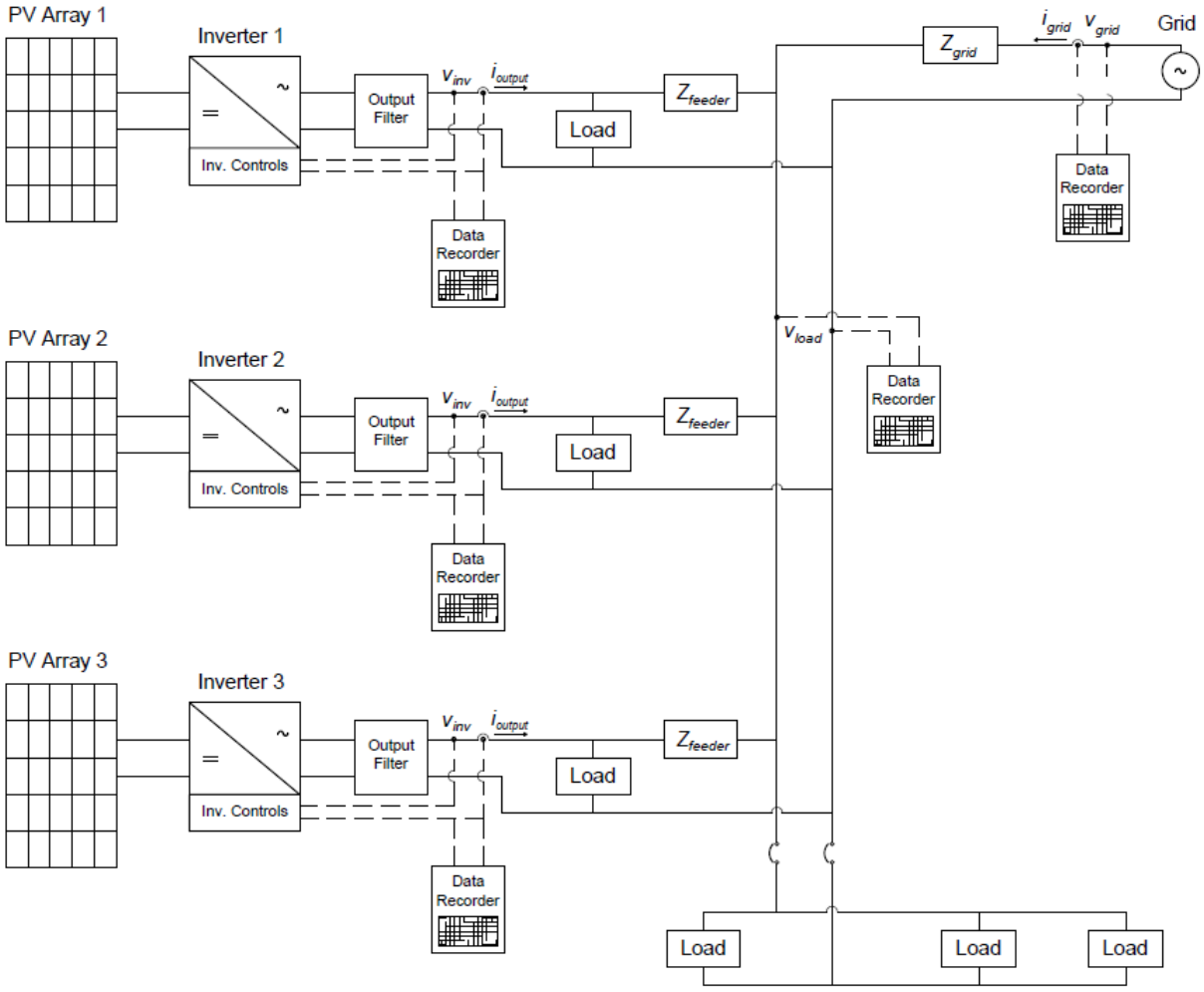

Figure 5.1 General Power System Diagram for Test Cases

5.2 Test Overview

The area of investigation of this thesis is discussed in Chapter 1. The general system that is used to perform this investigation is presented in Chapter 2. Certain physical variations are made to the system described in Chapter 2 in order to fully assess the area of investigation.

These variations are presented in the following Test Cases. The general power system one-line diagram being tested is shown in Figure 5.1.

These tests are developed with a focus on distributed generation in a low voltage residential distribution system, in North America. Thus, the nominal operating voltage is 240 VRMS, with a nominal frequency of 60 Hz. The line impedances are selected to be dominantly resistive (R/X >1), consistent with low voltage distribution systems. The load that is not separated from the inverter by impedance is intended to simulate a local load, such as a house with a rooftop mounted PV array. The loads that are separated from the inverters by impedance are intended to simulate remote loads, such as neighboring houses on the same distribution line. The size of the impedance can be considered relative to the distance between houses. Thus, a rural community would have larger line impedance values, while a suburban style neighborhood would have smaller line impedance values. The impedance between the loads and the central grid represents the line impedance between the neighborhood and the substation, or other voltage regulating point. The voltage regulating point (transformer) establishes the extent of the microgrid. This microgrid contains significant distributed generation capacity, relative to the microgrid load.

The tests are performed by running simulations in PSCAD. All of the simulations performed share a common initialization process. Each simulation commences with the grid supplying the loads. The inverter(s) turn on after 0.5 seconds and synchronize with the grid. The inverters operate in the droop control mode to manage power flow. The remainder of the simulation varies with each test and is explained in each test case.

The tests are grouped into Test Cases. Each test case seeks to demonstrate a different aspect of the system performance. Each test case is accompanied by a scenario description and power system diagram. A table lists the specific parameters that are varied and the specific setpoints used in each test. The Test Cases, scenario descriptions, table of parameters, and results are presented below. The summary of these results into final conclusions is presented in Chapter 6.

5.3 Test Case 1

The purpose of Test Case 1 is to demonstrate the droop functions of the controller. The function of droop control is to manage power flow out of the distributed generator in order to achieve voltage and frequency balancing. The inverter measures voltage and frequency at the output, and feeds these values into the droop controllers, as discussed in Chapter 4 -Droop Control. This test demonstrates that when voltage or frequency change in the system, the controller responds promptly and effectively by injecting real or reactive power in accordance with the droop curves.

5.3.1 Scenario for Test Case 1

This scenario consists of one inverter in parallel with the grid voltage source, and the load bus with the breaker open, as shown in Figure 5.2. The system, load and impedance parameters are as defined in Table 2.1. The droop coefficients are calculated using (4.23) and (4.24), and the calculation is shown below. The photovoltaic array is assumed to be rated for 25 KW. The maximum design injected reactive power is 5% of the rated power, consistent with the recommendations of the IEEE standard for interconnection of distributed energy resources with the grid [32]. The minimum voltage and the maximum frequency are consistent with the same standard.

$$k_v = \frac{210\ VAC - 240\ VAC}{25\ KW} = -1.2 \tag{5.1}$$

$$k_f = \frac{61.8\ Hz - 60\ Hz}{1.25\ KVAR} = 1.4 \tag{5.2}$$

To demonstrate proper operation of the droop controllers, two tests are run. In the first, the grid source voltage is manually varied according to Table 5.2. In the second test, the system frequency is manually varied according to Table 5.2. The manual change in grid voltage and frequency is used to simulate changes in load. The controller responds by feeding an error signal into the current and voltage control loops and generating a new reference waveform. This reference waveform drives changes to the real and reactive power that is injected into the grid.

Table 5.2 Voltage Setting and Corresponding Time of Voltage Change

RMS Voltage Setting	Simulation Time
240 VRMS	0 sec
250 VRMS	5 sec
240 VRMS	10 sec
230 VRMS	15 sec

Table 5.2 Frequency Setting and Corresponding Time of Change

Frequency Setting	Simulation Time
60 Hz	0 sec
60.05 Hz	5 sec
60 Hz	10 sec
59.95 Hz	15 sec

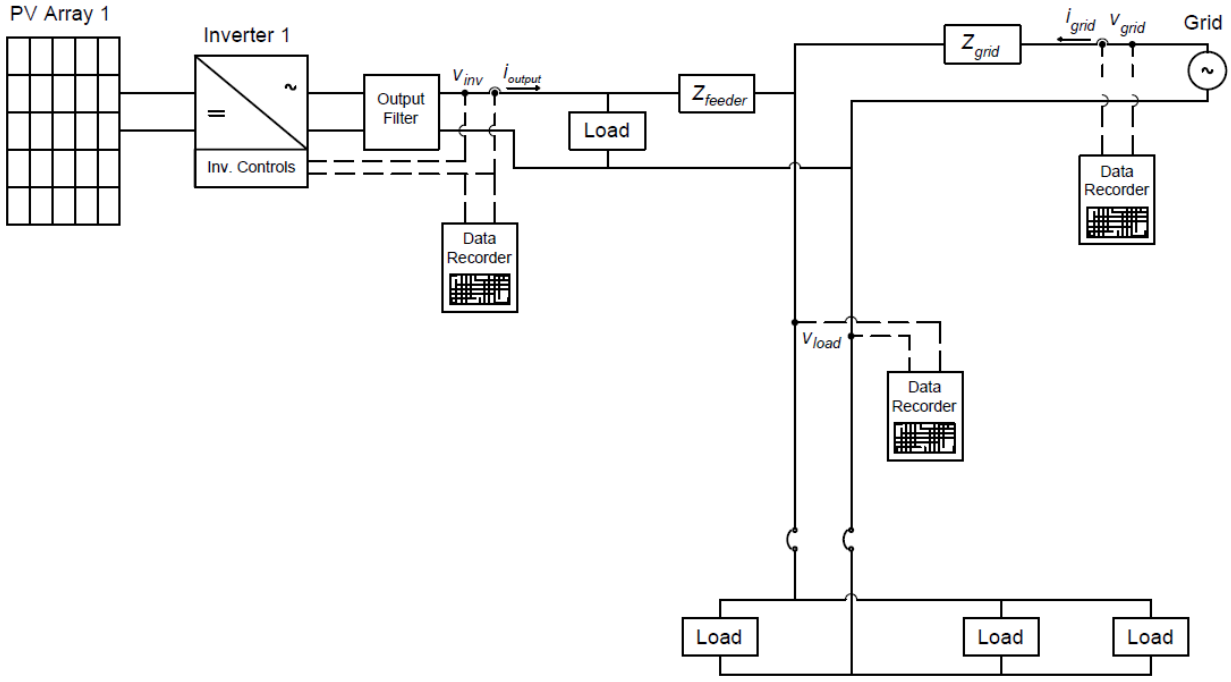

Figure 5.2 Test Case 1 Power System Diagram

5.3.2 Test Results

Select figures were generated to document each test. The figures and accompanying discussion for the tests of Test Case 1 follow.

5.3.2.1 Test 1

The changes in voltage of the first test can be seen in Figure 5.3 (a) which shows the grid RMS voltage setpoint overlaid with the RMS voltage measured at the inverter. The inverter voltage is immediately affected by changes in the grid voltage. The change in voltage measured at the inverter creates an error signal that feeds back into the current and voltage control loops. The control loops generate a reference waveform that causes active power to be exported, consistent with the droop equation. Figure 5.3 (b) shows the error signal acting on the controller, and the active power that is exported by the inverter. The previously derived (4.20) is restated below.

$$P_{ref} = P + \frac{V_{rms} - V_{0(rms)}}{(-k_V)} \tag{5.3}$$

The changes in grid source voltage cause a change in V_{rms} measured at the inverter. Meanwhile the reference value $V_{0(rms)}$ remains unchanged at 240 VRMS. Thus, at 5 seconds into the simulation, V_{rms} becomes greater than $V_{0(rms)}$. This generates a negative error that is subtracted from the present value of P being exported by the inverter, to establish a new, lower P_{ref}. The lower P_{ref} setpoint drives P downward. As P decreases due to this negative error, V_{rms} also decreases, reducing the error. Steady state is achieved when V_{rms} again equals $V_{0(rms)}$ and the inverter is outputting a lower active power.

At 10 seconds into the simulation, and again at 15 seconds, the opposite condition occurs. V_{rms} is suddenly reduced less than $V_{0(rms)}$. Each time generating a positive error. P increases with the positive error, causing V_{rms} to increase until V_{rms} is equal to $V_{0(rms)}$. Steady state is achieved each time with a higher value of output active power P.

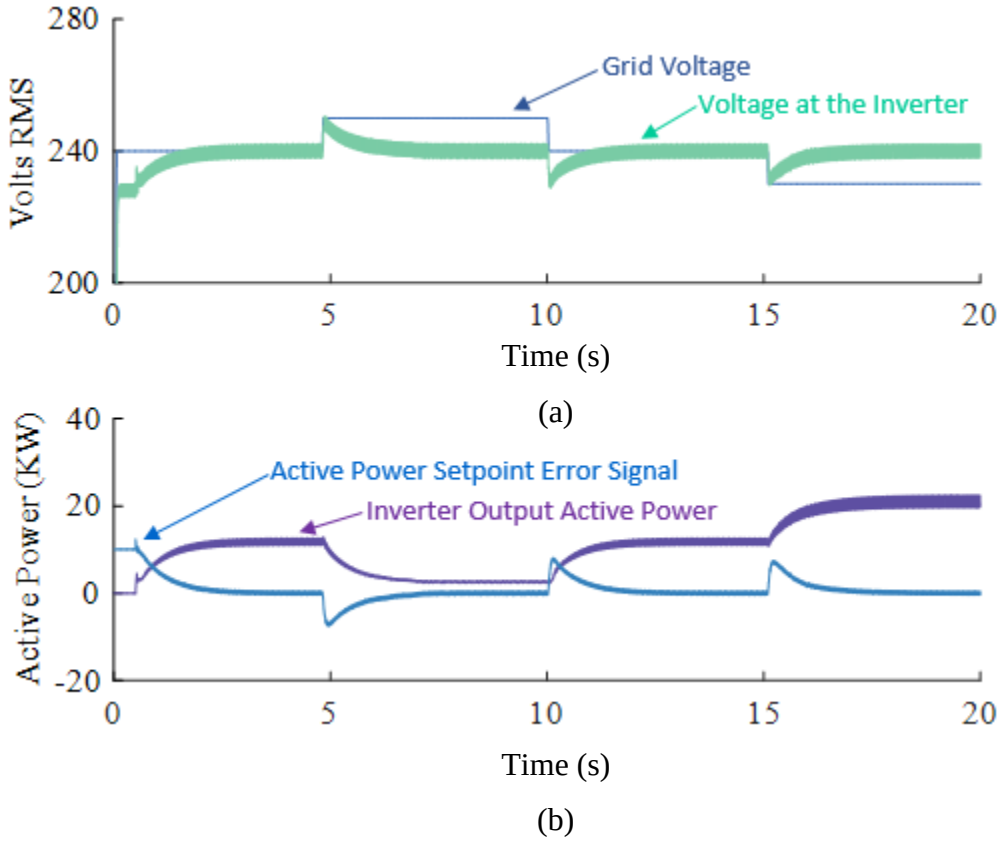

Figure 5.3 Test 1 Test Results demonstrating that changes in microgrid voltage effect compensating changes in inverter output power, as seen by (a) Inverter Output RMS Voltage Vs. Grid Setpoint RMS Voltage, and (b) Inverter Output Power Vs. Droop Controller Voltage Error Signal

Looking at the waveforms during each of these RMS voltage transients, shown in Figure 5.4, it can be seen that the waveforms measured at the inverter are not significantly affected. This can be attributed to the grid impedance which smooths the voltage and current transients. However, the variations in power can be observed by noting that the current waveform at 10 seconds is substantially smaller than the current waveforms of 5 and 15 seconds. This corresponds with the lower active power being output by the inverter at 10 seconds, as shown in Figure 5.3.

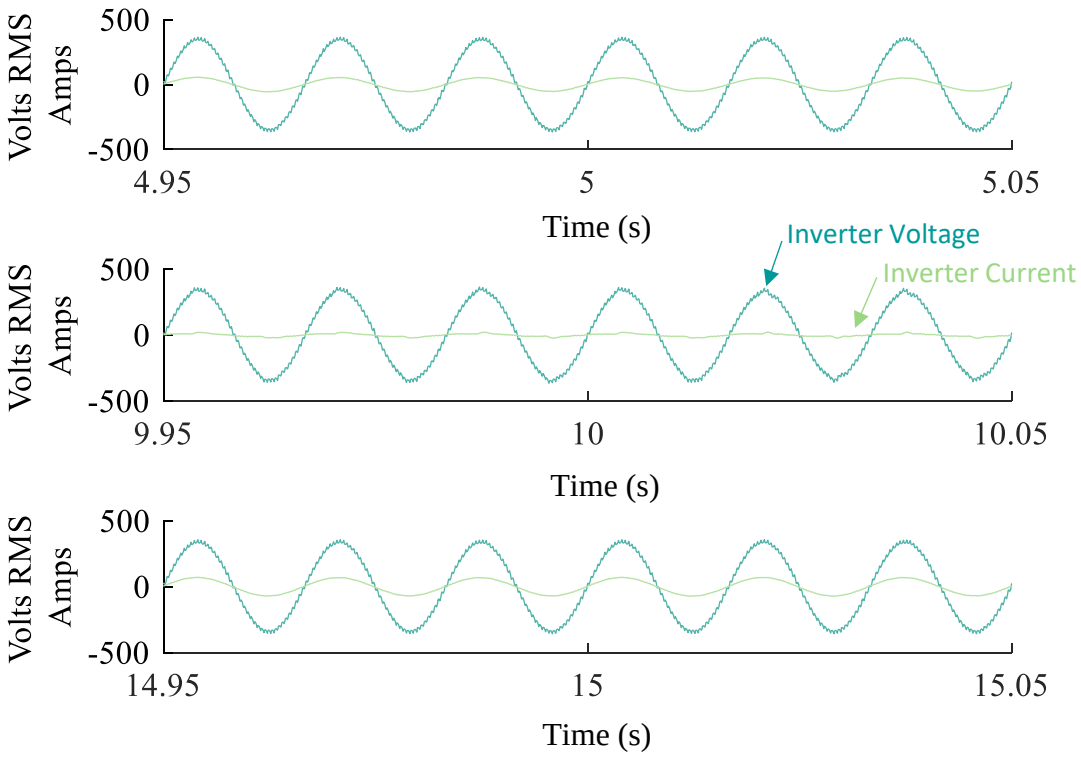

Figure 5.4 Inverter Output Voltage and Current Waveform at (a) 5 Seconds with the Grid Operating at 240 VRMS, (b) 10 Seconds with the Grid Operating at 250 VRMS, and (c) 15 Seconds with the Grid Operating at 240 VRMS

5.3.2.2 Test 2

This test validates the same inverter responses as test 1, but with regard to the reactive power setpoint. Changes are made to the system frequency at 5, 10 and 15 seconds. The change in frequency is detected at the inverter and a reactive power reference signal is generated. The measured reactive power is compared to the reference reactive power to generate the error signal for the controller. The error feeds the controller and raises or lowers the reactive power output, in accordance with (4.22) which is restated below.

$$Q_{ref} = \frac{f - f_0}{k_f} \tag{5.4}$$

The implementation of this equation can be seen in Figure 5.5. At 5 seconds into the simulation the system frequency f is raised above the nominal reference frequency f_0 that is programmed into the controller (60 Hz). A positive error signal is generated, increasing the reactive power reference signal. The measured reactive power at the output follows this reference signal, as is seen in Figure 5.5 (b)

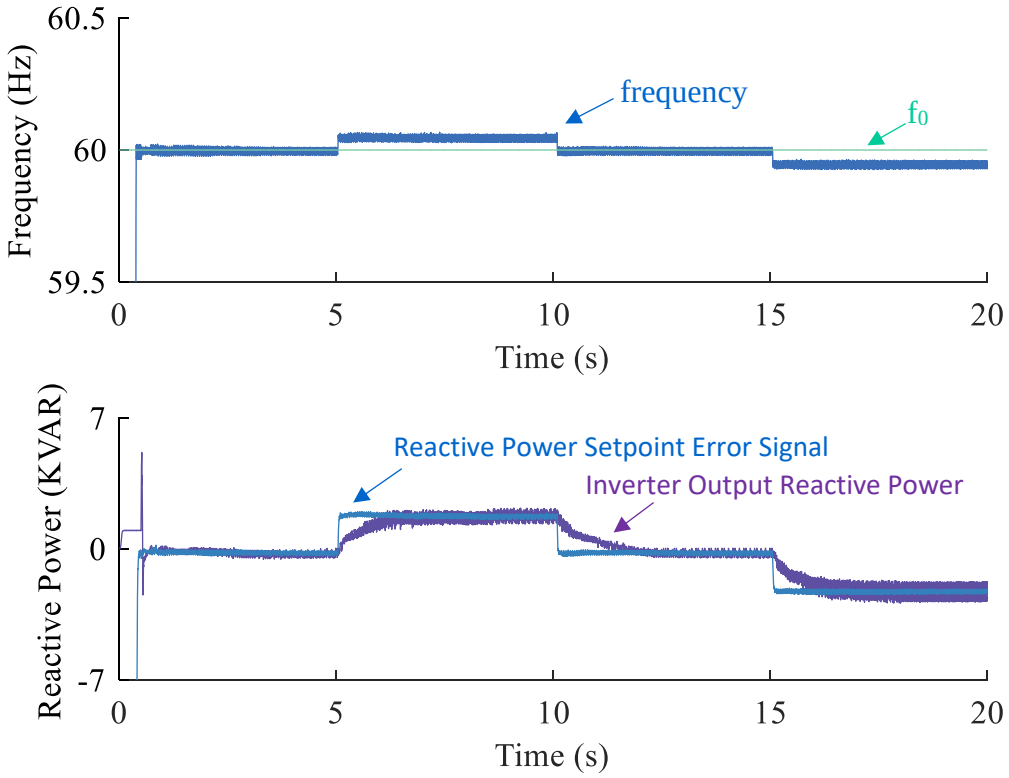

Figure 5.5 (a) Grid Frequency Plotted Against the Programed Nominal Frequency (f_0) of 60 Hz, and (b) the Reactive Power Setpoint Error Signal (Q_{ref}) Plotted Against the Reactive Power Measured at the Inverter

The waveforms shown in Figure 5.6 show that no significant change in active power occurs between these time intervals. The change in reactive power is only slightly perceptible by observing that the voltage leads the current at 10 seconds, consistent with a positive reactive power condition, while at 5 and 15 seconds the voltage and current are in phase. The change in frequency is imperceptible on these plots.

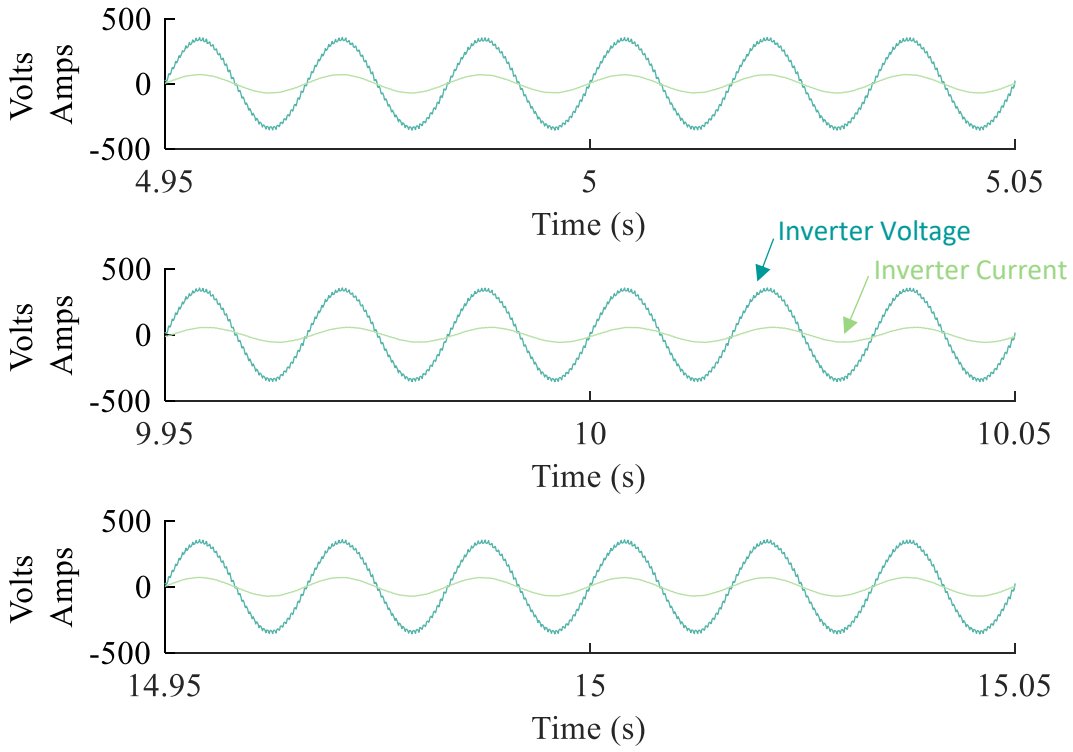

Figure 5.6 Voltage and Current Profiles at (a) 5 Seconds with the Grid Frequency Operating at 60 Hz, (b) 10 Seconds with the Grid Frequency Operating at 60.05 Hz, and (c) 15 Seconds with the Grid Frequency Operating at 59.95 Hz.

5.3.3 Conclusions from Test Case 2

The simulations performed confirm the proper implementation of the control figures and equations presented in Chapter 3 -Single-Phase Inverter Operation and Chapter 4 -Droop Control. Specifically, the presented controller performs as expected when presented with changes in voltage and frequency. The Inverter exports active and reactive power consistent with the resistive droop equations, represented graphically in Figure 4.2 and presented again in Figure 5.7.

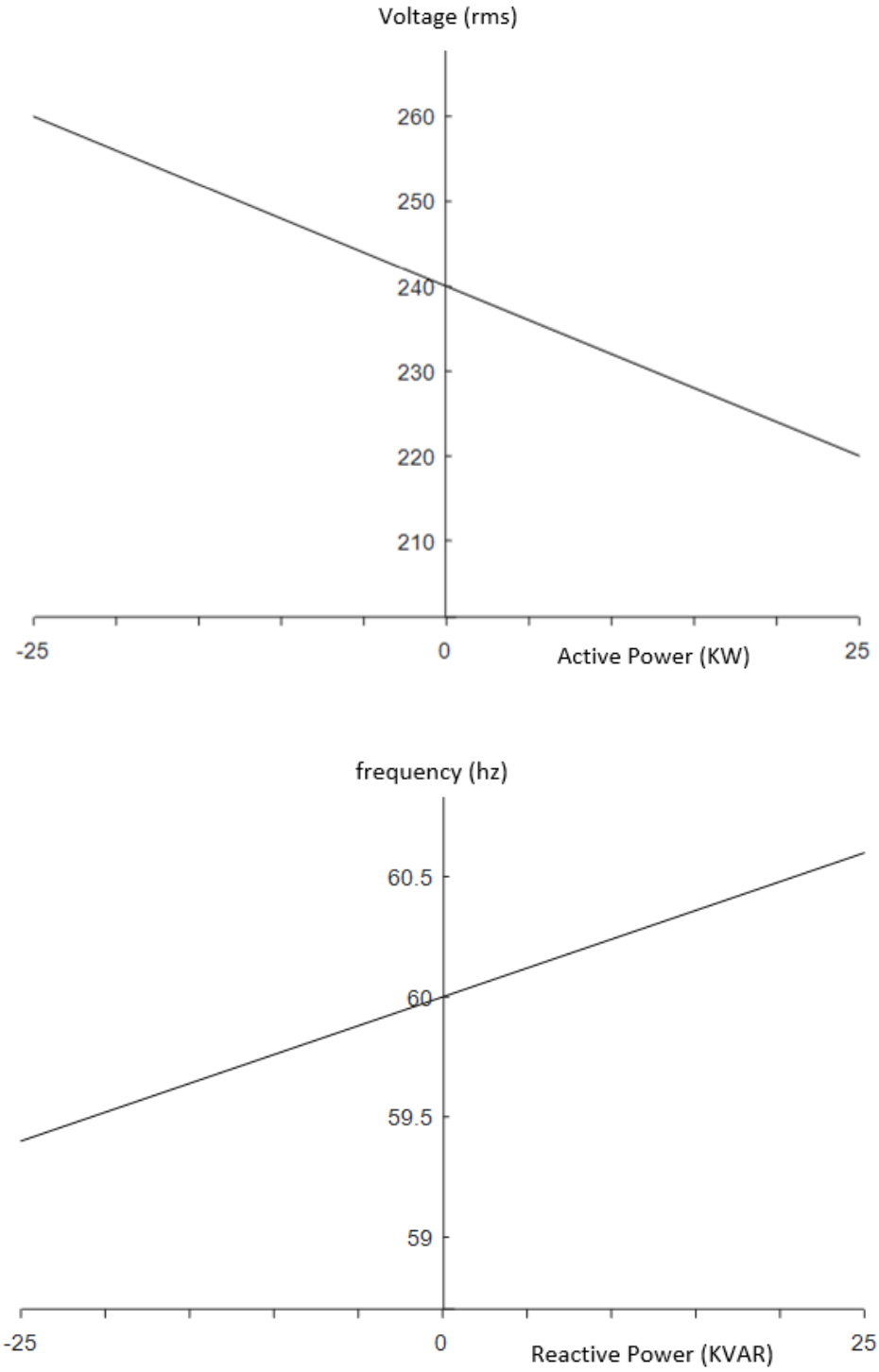

Figure 5.7 Resistive Droop Characteristics

5.4 Test Case 2

The purpose of this test case is to highlight the application of droop control in the presence of a local load. This test will demonstrate that in the ideal case of multiple inverters being directly applied to managing power at a local load bus, the inverters will export power according to the setpoint established by the programmed droop coefficient. However, in the case of multiple remote inverters attempting to manage voltage at a remote load, the droop coefficient no longer regulates the inverter output, and instead the inverter exports power as demanded by the system in order to manage the voltage drop. This test demonstrates the droop power sharing attribute in two ways, one with power shared to local loads only, and two with power shared to local and remote loads.

This test case is useful to the inverter designer since in many cases photovoltaic inverters and systems are desired to operate in the immediate vicinity of one another and a load, effectively forming a local bus. The designer must understand how power will be shared based on the presence or absence of a local bus at the system level.

5.4.1 Scenario for Test Case 2

The scenario for test case 2 consists of three inverters operating in parallel with three local loads. In the first test the feeder impedances are eliminated to represent multiple inverters and loads in close proximity. At 20 seconds into the simulation the load bus breaker shuts, introducing additional local load into the microgrid.

In the second test a feeder impedance is established, according to Table 2.1, resulting in each inverter having a small local load while managing the voltage at the remote bus. At 20 seconds into the simulation the load bus breaker shuts, introducing additional remote load to the microgrid.

The inverters are each distributing power from photovoltaic arrays of different capacities, as shown in Table 5.3. The power system diagram for both tests is presented in Figure 5.8.

Table 5.3 Photovoltaic Array Capacities for Test Case 2

Inverter Number	PV Capacity (KVA)
Inverter 1	30 KVA
Inverter 2	40 KVA
Inverter 3	50 KVA

Since each inverter has a different photovoltaic capacity, each inverter must also have a different droop coefficient in accordance with (4.23). Those droop coefficients are each calculated from that equation below.

$$k_{v(Inverter\ 1)} = \frac{210\ VAC - 240\ VAC}{30\ KW} = -1.0 \tag{5.5}$$

$$k_{v(Inverter\ 2)} = \frac{210\ VAC - 240\ VAC}{40\ KW} = -1.3 \tag{5.6}$$

$$k_{v(Inverter\ 3)} = \frac{210\ VAC - 240\ VAC}{50\ KW} = -1.7 \tag{5.7}$$

Only the active power droop coefficients are presented here, since in this test case no change in frequency is expected to occur, and therefore there will be no change in the reactive power control setpoint.

5.4.2 Test Results

Select figures were generated to document each test. The figures and accompanying discussion for the tests of Test Case 2 follow.

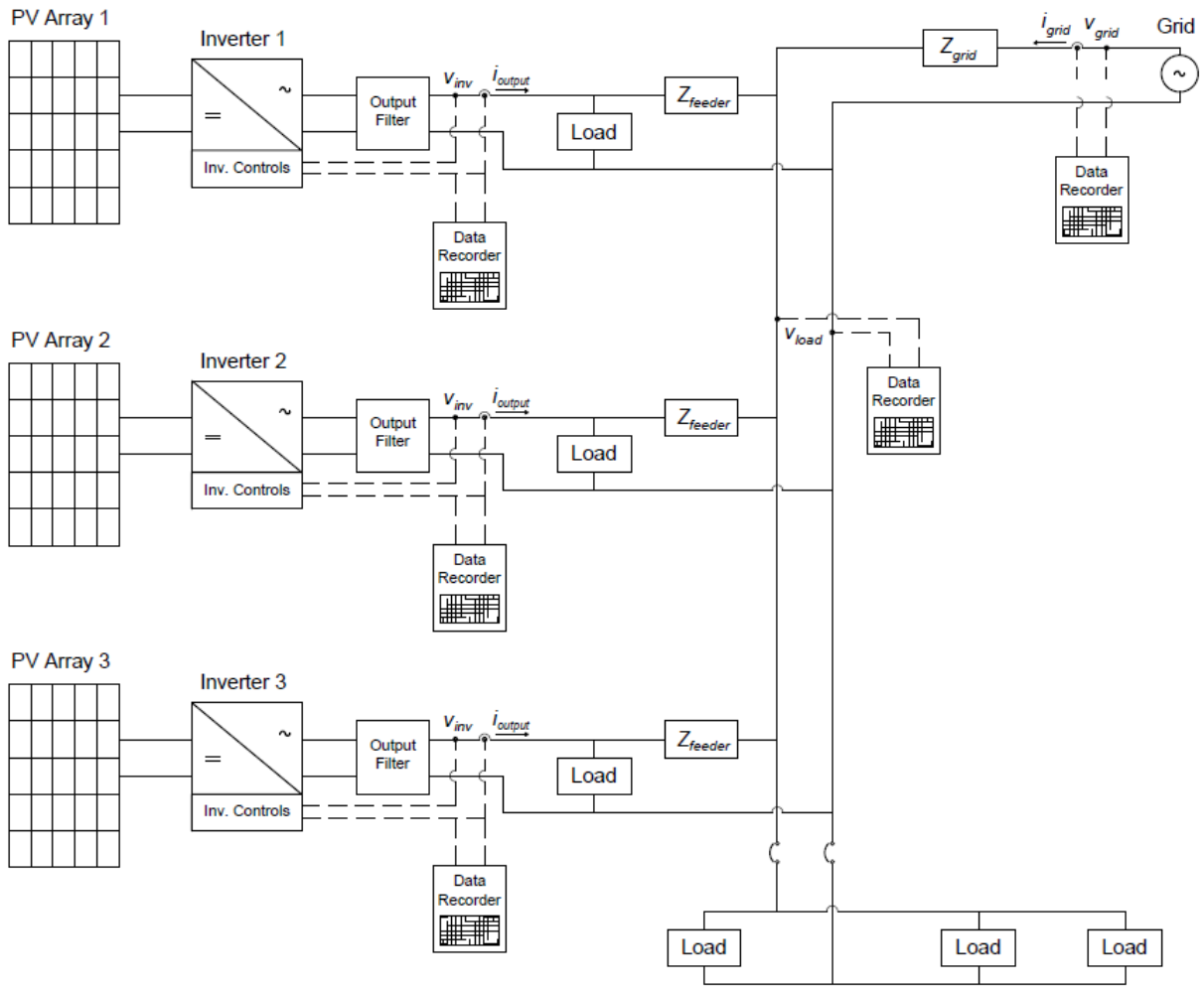

Figure 5.8 Power System Diagram of Test Case 2

5.4.2.1 Test 3

In this test the inverters are placed on service with no feeder impedance in order to demonstrate the effectiveness of the droop coefficients in droop control. In this case each inverter is targeting the same output voltage setpoint and has the same size load. However, because of their unique droop coefficients they each target a different power setpoint.

Inverter 3 has the highest photovoltaic capacity, and therefore the smallest droop coefficient (shallowest slope). This means for a given change in voltage, inverter 3 will establish the highest power setpoint at the controller.

On the other hand, inverter 1 has the smallest photovoltaic capacity, and therefore the largest droop coefficient (steepest slope). This means for the same change in voltage, inverter 1 will establish the lowest power setpoint at the controller.

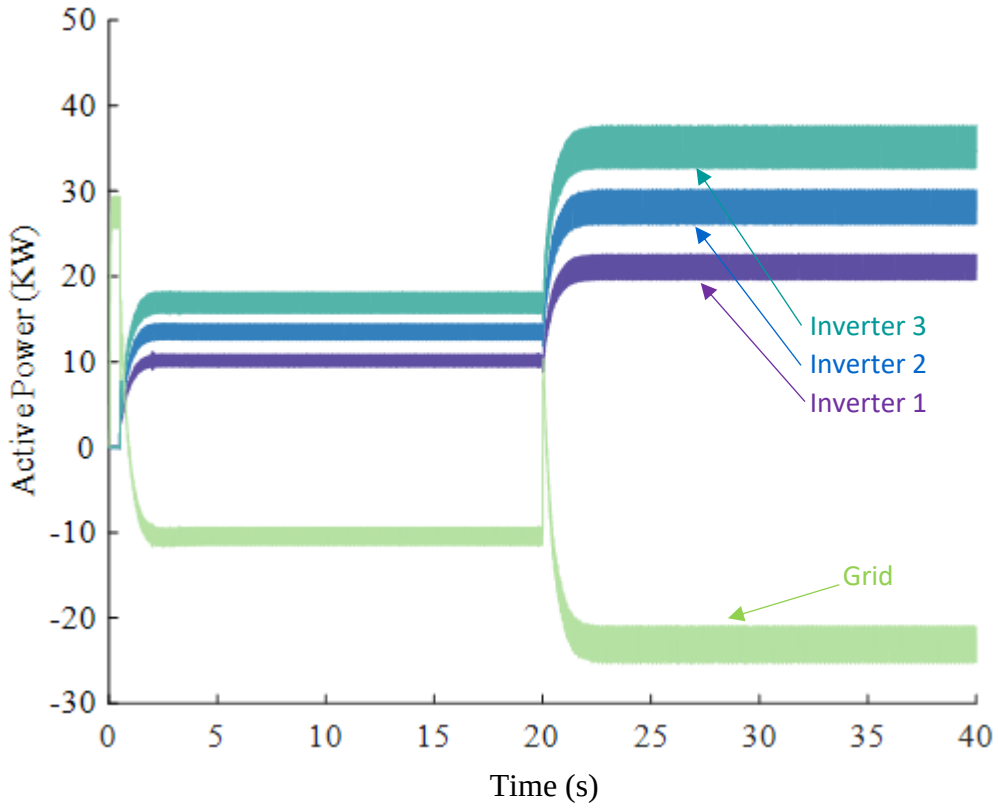

Figure 5.9 Active Power Output by Inverters and Injected by the Grid

As the inverters increase their output power the voltage across the entire grid is raised consistently. Thus, each inverter closes in on the voltage setpoint at the same time, and no hunting between inverters can occur. The result, shown in Figure 5.9, is that every inverter

settles into a steady state condition with a power output proportionate to the magnitude of the photovoltaic capacity that it is able to provide.

This response can also be seen by viewing the current waveforms being output by each inverter. Inverter 1 contributes the least to the loads, while inverter 3 contributes the most, as can be seen in Figure 5.10.

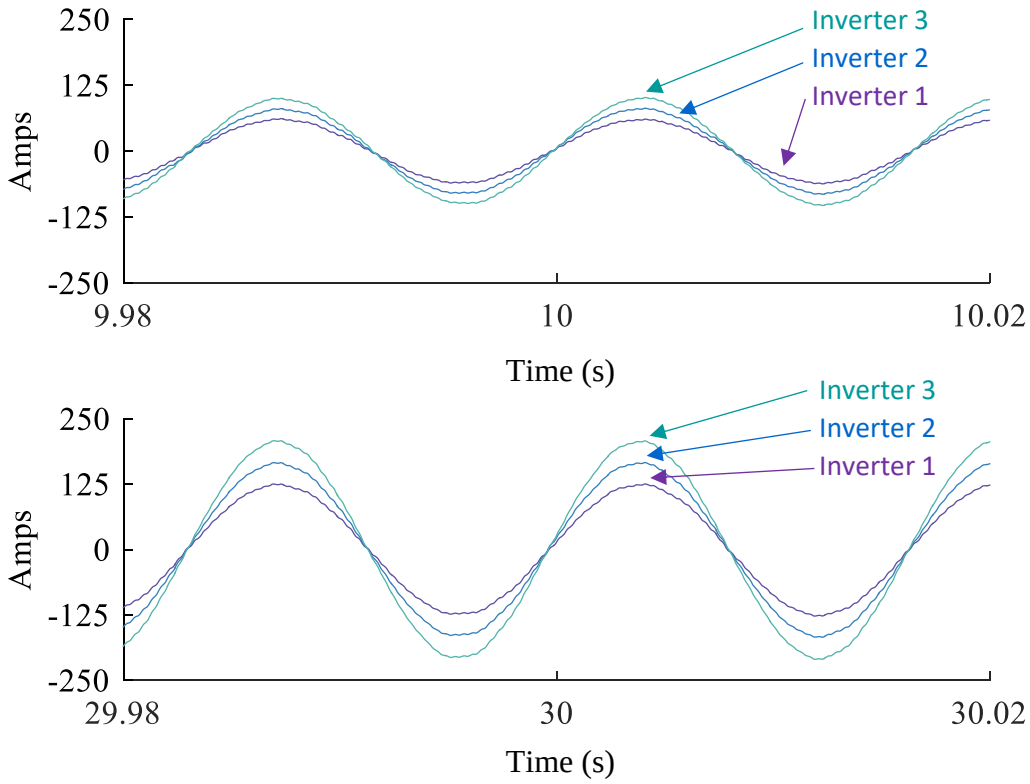

Figure 5.10 Current Waveforms of Each Inverter Prior to Applying the Load Bus (a) and After the Load Bus is Connected (b)

5.4.2.2 Test 4

In this test the feeder impedance is reinserted into the feeders, providing an effective control separation between each inverter and between the inverters and the remote loads. The

impedance dominates the regulation of voltage and the droop coefficient no longer influences steady state power sharing as seen in Figure 5.11.

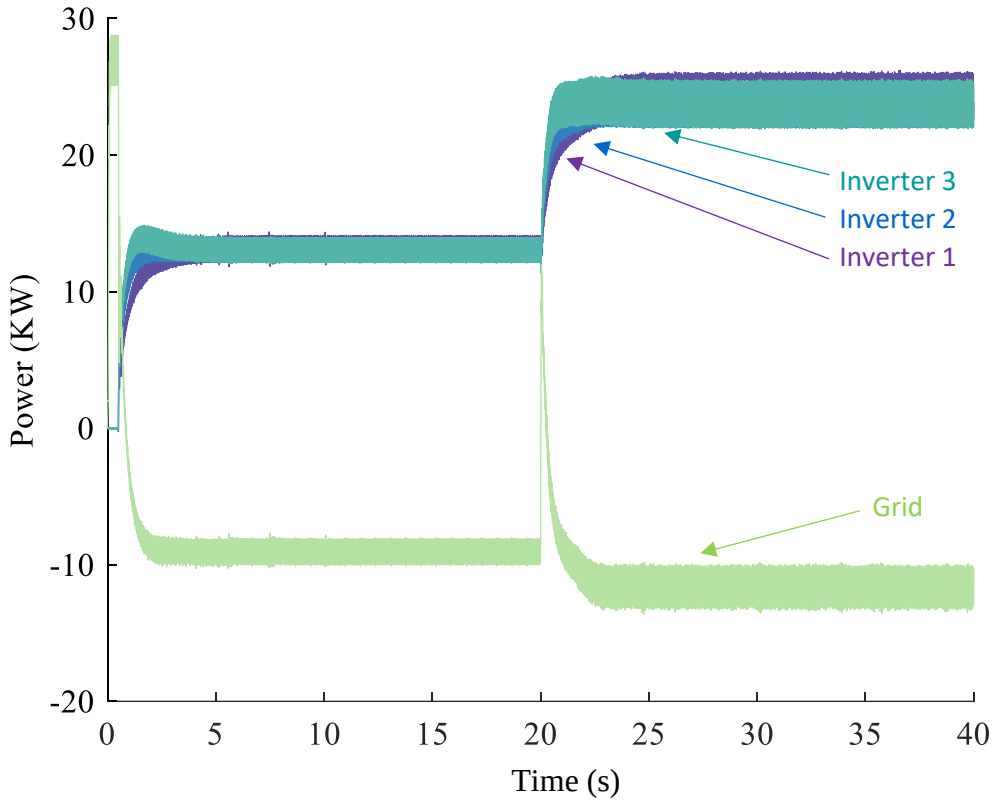

Figure 5.11 Active Power Output From Each of the Inverters, and Active Power Output Injected by the Grid, in Remote Configuration

This observation requires more explanation than the previous test. Observing only the first 20 seconds of the simulation, each inverter experiences a voltage drop across the impedance and local load. Since each feeder impedance is set to be equal, the observed voltage drop is identical at each inverter, and a unique active power setpoint is established based on the inverter's photovoltaic capacity and droop coefficient.

As power is exported from the inverters the voltage at the load bus is increased. However, each inverter contributes to raising the voltage a different amount, unlike the previous test,

where the voltage level is constant across the grid. The voltage at the load bus can be defined by the following steady state equations.

$$v_{load} = (v_{inv1} - \Delta v_{inv1}) = (v_{inv2} - \Delta v_{inv2}) = (v_{inv3} - \Delta v_{inv3}) \tag{5.8}$$

$$\Delta v = iZ_{feeder} \tag{5.9}$$

In these equations Δv is the voltage droop across the feeder, v_{load} is the voltage at the load bus, and *v* and *i* are the denoted inverter output voltage and current. Additionally, it must be remembered that the feeder impedance is the same for each inverter feeder, and the inverter voltage is defined by the following steady state equation.

$$v_{inv1} = v_{inv2} = v_{inv3} = v_0 \tag{5.10}$$

From this it can quickly be seen that each inverter must contribute equally to establishing the voltage at the load bus. This can only occur when every inverter outputs an equal portion of current, and therefore, active power. Thus, load sharing occurs naturally, independent of droop coefficients or inverter capacity, so long as the feeder impedance is equal.

From (5.8) it can also be concluded that differences in feeder impedance will result in each inverter contributing uniquely to the load bus voltage, proportional to the impedance value. If inverter 1 had a larger impedance than inverters 2 and 3, the voltage drop across the feeder would be larger. The voltage contribution to the load bus would therefore be smaller, and the other two inverters would have to contribute more current, and respectively, power.

In Figure 5.12, setpoint hunting is observed until about 5 seconds into the simulation at which point each inverter is producing the same output power, voltage and current. Additionally, it can be seen that all inverters are outputting power beyond that which is required by the load by observing the negative power value at the grid, representing power being exported out of the microgrid. Each local load is approximately 10 KW, as is shown in Table 2.1. Thus, with each inverter exporting approximately 13 KW, it is justified that the grid will be exporting approximately 9 KW.

During the next 20 seconds, the same effect is realized, however the load is increased by 30 KW of remote loads, or 10KW per inverter. The only difference to the inverters is that the voltage drop is larger, however the response is the same as previously discussed.

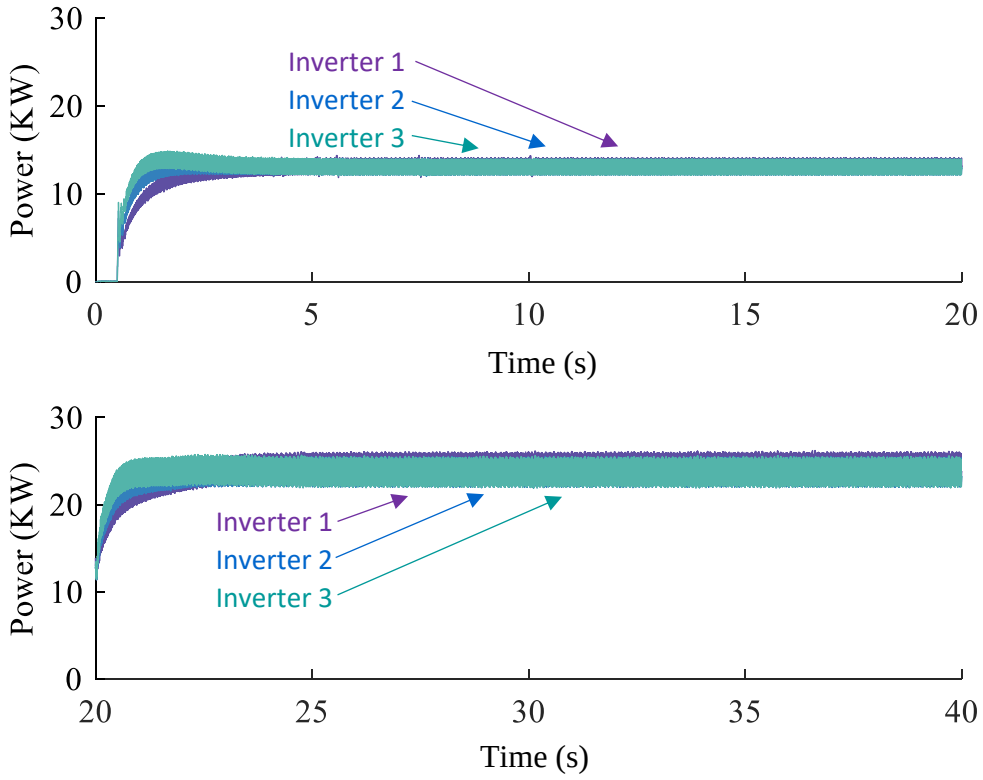

Figure 5.12 Active Power Exported by Each of the Inverters in Remote Configuration During the First 20 Seconds (a) and the Last 20 Seconds (b)

5.4.2.3 Test 5

In this test, the above stated assertion, that power will be shared at the load bus proportional to the feeder impedance, is demonstrated. Three unique impedance values are inserted. All values used are resistive in nature (R/X is greater than 1). The selected values are shown in Table 5.4.

Table 5.4 Values of Inverter Feeder Impedances for each Inverter

Inverter Number	L	R	R/X
Inverter 1	0.1mH	0.1884	5
Inverter 2	0.1mH	0.2939	7.8
Inverter 3	0.1mH	0.3768	10

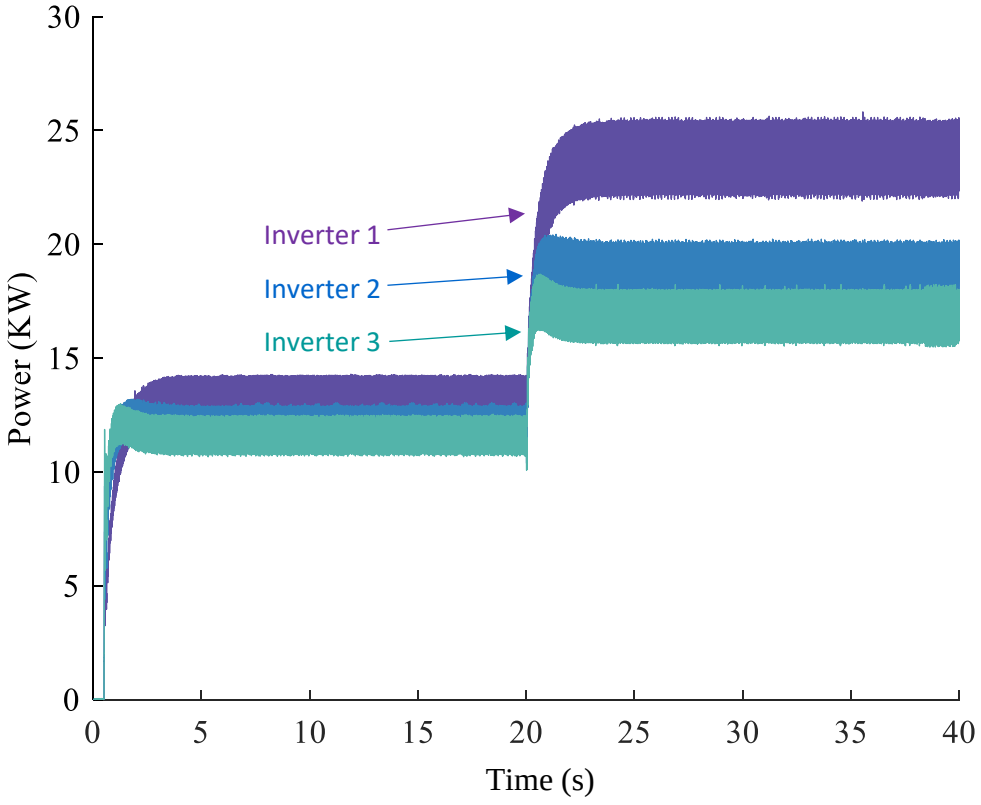

Figure 5.13 Inverter Active Power Profile for Each Inverter Where Inverter 1 Has the smallest Feeder Impedance, Followed by Inverter 2 and Inverter 3.

The impedance values are representative of inverter 1 being closest to the load bus, with inverter 2 next, and inverter 3 being farthest from the load bus. Since the inverters export power based on the voltage setpoint the result can again be explained using (5.8) and (5.9). The feeder impedances vary, however the Δv_{inv} must remain unchanged. Therefore, when the feeder impedance goes up for any given inverter, i_{inv} must go down for the same inverter. In other words, inverter 1, with the lowest feeder impedance is expected to output the most power, while inverter 3, with the highest feeder impedance, is expected to output the least power. Figure 5.13 confirms this conclusion.

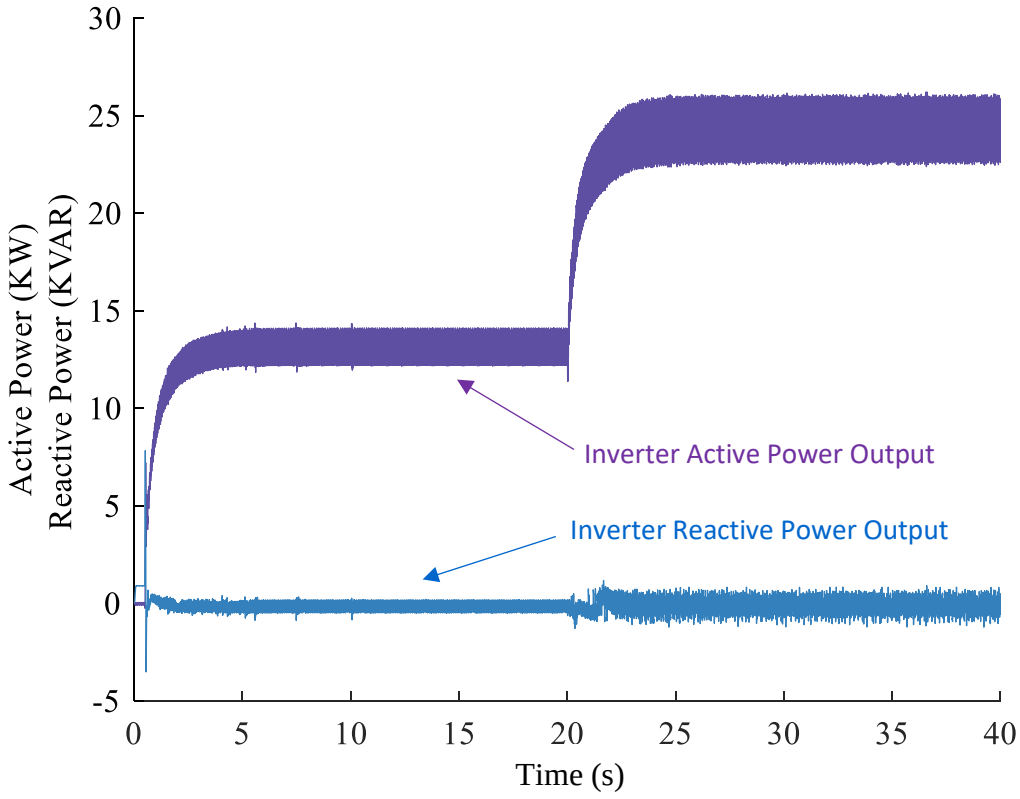

Figure 5.14 Inverter 1 Active and Reactive Power Output

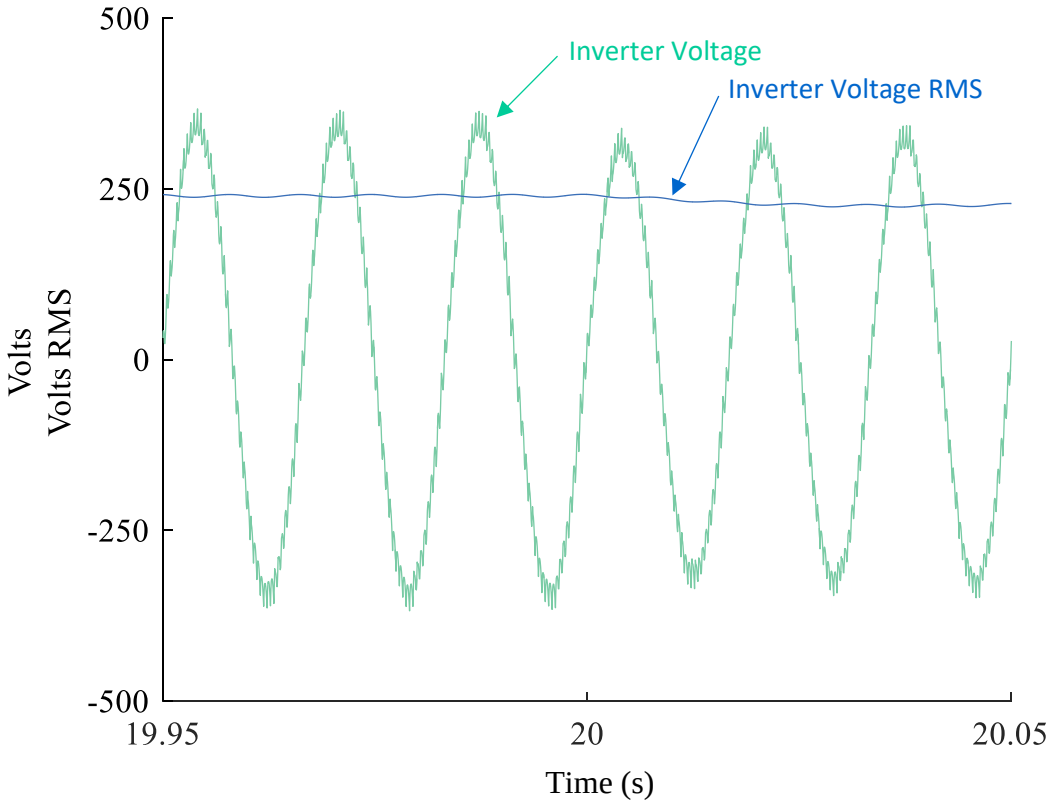

Figure 5.15 Inverter 1 Voltage Waveform and RMS Voltage During Load Transient.

5.4.2.4 Test 6

This test documents other aspects of the microgrid that are not presented in test 4. The conditions for the test are the same as test 4, including the presence of feeder impedance. Since no change in frequency is expected in this scenario, it can be concluded that reactive power will remain unchanged during the simulation. This is confirmed by Figure 5.14 which plots Inverter 1 Active and Reactive power on the same axis. It can be seen that the reactive power measurement is noisier during the last 20 seconds. This can be attributed to measurement error due to the meter having to read higher current values.

Since reactive power is unchanged, the observed change in active power can be entirely attributed to the voltage difference driving the droop equation. The voltage drop is seen in the

voltage waveform plot in Figure 5.15. When the load breaker shuts at 20 seconds, a reduction in RMS and peak voltage can be observed at the inverter.

5.4.3 Conclusions from Test Case 2

Test case 2 demonstrates the attribute of power sharing between droop controlled inverters in the case of a local bus, as well as a remote load bus. In the case of a local bus, the role of droop coefficients in managing power sharing between inverters in close proximity to each other is shown. Specifically, it is demonstrated that when droop coefficients are calculated with respect to photovoltaic capacity, the inverter for the array with more photovoltaic capacity will export more power than another inverter with less photovoltaic capacity.

Additionally, this test case demonstrates how power sharing between the same inverters is different when applied to a system with a remote bus. Specifically, it is shown that when the inverters are not close together, and therefore separated by an impedance the value of the impedance will determine the amount of power shared at any given remote load. In the case of two inverters, regardless of their photovoltaic capacity, the inverter that is closer to the remote load (has lower feeder impedance) will provide more power than the inverter that is further away (has greater feeder impedance).

5.5 Test Case 3

The purpose of this test is to demonstrate some benefits of the resistive droop control method to the future smart grid. Three key elements of a smart grid are improved reliability, availability and efficiency. A high capacity microgrid, like the one presented in this paper contributes to the greater grid's efficiency when it is able to consistently and fully supply its own needs. It has the potential to achieve greater reliability as technologies are put into place to enable it to operate in islanded mode during a grid fault. Availability is increased through design simplicity and redundancy. Design simplicity is achieved by accomplishing microgrid power management without the need for intercommunication systems. Redundancy is an inherent benefit of multiple distributed generators taking over the roll of a single central generator.

Many researches have investigated methods to control power flow in microgrids. Early focus was on the use of line interactive UPS as establishing the microgrid parameters via communication to an interactive bypass switch to allow independent microgrid operation and islanding [31]. More sophisticated hierarchical control is presented in [33] which again depends on the voltage and current measurements at the point of coupling between the grid and microgrid and wired communication between devices. In [34] it is seen that without wired communication or a perfect knowledge of the feeder impedances and distributed generator capacities, autonomous management of grid connected power flow is not possible by the use of droop control alone. However, it can also be inferred from these studies that if the voltage and current parameters at the point of connection between the grid and microgrid are known, the grid power flow can be controlled. Leveraging the concept of smart transformers, which are summarized in [35], it can be concluded that microgrid voltage can be controlled, based on current and voltage measurements at the point of connection between the grid and microgrid. By applying the droop control method to determining the voltage setpoint for the microgrid, power flow between the grid and microgrid can be managed without the need for communication cables.

This test demonstrates that, without the complexity and cost of intercommunication, a reverse application of the droop control method can be applied to a voltage controlling transformer on the grid side of the microgrid to compliment the droop control method being employed by the inverters, enabling the microgrid to fully supply its own demand. The result is a microgrid that is better able to contribute to the reliability, availability and efficiency of the overall grid.

Two tests are performed in this test case. The first demonstrates how the reverse application of the droop control method to the grid side voltage regulating transformer accurately and automatically allocates the microgrid's loads to the microgrid power sources. The second demonstrates that as the load approaches the distributed generator capacity, the microgrid will maximize the individual output of each distributed generator to cover the microgrid load. This test also shows that when the load does exceed the capacity of the distributed generators the grid will seamlessly supply the deficit.

5.5.1 Scenario for Test Case 3

The scenario for Test Case 3 consists of three parallel inverters, each with a local 10KW load, separated by an impedance from the load bus and the main grid. The grid is assumed to be connected to the microgrid via a voltage controlling transformer with logic and setpoint control capability. At 5 seconds into the simulation the transformer begins regulating the microgrid voltage to shift all load to the distributed generators. The load bus is applied to the microgrid at 20 seconds into the simulation with different loads in each test, in accordance with Table 5.5.

Table 5.5 Test Case 3 Loads Applied

Test Number	Load Bus Load (KVA)
Test 7	30 KVA
Test 8	120 KVA

In order to transfer all load to the distributed generators, the transformer is programmed with a voltage setpoint controller. The basis for this controller can be derived from the voltage balance equation presented in (5.8) and presented again below in a different form.

$$(v_{grid} - i_{grid}Z_{grid}) = (v_{load}) = (v_{inv} - i_{inv}Z_{inv}) \tag{5.11}$$

In order for all load to be transferred to the distributed generators, the grid current must be set to zero. From the equation above it can be seen that if the grid voltage is lowered to equal the load voltage the load current will have to be provided by the inverters. A voltage setpoint can be determined using (4.16), which is presented in a slightly different form below.

$$(v_{grid(rms)} - v_{load(rms)}) = k_v(P_{grid}) \tag{5.12}$$

The load voltage can be made into the setpoint for this equation. Making this change and rearranging to solve for the voltage setpoint yields the following control equation.

$$v_{setpoint} = v_{grid(rms)} - k_v(P_{grid}) \quad (5.13)$$

Using (5.13) to generate the transformer voltage setpoint allows the microgrid voltage to be used as a medium to drive the inverters to change their power output until the grid is fully powered by the inverters, while also ensuring no excess power is produced. This feature is demonstrated using the same scenario as is used in Test Case 2, but with the addition of the previously discussed voltage control at the transformer. The droop coefficient of the transformer (k_v) can be generated using the same method as used for the inverters. For these simulations, a larger transformer capacity of 125 KVA is selected. However, unlike the inverters, the transformer must assume nominal voltage is achieved at median power transfer, allowing deviations from nominal to raise or lower the power transfer. Additionally, the voltage band must be maintained tight to prevent over or undervoltage conditions on the microgrid. Therefore, a band of 230 to 250 VRMS is selected. Hard limits are applied to the transformer to prevent operation outside of this band.

$$k_{v(transformer)} = \frac{250\ VAC - 230\ VAC}{125\ KVA} = 0.16 \quad (5.14)$$

5.5.2 Test Results

Select figures were generated to document each test. The figures and accompanying discussion for the tests of Test Case 3 follow.

5.5.2.1 Test 7

In this test the simulation is run for 40 seconds. During the first 5 seconds the grid transformer outputs the nominal setpoint of 240 VRMS. At 5 seconds into the simulation the transformer switches to the previously discussed voltage control mode. The grid RMS voltage immediately raises, causing an increase in microgrid voltage. The inverters respond by reducing their power output, eliminating the power that was being exported from the grid. At 20 seconds into the simulation the load breaker shuts, lowering the grid voltage. The transformer and the inverters respond simultaneously, retaining microgrid voltage within bounds while increasing the inverter power output exactly to match the increased demand.

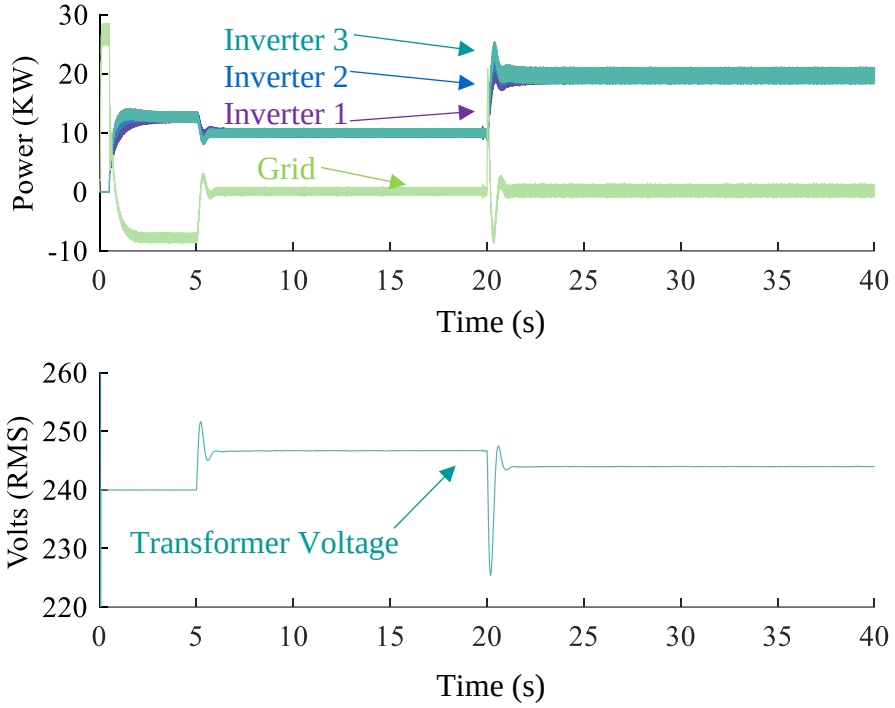

Figure 5.16 (a) Grid and Distributed Generators Output Power, (b) RMS Voltage Measured at the Grid Transformer

5.5.2.2 Test 8

This test adds additional load to the load bus, totaling 120 KW, in order to exceed the distributed generator capacity. Each inverter has a distinct photovoltaic capacity, in accordance with Table 5.3. During the first 5 seconds the grid transformer outputs the nominal setpoint of 240 VRMS. At 5 seconds into the simulation the transformer switches to the previously discussed voltage control mode. The response is consistent with the previous test. At 20 seconds into the simulation the excessive load is added, resulting in the grid voltage lowering to maximize each inverter output. Once each inverter has achieved its full capacity, the voltage continues to lower until it reaches the operational limit. At that point voltage is held steady and the grid picks up the remainder of the load.

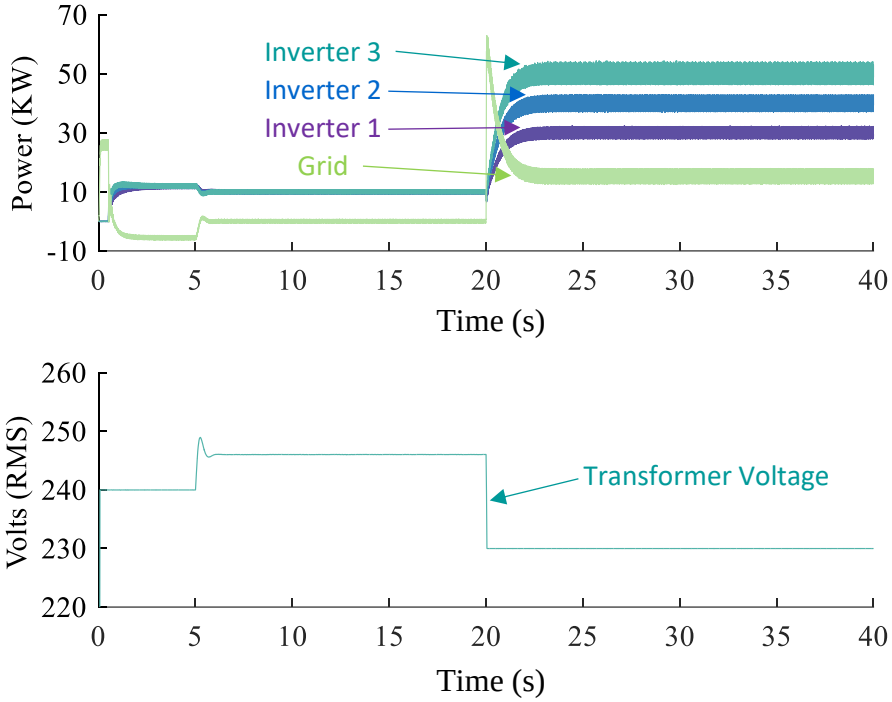

Equation 5.15 (a) Grid and Distributed Generators Output Power, (b) RMS Voltage Measured at the Grid Transformer

5.5.3 Conclusions from Test Case 3

From these tests a useful decentralized integrated microgrid control function is demonstrated. These test successfully demonstrated that a variation of the droop equations can be applied to the grid transformer in order to establish a voltage setpoint. This feature allows the transformer to work with the distributed generators to force the microgrid to be entirely self-powered up to the limits of the distributed generators. As long as the capacity is sufficient to carry the microgrid, the main grid can operate unaffected by the microgrid. Thus, fluctuations in microgrid load will have no effect on the main grid load. Additionally, the microgrid will have no power transfer with the main grid during steady state conditions, placing the microgrid in the ideal state for seamless islanding in the event of the loss of the main grid. Finally, it was shown that by incorporating operational voltage limits to the transformer, the microgrid voltage is maintained within proper limits to supply the needs of the load. These limits also

ensure that in the event that the microgrid is unable to meet the load demands the grid will accurately and automatically assume the remaining load.

Chapter 6 - Conclusion and Future Work

6.1 Introduction

The purpose of this chapter is to summarize key elements learned from this study and present some of the questions not answered by this study as ideas for future research.

6.2 Summary of Key Observations

The scenarios developed and the tests performed in this work evaluate the use of droop control with grid connected photovoltaic inverters in a microgrid environment where capacity is able to exceed the local loads. While today it is not common to find microgrids of this sort, this scenario is likely to be prevalent in the near future. With new technologies enabling lower cost photovoltaic cells, and creative business structures allowing for upfront costs of photovoltaic installations to be paid during the systems lifetime, distributed generation is becoming more readily available to many property owners in the United States. It is likely that this trend will continue.

While today's reality that a photovoltaic installation will take years to provide a return on investment, and therefore must be used in maximum power point tracking mode to maximize investment return, changes in technology may overcome this reality. In a future state, we may find that investment in photovoltaic generators is worthwhile for other benefits such as continuity of power, or contribution to greenhouse gas reduction. When this reality occurs, photovoltaic resource owners will no longer be compelled to operate in maximum power point tracking grid feeding mode. Then the additional benefits of communal power sharing will begin to be realized.

Benefits of operating microgrids with droop controlled grid supporting inverters include the following.

1. Better voltage regulation at the load bus.

2. When used in conjunction with a grid forming converter or transformer, the microgrid is able to operate islanded, thereby improving reliability for the consumers.

3. Power sharing between inverters prevents inverters from operating at maximum capacity, potentially reducing wear and improving longevity of limiting components.

In this paper, resistive droop control is presented. Traditional droop control is also possible on primarily resistive microgrids, however the droop control method presented here can be advantageous, specifically as follows.

1. Resistive droop control manages active power sharing via voltage drop, making it effective for microgrids without inertia, as long as the microgrid loads have a power factor near 1.

2. Resistive droop control provides a droop control method that can be directly applied to an AC or DC microgrid.

As has been previously suggested, many changes may be observed in the grid structure in the coming years. Many researchers have studied droop control methods between distributed generators as a useful element of future grids. Though the future state of the electrical grid is unknown, it is certain that distributed generation is playing a role in causing change. Regardless of what form the future grid takes, so long as distributed generation is included the following observations of this research will be beneficial.

1. The use of droop control on a large grid with actual impedances is an effective means of managing power flow between distributed generators without the use of communication cables.

2. When a large central generator is used to establish reference voltage and frequency for clusters of distributed generators, the power contribution of those distributed generators can be easily controlled by small variations in the voltage and frequency setpoints of the central generator.

While it is unknown what changes will come in solar and inverter technology, it is likely that these changes will build on lessons from the past. Droop control has long been an important part of achieving load sharing among large central generators in our current power system. This control strategy poses many possible benefits in future control systems as well.

6.3 Smart Grid Applications

Test case 3 opens the door to a number of interesting future applications for smart grid. Specifically, it shows that when the microgrid developed by this paper is used in conjunction with a smart transformer, the transformer can establish microgrid power sharing without the need for communication with the inverters. When this method is applied to remove all load from the grid, the microgrid ends up in a condition where it can be seamlessly islanded during a grid outage, and where changes in microgrid load can be managed by the microgrid itself. This has the potential to increase the overall grid efficiency.

For example, so long as distributed generator capacity supports, all local load transients are managed at the microgrid by the distributed generators. Thus, changes in microgrid loading is not observed at the central grid during the period in which the distributed generators are supporting the microgrid. This benefits the larger grid by making the microgrid load profile more predictable.

When the larger grid consists of multiple such microgrids the central generator will greatly benefit from a much more predictable load profile during periods of peak generation. In the case of photovoltaic distributed generators, as efficiency and capacity are increased, the central generator could benefit from minimal load variability during daytime hours when the microgrids are operating autonomously. Typically, daytime hours are characterized by the largest load variations, while nighttime hours are characterized by lower and more stable demand profiles. Thus, during nighttime hours, the microgrid loads would transfer to the central generator and still the load profile will remain lower and more stable than is presently seen by the central generator during the day. These improvements can yield better overall power distribution efficiency, resulting in lower costs for all.

With more stable and consistent load profiles comes the additional benefit of predictability when planning for preventive maintenance. The grid will be able to achieve higher availability by scheduling and executing preventive maintenance on grid distribution equipment during periods when the grid is not needed because the microgrids are operating autonomously. Additionally, distributed generator maintenance can be performed during periods when the generator is unable to produce power (after sunset). Thus, both power sources have large offset maintenance windows such that power consumption does not need to be impacted by preventive maintenance. The large no-impact maintenance windows allow for greater flexibility and contingency plan execution during maintenance. Overall these benefits yield greater power system availability.

Besides these direct benefits of greater availability and efficiency in the power system, another beneficial feature in future smart girds is increased control and communication. Many researchers have concluded that wired communication is necessary to achieve the level of control desired for future grid systems. Implementing the infrastructure for wired communication has drawbacks included greater complexity which can negatively impact reliability and availability, and greater cost. The information gained through improved communication, on the other hand can improve efficiency, and has the potential of offsetting the additional cost. The truly viable financial and technical solution will most likely be a blend of wired and decentralized solutions.

The microgrid in this paper would function successfully in a blended smart grid like the one presented in Figure 2.1. In this concept, the central generator oversees distribution and is able to monitor the voltage setpoint of the smart transformers at the point of connection of each microgrid. The voltage setpoint can be interpolated to establish the microgrid capacity and load. Two way communication would allow the central operator to island a stable microgrid by de-energizing the smart transformer where microgrid conditions and equipment support, in order to accomplish distribution system maintenance while minimizing consumer interruptions. Additionally, with the increase in electronic and computer loads, some consumers may find it advantageous to maintain DC microgrids to eliminate the damaging effect of harmonics. As

previously stated, the droop control method presented in this paper functions equally well in a DC microgrid environment.

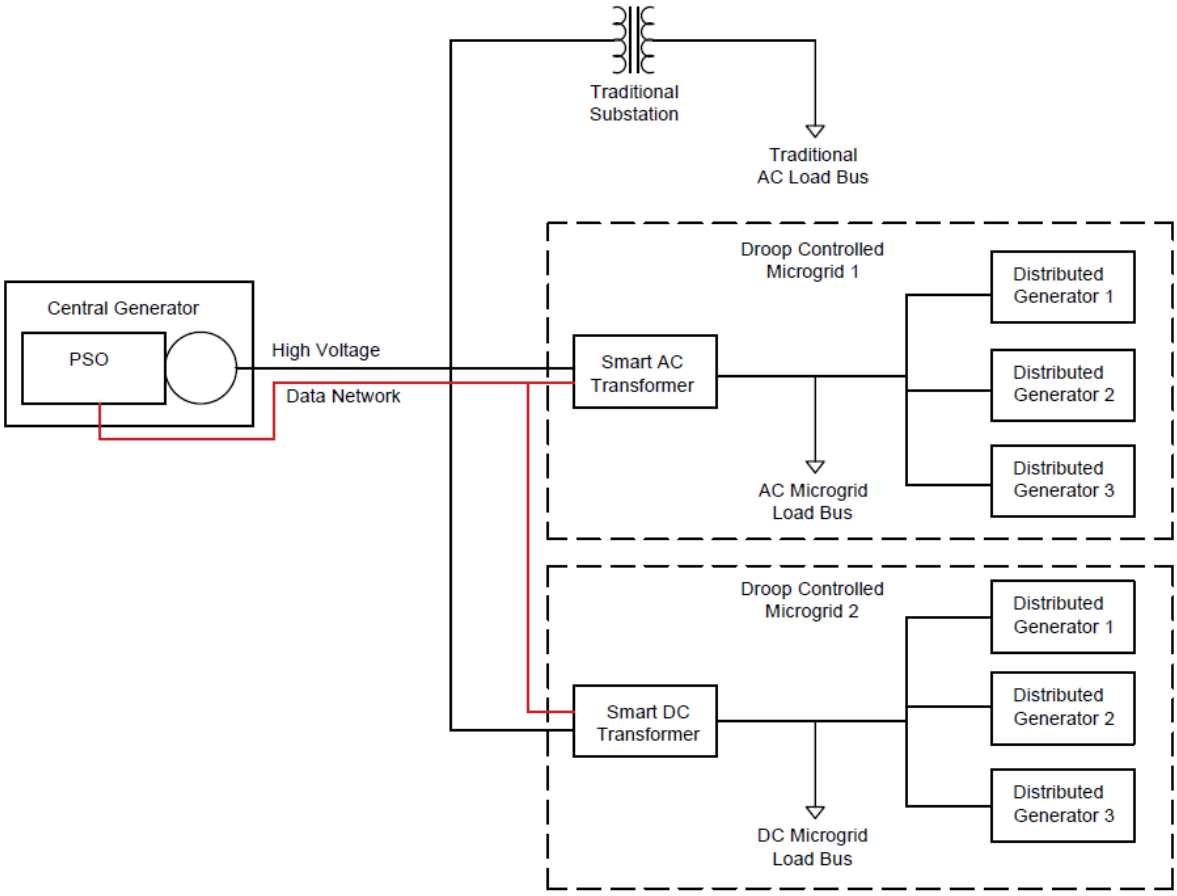

Figure 6.1 Theorized Future Smart Grid with Droop Controlled Microgrids

Despite the many benefits presented for the use of smart transformer managed autonomous microgrids, there is a cost to the distributed generator. By choosing to operate in the droop control mode rather than the maximum power point tracking mode the average inverter output over time will be lower. With the desire to maximize the rate of return on investment in distributed generation, the benefits of droop control may not outweigh the cost of reduced average production. Thus, the efficiency of distributed generators must improve in order for

the cost and payback period of the distributed generators to be reduced to the point where droop controlled microgrids become advantageous to the distributed generator.

In summary, the benefits and challenges of autonomous droop controlled microgrids, with grid power contribution managed by smart transformers, are as follows.

1. A more stable and predictable load profile yields increased grid efficiency.
2. The existence of a larger no-impact window for planned maintenance of grid distribution equipment yields increased availability.
3. In microgrids where grid forming technology is implemented, by maintaining microgrids in an Island ready condition to continue operation after a grid fault, greater reliability can be realized.
4. The needed communication functions of the microgrid are achieved without the need for communication wires within the microgrid.
5. The droop control mode lengthens the payback period for the distributed generator, but will become viable when distributed generator prices decline.

6.4 Future Work

Though this work touches on some of the benefits of droop control use in distributed generation systems, more work is needed in preparation for this future state. Of particular importance is a greater understanding of transitioning distributed generators from grid connected to islanded. Another interesting transition worth investigating is the transition from a microgrid with load that is greater than distributed generation capacity, to a microgrid with load that is less than distributed generation capacity. Specific topics could include the following:

1. Investigation into the transition of microgrids of distributed generators between grid connected and islanded, while operating in droop control.

2. Investigation into managing reactive power flow in Inertialess AC microgrids.

3. Investigation into the application of droop control in DC microgrids.

4. Investigation into smart transformer technologies for supervising power flow in droop controlled microgrids.

These and other topics can lead to better understandings that may help grid operators and developers, and related technologies companies develop the technologies and methodologies of the future.

There is no question that the grid is changing. There is also no question that distributed generation is playing a role in that change. There are many hinge points still ahead of us in the development of the future grid. Investigations of this sort are essential to enable wise decision making during these early hinge points, each of which will play a role in determining the future state of power distribution. It has been said that the world runs on "energy" and so these changes to our energy infrastructure have the ability to impact for good the very way the world runs. Continued research on these topics will enable us to achieve a future state that exceeds even our current expectations.

References

[1] J. G. de Matos, F. S. F. e Silva and L. A. de S. Ribeiro, "Power Control in AC Isolated Microgrids with Renewable Energy Sources and Energy Storage Systems," *IEEE Transactions on Industrial Electronics,* vol. 62, no. 6, pp. 3490 - 3498, 2015.

[2] H. mahmood, D. Michaelson and J. Jiang, "Reactive Power Sharing in Islanded Microgrids Using Adaptive Voltage Droop Control," *IEEE Transactions on Smart Grid,* vol. 6, no. 6, pp. 3052-3060, 2015.

[3] A. Bendib and A. Chouder, "Droop Controller Based Primary Control Scheme for Parallel-Connected Single-Phase Inverters in Islanded AC Microgrid," *The 5th International Conference on Electrical Engineering - Boumerdes (ICEE-B),* 2017.

[4] J. Rocabert, A. Luna, F. Blaabjerg and P. Rodriguez, "Control of Power Converters in AC Microgrids," *IEEE Transactions on Power Electronics,* vol. 27, no. 11, pp. 4734 - 4748, 2012.

[5] J. M. Guerrero, J. Matas, L. Garcia de Vicuna, M. Castilla and J. Miret, "Decentralized Control for Parallel Operation of Distributed Generation Inverters Using Resistive Output Impedance," *IEEE Transactions on Industrial Electronics,* vol. 54, no. 2, pp. 994-1004, 2007.

[6] C. K. Sao and P. W. Lehn, "Control and Power Management of Converter Fed Microgrids," *IEEE Transactions on Power Systems,* vol. 23, no. 3, pp. 1088-1098, 2008.

[7] J. M. Guerrero, J. Matas, L. Garcia de Vicuna, Castilla, Miguel and J. Miret, "Wireless-Control Strategy for Parallel Operation of Distributed-Generation Inverters," *IEEE Transactions on industrial electronics,* vol. 53, no. 5, pp. 1461 - 1470, 2006.

[8] Institute of Electrical and Electronic Engineers, *IEEE Recommended Practice for Industrial and Commercial Power Systems Analysis,* New York: The Institute of Electrical and Electronics Engineers, Inc., 1997.

[9] D. Beeman, Industrial Power Systems Handbook, New York: McGraw-Hill Book Company, Inc., 1955.

[10] S. Saha and V. P. Sundarsingh, "Novel grid-connected photovotaic inverter," *Proc. Inst. Elect. Eng.,* vol. 143, no. 2, pp. 143-156, 1996.

[11] P. G. Barbosa, H. A. C. Braga, M. D. C. B. Rodrigues and E. C. Teixeira, "Boost current multilevel inverter and its application on single-phase grid-connected photovoltaic systems," *IEEE Transactions on Power Electronics,* vol. 21, no. 4, pp. 1116-1124, 2006.

[12] B. M. T. Ho and H. S.-H. Chung, "An integrated inverter with maximum power tracking for grid-connected PV systems," *IEEE Transactions on Power Electronics,* vol. 20, no. 4, pp. 953-962, 2005.

[13] Y. Yongheng and F. Blaabjerg, "Overview of Single-Phase Grid-Connected Photovoltaic Systems," *Electric Power Components and Systems,* vol. 43, no. 12, pp. 1352-1363, 2015.

[14] R. A. Messenger and J. Ventre, Photovoltaic Systems Engineering, Boca Raton: Taylor and Francis Group, LLC, 2010.

[15] D. F. Zaions, A. J. Balbino, C. L. Baratieri and A. L. Stankiewicz, "Comparative Analysis of Buck and Boost Converters Applied to Different Maximum Power Point Tracking Techniques for Photovoltaic Systems," *Power Electronics Conference, 2017 Brazilian,* pp. 19-22, 2017.

[16] R. W. Erickson and D. Maksimovic, Fundamentals of Power Electronics, Norwell, MA: Kluwer Academic Publishers, 2001.

[17] S. Buso and P. Mattavelli, Digital Control in Power Electronics, USA: Morgan & Claypool, 2006.

[18] R. H. Muhammad, Power Electronics Handbook (4th Edition), Elsevier, 2018.

[19] M. P. Kazmierkowski and L. Malesani, "Current Control Techniques for Three-Phase Voltage-Source PWM Converters: A Survey," *IEEE Transactions on Industrial Electronics,* vol. Vol. 45, no. No. 5, pp. 691-703, October 1998.

[20] L. Malesani and P. Tomasin, "PWM Current Control Techniques of Voltage Source Converters - A Survey," *Proceedings of the IECON '93., International Conference on Industrial Electronics, Control and Instrumentation,* pp. 670-675, 1993.

[21] P. C. Krause, O. Wasynczuk and S. D. Sudhoff, Analysis of Electric Machinery, Second Edition ed., John Wiley & Sons, Inc, 2002.

[22] R. Zhang, M. Cardinal, P. Szczesny and M. Dame, "A Grid Simulator with Control of Single-Phase Power Converters in D-Q Rotating Frame," *IEEE,* pp. 1431-1436, 2002.

[23] L. Cui, L. Zhenxing and Z. Botao, "Control for Single-phase Power Inverter System Based on Lead Signal and dq Transform," *IEEE; 27th Chinese Control and Decision Conference,* pp. 3481-3484, 2015.

[24] B. Crowhurst, E. F. El-Saadany, L. El Chaar and L. A. Lamont, "Single-Phase Grid-Tie Inverter Control Using DQ Transform for Active and Reactive Load Power Compensation," *IEEE International Conference on Power and Energy,* pp. 489-494, 2010.

[25] M. Gonzalez, V. Cardenas and F. Pazos, "DQ Transformation Development for Single-Phase Systems to Compensate Harmonic Distortion and Reactive Power," *IEEE,* pp. 177-182, 2004.

[26] Y. Xue, L. Chang, S. B. Kjaer, J. Bordonau and T. Shimizu, "Topologies of Single-Phase Inverters for Small Distributed Power Generators: An Overview," *IEEE Transactions on Power Electronics,* vol. 19, no. 5, pp. 1305-1314, 2004.

[27] S. Jain and V. Agarwal, "A Single-Stage Grid Connected Inverter Topology for Solar PV Systems With Maximum Power Point Tracking," *IEEE Transactions on Power Electronics,* vol. 22, no. 5, pp. 1928-1940, 2007.

[28] R. O. Caceres and I. Barbi, "A Boost DC-AC Converter: Analysis, Design, and Experimentation," *IEEE Transactions on Power Electronics,* vol. 14, no. 1, pp. 134-141, 1999.

[29] C.-M. Wang, "A Novel Single-Stage Full-Bridge Buck-Boost Inverter," *IEEE Transactions on Power Electronics,* vol. 19, no. 1, pp. 150-159, 2004.

[30] N. Vazquez, J. Almazan, J. Alvarez, C. Aguilar and J. Arau, "Analysis and Experimental Sudy of the Buck, Boost and Buck-Boost Inverters," *IEEE Power Electronics Specialists Conference,* vol. 99, pp. 801-806, 1999.

[31] J. M. Guerrero, J. C. Vasquez, J. Matas, M. Castilla and L. Garcia de Vicuna, "Control Strategy for Flexible Microgrid Based on Parallel Line-Interactive UPS Systems," *IEEE Transactions on Industrial Electronics,* vol. 56, no. 3, pp. 726 - 736, 2009.

[32] IEEE Standard 1547-2018, *IEEE Standard for Interconnection and Interoperability of Distributed Energy Resources with Associated Electric Power Systems Interfaces,* New York, 2018.

[33] J. M. Guerrero, J. C. Vasquez, J. Matas, L. G. de Vicuna and M. Castilla, "Hierarchical Control of Droop-Controlled AC and DC Microgrids - A General Approach Toward

Standardization," *IEEE Transactions on Industrial Electronics,* vol. 58, no. 1, pp. 158-172, 2011.

[34] H. Han, X. Hou, J. Yang, J. Wu, M. Su and J. M. Guerrero, "Review of Power Sharing Control Strategies for Islanding Operation of AC Microgrids," *IEEE Transaction on Smart Grid,* vol. 7, no. 1, pp. 200-215, 2016.

[35] H. Helali, A. Bouallegue and A. Khedher, "A Review of Smart Transformer Architectures and Topologies," *17th International Conference on Sciences and Techniques of Automatic Control and Computer Engineering,* pp. 449-454, 2016.

[36] J. Thornycroft and T. Markvart, "Grid Connection of PV Generators: Technical and Regulatory Issues," in *Practical Handbook of Photovoltaics*, 2012.

[37] International Energy Agency, "Demonstration Test Results for Grid Interconnected Photovoltaic Power Systems," *IEA Report PVPS T5-02,* 1999.

[38] International Energy Agency, "Probability of Islanding in Utility Networks Due to Grid Connected Photovoltaic Power Systems," *IEA Report PVPS T5-07,* 2002.

[39] IEEE Standard 929-2000, *Recommended Practice for Utility Interface of Photovoltaic Systems,* 2000.

[40] N. Mohan, T. M. Undeland and W. P. Robbins, Power Electronics; Converters, Applications, and Design. Third Edition, John Wiley & Sons, Inc, 2003.

[41] D. N. Zmood and D. G. Holmes, "Stationary Frame Current Regulation of PWM Inverters With Zero Steady-State Error," *IEEE Transactions on Power Electronics,* vol. 18, no. 3, pp. 814-822, May 2003.

[42] IEEE, *1547-2018 IEEE Standard for Interconnection and Interoperability of Distributed Energy Resources with Associated Electric Power Systems,* New York: Institute of Electrical and Electronics Engineers, Inc., 2018.

[43] A. Adib and B. Mirafzal, "Virtual Inductance for Stable Operation of Grid-Interactive Voltage Source Inverters," *IEEE Transactions on Industrial Electronics,* vol. 8, no. 66, pp. 6002-6011, 2019.

[44] A. Singh and B. Mirafzal, "An Efficient Grid-Connected Three-Phase Single-Stage Boost Current Source Inverter," *IEEE Power and Energy Technology Systems Journal,* vol. 3, no. 6, pp. 142-151.

[45] A. Adib, J. Lamb and B. Mirafzal, "Ancillary Services via VSIs in Microgrids With Maximum DC-Bus Voltage Utilization," *IEEE Transactions on Industry Applications,* vol. 2, no. 54, pp. 1663-1670, 2018.

Appendix A: Modeling a Single Phase Inverter in PSCAD

A.1 Introduction

To perform the tests discussed herein, a model was constructed using PSCAD X4 power system simulation software, a product of the Manitoba HVDC Research Center. This software allows for modeling power, control and logic circuits for power system research. The following provides the needed information for a user familiar with the PSCAD environment to build the test model used for the research in this thesis.

A.2 Distribution Grid

The distribution grid (Figure A.1) is described in Chapter 2. The power source is ideal to eliminate voltage drop on the 240 VRMS network. In lieu of using the photovoltaic array building block in PSCAD, a simple DC source is used. Since this study does not benefit from the added complexity of calculating luminescence, insolation, and photovoltaic array characteristics, a simple DC source can be used. Included in this simplification is the assumption that current is available to the inverter, sufficient to supply the defined power. Therefore, it becomes necessary also to artificially limit power from exceeding the defined parameter. For this reason, power limiters are used within the inverters to ensure no inverter supplies power beyond what its associated photovoltaic array would be capable of.

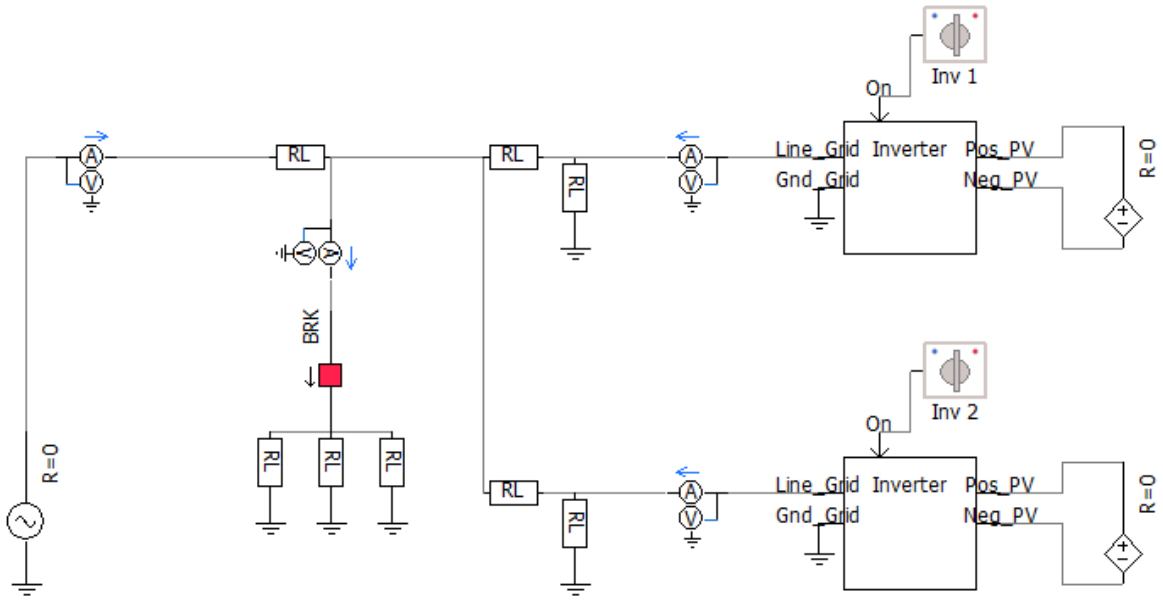

Figure A.1 Distribution Grid Circuit Diagram in PSCAD

A.3 Inverter

The inverter module is a custom PSCAD component with four electrical input/output ports, and one logical input port. The logical input port is used to turn the inverter 'on' and 'off'. Two electrical ports are for connecting the two lines of the AC distribution grid. Two electrical ports are used for connecting the two sides of the DC photovoltaic array.

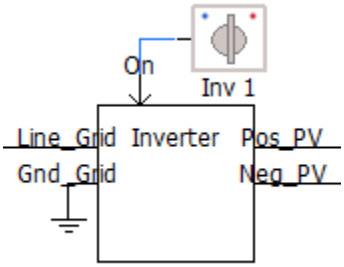

Figure A.2 PSCAD Inverter Component

The Inverter component contains two portions. First is the power electronic circuit that performs the power transfer from the DC voltage source to a modulated AC output waveform. Second is the control system that provides the firing pulse train to the full bridge inverter of the power electronic circuit. Those two portions are presented below.

A.3.1 Power Electronic circuit

The inverter power electronic circuit (Figure A.3) is described in chapter 3. In the circuit diagram below power flows from right to left, from the DC source to the grid. The full bridge inverter consists of four switches. Each switch is controlled by the firing pulse train generated by the full bridge inverter controller. The output waveform is passed through a filter to the grid.

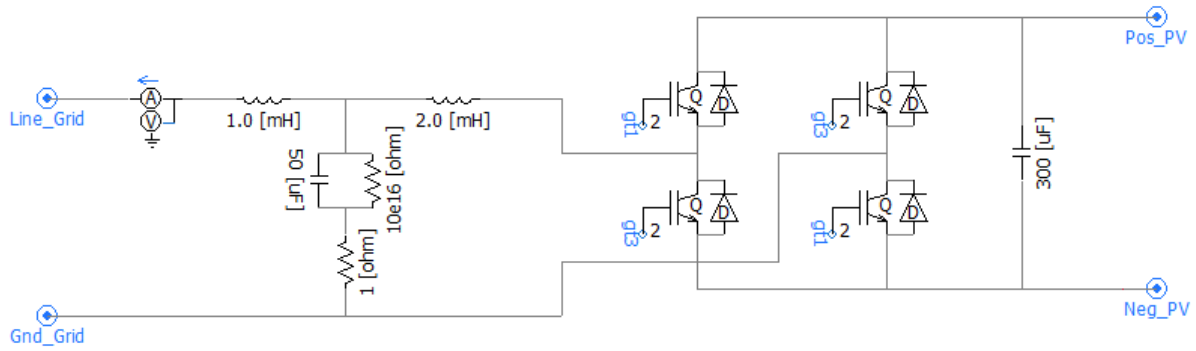

Figure A.3 Inverter Power Electronic Circuit Diagram in PSCAD

A.3.2 Full Bridge Inverter Controller

The full bridge inverter controller is realized in 10 steps.

1. Converter startup sequence
2. Phase locked loop reference angle generator
3. Single phase d-q transformation
4. Droop Controllers
5. Current and Voltage Control Loops
6. Inverse d-q transformation

7. Pulse width modulator and firing pulse generator

A.3.2.1 Startup sequence

The purpose of the startup sequence is to allow the system to normalize prior to initiating inverter operation. This is accomplished by inputting the simulation time component into a single input level comparator. The level comparator uses a threshold input value of 0.5sec, a low output of 0 and a high output of 1.

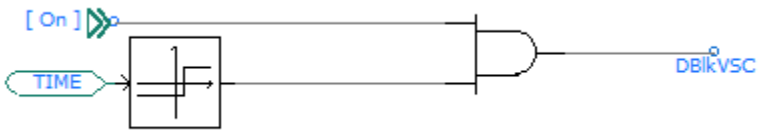

Figure A.4 Inverter Startup Sequence Circuit Diagram in PSCAD

A.3.2.2 Phase Locked Loop

The phase locked loop generates the phase angle for the dq controllers. This is accomplished via a custom block which uses the quadrature component of the voltage (vq) as an input. The vq value is generated in the DQ transformation block, which requires input from the phase locked loop. These two components communicate back and forth until they are able to provide the proper setpoints to each other. The outputs of the phase locked loop are the phase angle and the frequency.

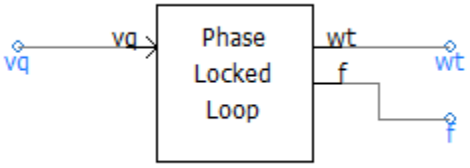

Figure A.5 Phase Locked Loop Component

The phase locked loop functions by finding the phase angle when vq is equal to 0, and this indicates phase alignment with the dq transformation. The phase angle is brought to 0 via a PI controller and the error signal is add to the nominal value of $2\pi f$. This generates the angular velocity which is integrated over time to find the angular velocity over time (ωt). The angular velocity can be divided by 2π to find the frequency.

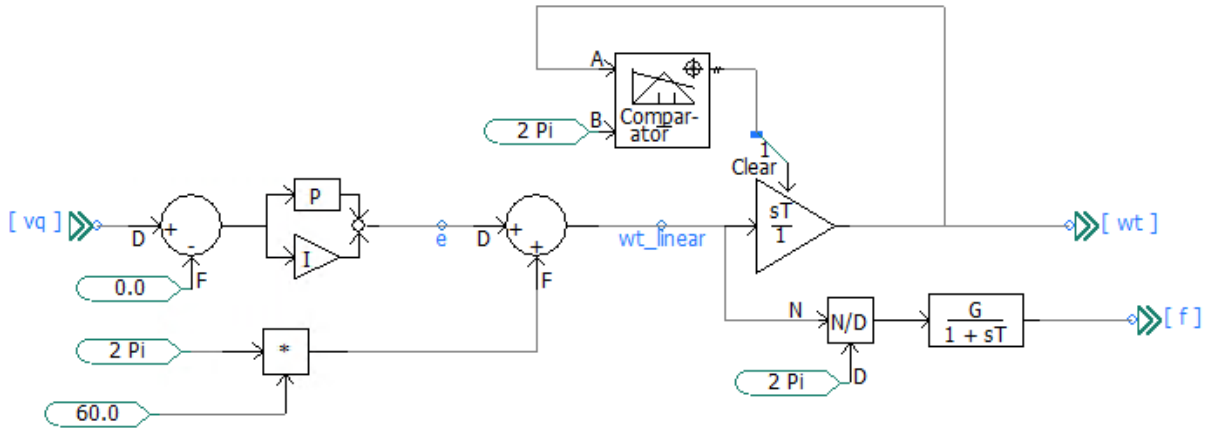

Figure A.6 Phase Locked Loop Circuit Diagram in PSCAD

A.3.2.3 DQ Transformation

The DQ transformation is performed on both the measured voltage and current signals. These signals are measured on the grid side of the output filter. The output of the phase locked loop is supplied to both blocks. The transformation generates the d and q components of the input voltage or current signal.

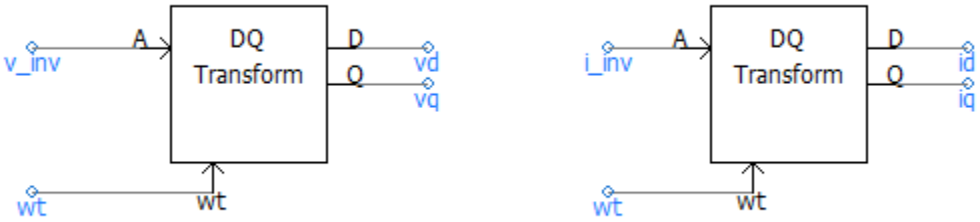

Figure A.7 DQ Transform Component Model in PSCAD

The dq transformation functions by first determining an imaginary orthogonal component of the input signal. This is accomplished by instituting a quarter phase delay. This is completed by sampling each quarter period 8 times and storing the value for a half period. To do this, the sampling period is established as 32 times the frequency, as implemented by the multiplier component. The sampling period is provided as an input to a pulse train to generate a pulse at the required frequency. The pulse train oscillates between 1 and 0 at the input frequency. The output of the pulse train is provided to two edge detectors. One edge detector operates when a pulse of value 1 is received. The other operates when a pulse of value 0 is received. When the edge detectors operate, they output an instantaneous value of 1. Otherwise they output 0. The edge detectors provide an alternating timing input to a series of sixteen pulse samplers. The pulse samplers are set to operated using a non-interpolated pulse train input signal. When the pulse samplers operate, they pass the input value to the output and store the next input value.

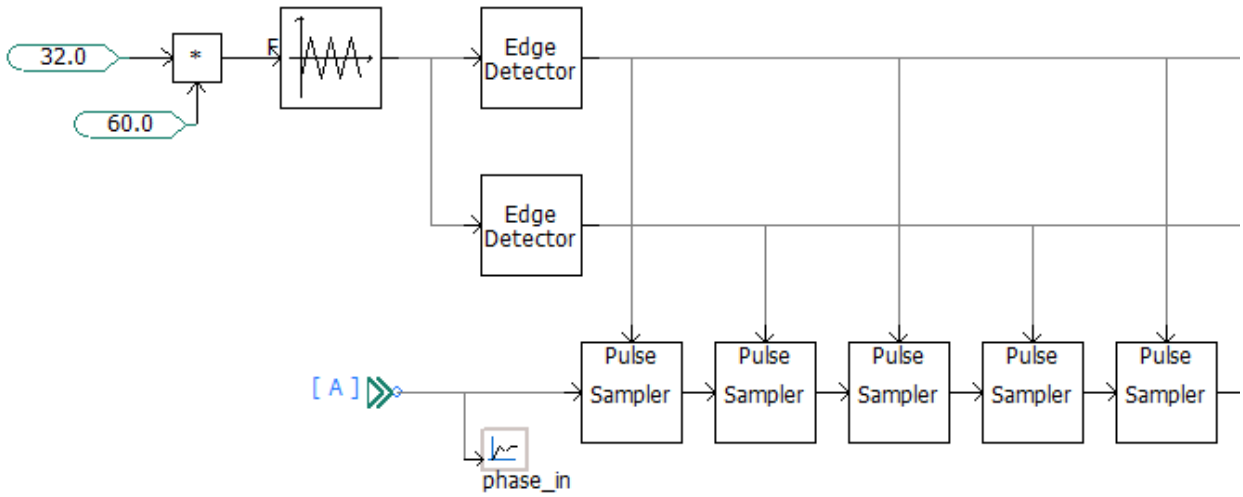

Figure A.8 Imaginary Orthogonal Signal Generator Circuit Model in PSCAD

The output of the imaginary orthogonal signal generator is supplied to a mathematical transformation to calculate the direct and quadrature components of the two signals.

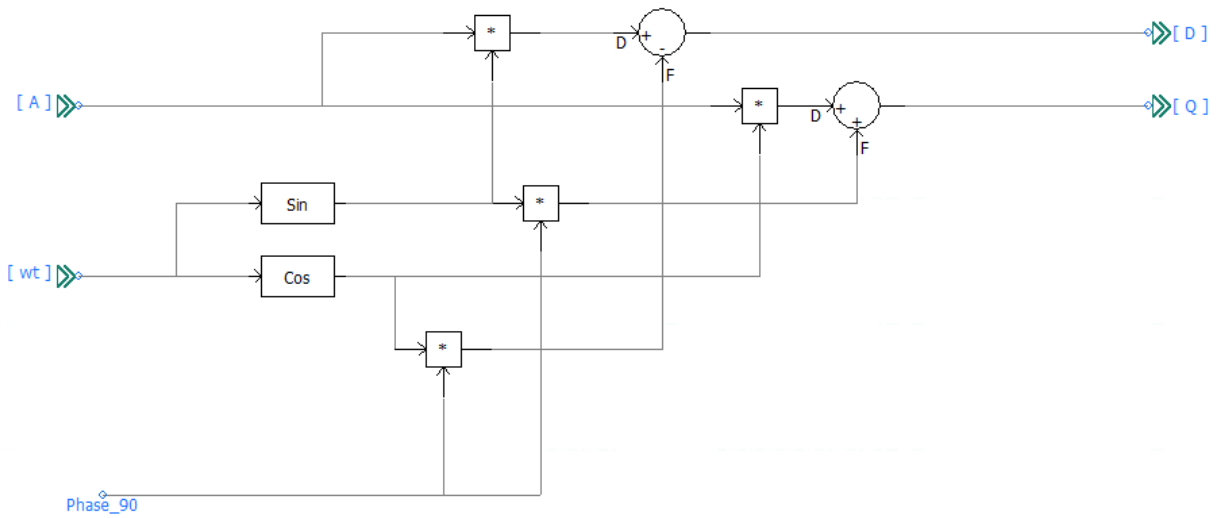

Figure A.9 Single Phase d-q Transformation Circuit Model in PSCAD

A.3.2.4 Droop Controllers

The droop control blocks are unique for the active and reactive power controllers. Active power control is managed by comparing the system RMS voltage to the nominal system voltage. The difference is divided by the droop coefficient and added to the active power measurement. This value is passed through a limiter to establish a maximum capacity for each inverter. The active power measurement is then subtracted from the target power to create an error setpoint signal that can be fed into the current and voltage control loops.

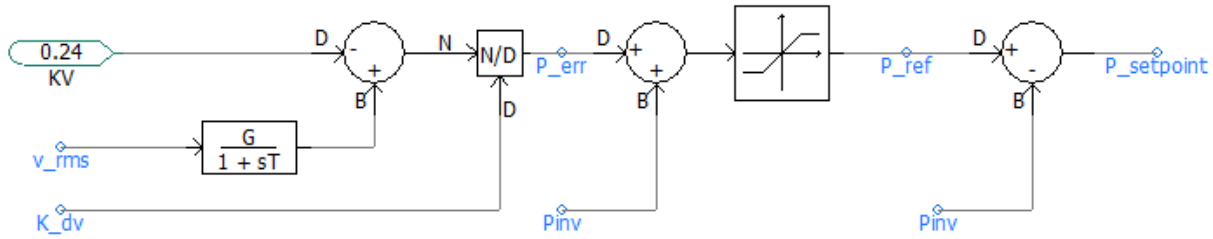

Figure A.10 Active Power Droop Control Circuit Model in PSCAD

The reactive power control is managed by comparing the measured system frequency to the nominal frequency. The difference is divided by the droop coefficient and subtracted from the

measured reactive power. The difference is the error setpoint signal that can be fed into the current and voltage control loops.

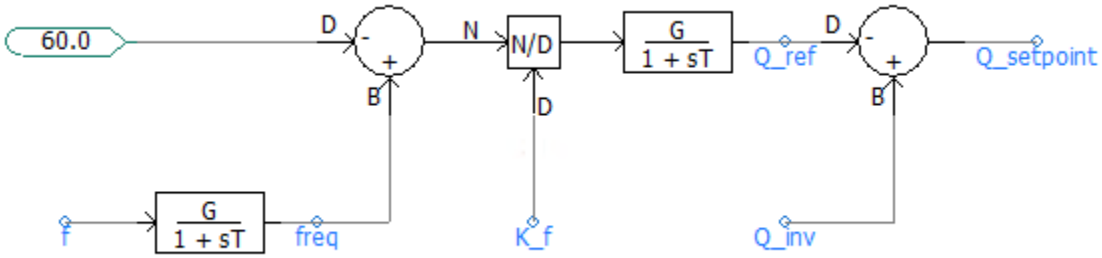

Figure A.11 Reactive Power Droop Control Circuit Model in PSCAD

A.3.2.5 Current and Voltage Control Loops

1. The current and voltage control loops receive an input error signal from either the maximum power point tracker or from the droop controllers. The error signal is fed

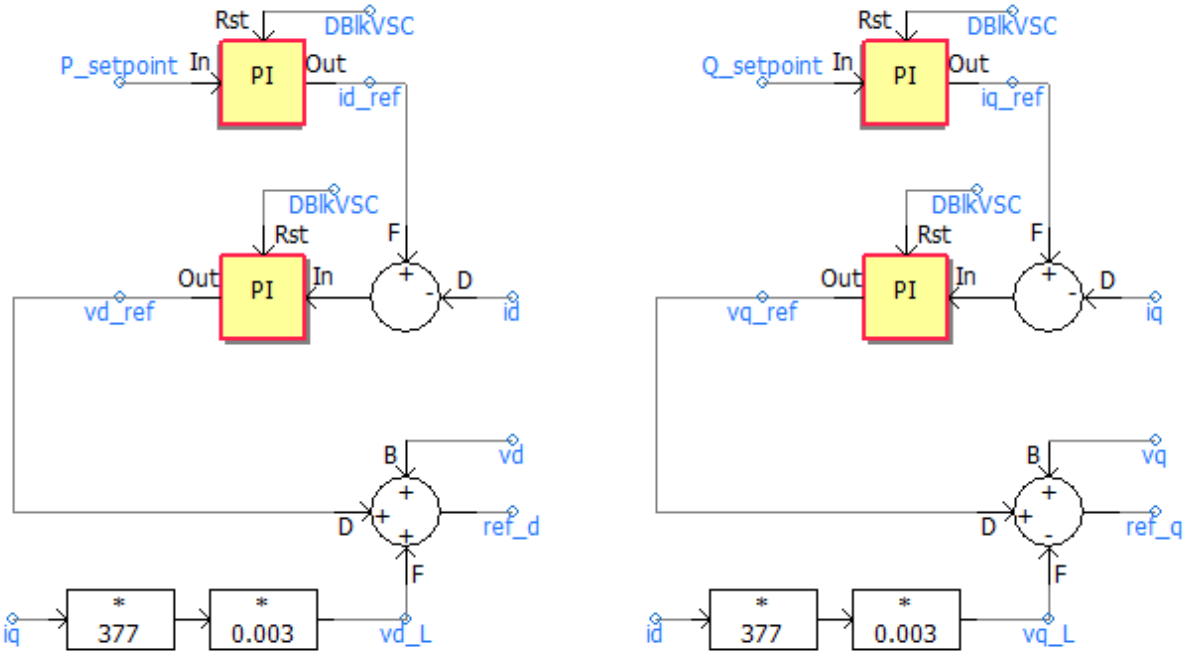

Figure A.12 Current and Voltage Control Loop Circuit Models

through a proportional integral block and the output signal is compared to the applicable current component. The error from that comparison is fed through a second proportional integral block and the output signal is added to the applicable voltage components to generate the reference signal.

A.3.2.6 Inverse dq transformation

The output of the current and voltage loops is the direct and quadrature components of the reference waveform that will be fed to the pulsewidth modulator. These components must be transformed back to the time domain using an inverse DQ transformation.

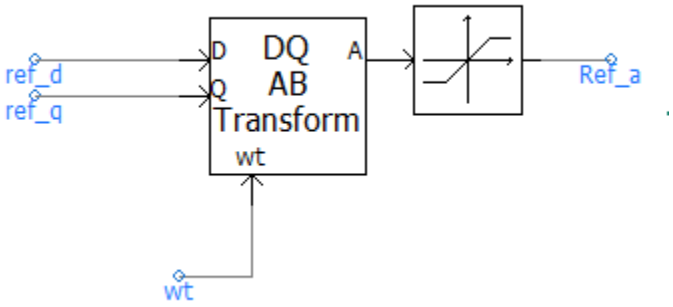

Figure A.13 Inverse DQ Transformation Component

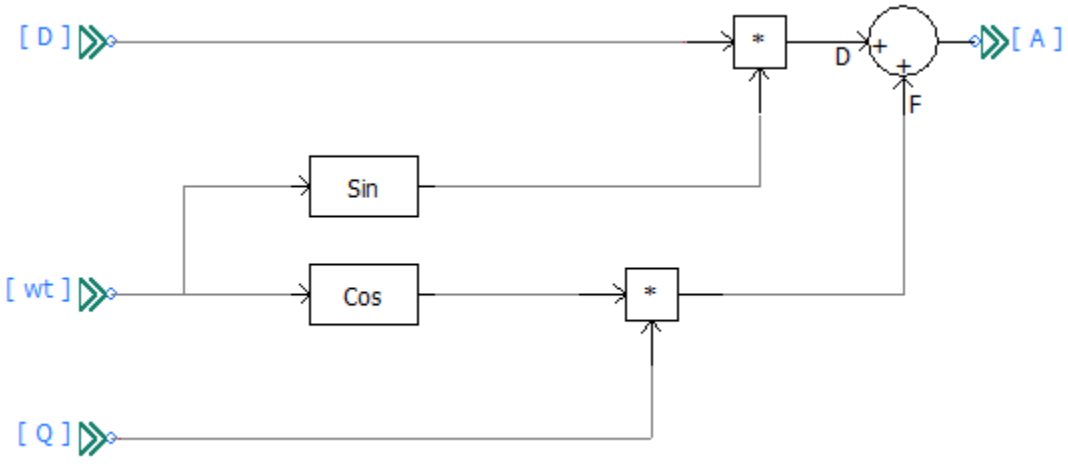

Figure A.14 Inverse dq Transformation Circuit Model in PSCAD

The same phase angle is used on the inverse transformation as was used on the original dq transformation. The output is limited from -1.1 to 1.1 to prevent saturation during a transient. The transformation is performed mathematically, with the orthogonal component not being used.

A.3.2.7 Pulsewidth Modulator

The pulse width modulator and firing signal generator is used to generate a firing pulse train to supply the full bridge converter thyristors. A saw tooth signal generator component is used to supply a sawtooth waveform with a voltage of -1 to 1. The output of the sawtooth waveform component is compared the AC modulating reference signal at two interpolating firing pulse components. The output of one interpolated firing pulse component provides the firing signals for the positive set of full bridge thyristors. The output of the other interpolated firing pulse component provides the firing signals for the negative set of full bridge thyristors. The blocking signal prevents inverter operation prior to converter startup.

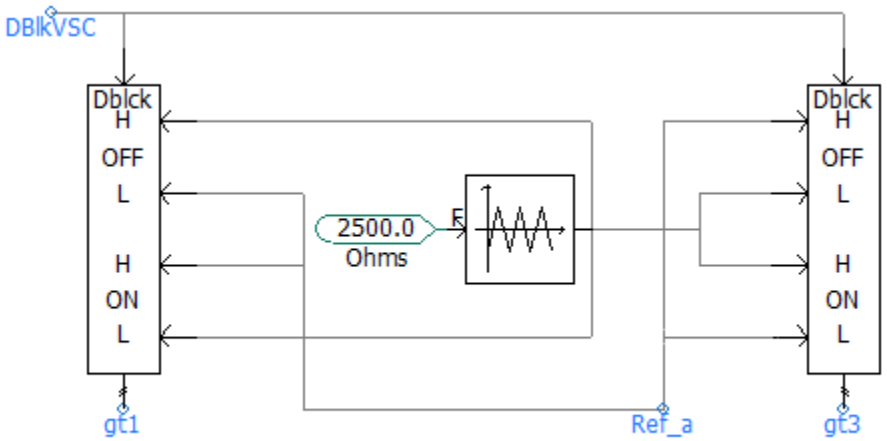

Figure A.15 Pulse Width Modulator and Firing Signal Generator Circuit Model

A.4 Conclusion

The circuit models presented in this appendix are intended to provide a helpful reference for designers in PSCAD to replicate various aspects of the performed study. Though not every feature is fully defined in this appendix, the basic flow and approach can be understood by users familiar with the PSCAD environment.